The Hong Kong Polytechnic University

Department of Health Technology and Informatics

DEVELOPMENT OF A COMPUTATIONAL FOOT MODEL FOR BIOMECHANICAL EVALUATION OF HIGH-HEELED SHOE DESIGNS

By

YU JIA

B. Eng., M. Eng.

A thesis submitted in partial fulfilment of the requirements for

the Degree of Doctor of Philosophy

January 2009

CERTIFICATE OF ORIGINALITY

I hereby declare that this thesis is my own work and that, to the best of my knowledge and belief, it reproduces no material previously published or written, nor material that has been accepted for the award of any other degree or diploma, except where due acknowledge has been made in the text.

____ ____ ____ ____

(YU Jia)

ABSTRACT

Foot problems such as corn, callus, ulceration, bunion and bone fracture may result from improperly or incorrectly fitted footwear. Wearing high-heeled shoes (HHS) may cause discomfort and eventually lead to foot problems such as hallux valgus, metatarsalgia, knee osteoarthritis and lower back pain. Many experimental techniques were developed and employed to quantify the biomechanical interactions of foot and footwear, such as in-shoe pressure measurement, motion analysis, in-shoe thermal measurement and skin blood flow measurement. However, direct biomechanical measurement of internal stress and strain on bony, ligamentous and intramuscular structures of the foot remains unavailable or highly invasive. Our understanding and quantification of HHS design from biomechanical aspects are still far from complete.

In this study, a comprehensive finite element (FE) model of a female foot with HHS was developed. The model used real three-dimensional foot geometry, and incorporated nonlinear material properties, large deformations and interfacial slip/friction conditions. The results of the computational model were validated by comparison of pressure distributions, shape deformations and cadaveric experiments. In general, the FE predictions were in good agreement with experimental measurements.

For the parametric study on heel height from 0-inch to 3-inch, an increase in heel height resulted in a decrease in arch deformation from 8.8 mm to 1.1 mm, which was

consistent with measured deformations. It was found that wearing HHS may help to reduce arch deformation of the weight-bearing feet. There was a general increase in predicted maximum von Mises stress of foot bones with increasing heel height of foot supports from 0-inch to 3-inch. In the forefoot region, relatively high von Mises stresses concentrated at the second to the fourth metatarsals. With 2-inch high-heeled foot support, the strain and total tension force in the plantar fascia was minimum in all calculated cases. Moderate heel elevation may help to reduce the strain of in plantar fascia. This finding copes with existing conservative treatment strategy for plantar fasciitis. Comparing the FE predictions of static standing on flat support and HHS, no noticeable rotation movement in transverse plane of the first metatarsophalangeal (MTP) segment was found, which was consistent with cadaveric experiment. A pronounced increase in peak von Mises stress in the first MTP joint was predicted in HHS condition compared to flat support. Therefore, heel elevation was not found to be a direct biomechanical risk factor for hallux valgus deformity. However, combined effects with tight toe box may impose risk of hallux valgus deformity. Heel elevation could be a triggering factor and should be confirmed in further study.

For the parametric study on outsole stiffness, comparison of von Mises stress in outsole with and without shankpiece suggested that embedded steel shankpiece is an important component of HHS, which sustains most of the loading of outsole and prevents outsole from collapsing and distorting.

For the parametric study on coefficient of friction, the model predicted that reduction of coefficient of friction will result in reduction in peak shear stress, whereas the peak plantar pressures remain approximately the same. The ground reaction force (GRF) in anterior-posterior direction increased by 55.5% with the reduction of coefficient of friction from 0.6 to 0.2.

Comparing mid-stance phase to standing from the FE predictions, arch deformation increased 98.3% from 5.9 mm to 11.7 mm. Tension and peak strain of plantar fascia increased 243.6% and 250.5%, respectively. While comparing walking with 2-inch HHS to balanced standing on flat support, tension force of plantar fascia increased by 31.1%. Results from gait analysis showed that increasing heel height from 0-inch to 4-inch increased the peak pressure and pressure-time integral in the forefoot region by 33% and 54%, respectively, whereas corresponding values in the heel region decreased. Moreover, for the GRF, the maximal propulsive force and maximal braking force with HHS was larger than those of the flat condition. The results imply that wearing HHS may be a possible risk factor of metatarsalgia.

It should be noted that current FE predictions were carried out with HHS without the shoe upper structures such as toe box and heel counter. In addition, high loading-bearing stance phases such heel strike and push off were not simulated in this study. Therefore, further investigations and simulations should be conducted before a solid conclusion about the biomechanical effects of wearing HHS can be made.

The biomechanical effects of different parameters, such as heel height, material properties and friction of HHS obtained from this study will be useful for better understanding HHS related foot problems and designing proper HHS. Meanwhile, much work still needs to be done to change footwear selection habits and public health cognition.

PUBLICATIONS ARISING FROM THE THESIS

Peer-reviewed Journals

1. Yu J, Cheung JT, Fan Y, Zhang Y, Leung AK, Zhang M，2008. Development of a finite element model of female foot for high-heeled shoe design. Clin Biomech. 23, Suppl 1, 31-38.
2. JT Cheung, J Yu, M Zhang, 2009. Review of computational models for footwear design and evaluation. Korean J of Sport Biomech.19,1-12.
3. JT Cheung, J Yu, WC Wong, M Zhang. Current methods in computer-aided engineering for footwear design. Footwear Science. (in press).
4. Yan Luximon, Jia Yu, Ameersing Luximon, Ming Zhang. Effect of heel height and weightbearing condition on the plantar load transfer, Acta Mechanica Sinica (submitted).
5. Yu J, Zhang M, 2008. Finite element analysis of foot and its clinical applications. Chin J Orthop Trauma (Chinese). 10, 113-115.
6. Zhang M, Cheung JT, Yu J, Fan Y, 2007. Human foot three-dimensional finite element of modelling and its biomechanical applications. J of Med Biomech (Chinese). 22, 339-344.
7. M Zhang, J Yu, JTM Cheung, AKL Leung and YB Fan，2007. Computational Foot Models for High-Heeled Shoe Design. J of Med Biomech (Chinese). 22 Suppl, 15-16.
8. Yu J, Zhang M, 2006. Finite element analysis on the effects of high-heeled shoes on foot biomechanics. J of Med Biomech (Chinese). 21 Suppl, 52.

Book Chapters

1. JT Cheung, J Yu, M Zhang, 2009. Development of foot biomechanical model and its and applications. Digital Medicine Progress (Chinese). In press.

Conference Proceedings

1. J Yu, JT Cheung, M Zhang, A 3D finite element female foot model for biomechanical evaluation of high-heeled shoe designs. World Congress on Bioengineering. 26-29 July, 2009. Hong Kong. (accepted).
2. JT Cheung, J Yu, M Zhang, Computational simulation of high heeled shoe fitting and walking. IX Biennial Footwear Biomechanics Symposium. 10-12 July 2009. South Africa. (accepted).

3. Yu J, Cheung JT, Zhang M, A finite element female foot Model for the design of High-heeled shoes. The 12th World Congress of the International Society for Prosthetics and Orthotics, Vancouver. 2007, pp109.
4. Yu J, Zhang M, VIMS-II conference & Workshop, Beijing, China, 2007, Oct 12-14. CD-ROM.
5. J Yu, JT Cheung, M Zhang, A 3-D finite element model of female foot with high heeled shoe. In: Proceedings of the BME 2006, Hong Kong, 21-23 Sept, 2006, pp75-76.
6. Y. Zhang, J Yu, MC Ho, M Zhang, Effect of heel height on plantar pressure distribution and subjective measure. In: Proceedings of the BME 2006, Hong Kong, 21-23 Sept, 2006, pp149-151.

ACADEMIC AWARDS

2006 Young Engineers Papers Competition Champion Award at Biomedical Engineering Conference 2006 Organized by Biomedical Division of the Hong Kong Institution of Engineer

ACKNOWLEDGEMENTS

Time runs fast, postgraduate study life is precious. I would like to thank the most important person, Prof. Ming Zhang, chief supervisor of my PhD study, who provided all necessary support, helpful guidance, constructive advice and great patience throughout my more than one thousand days on perusing PhD degree.

I must particularly thank Dr. Jason T.M. Cheung, my fellow for his invaluable suggestions on the development of foot model of my PhD study and his constructive comments and recommendations given on my drafted papers and thesis.

I must also thank Prof. Kai-Nan An, Chair and Professor of Department of Orthopaedic Surgery, Mayo Clinic, my supervisor during my attachment programme at Mayo Clinic for his support and invaluable suggestions on cadaveric experiment at Mayo Clinic. I would like to express my sincere thanks all my fellow researchers at Mayo Clinic, Prof. Kitaoka Harold, Prof. Kaufman Kenton, Dr. Kristin Zhao, Dr. McCullough Matthew, Dr. Ikoma Kazuya, Dr. Hirano Takaaki and Mr. Lawrence Berglund, who helped me on the cadaveric foot experiment with high-heeled shoes.

I would like to thank Prof. Arthur F.T. Mak, Head of our department, Prof. Daniel H.K. Chow, Dr. Aaron K.L. Leung, Dr. Mo Yang and Dr. M.S. Wong who gave me invaluable suggestions on my confirmation examination and student seminar.

I am pleased to acknowledge all my fellow students and colleagues who contributed in my research studies. Of particular, I must first extend my sincere thanks to Mr. Duo W.C. Wong for his invaluable comments on my drafted thesis. I would like to thank Dr. Yan Luximon, who helped me on high-heeled shoes design, gave me suggestions on gait analysis experiment and helped me on static validation measurements. I would like to thank Miss Yan Cong, who assisted me on gait experiments. Appreciation also goes to Dr. Alison Wong and Mr. Kobayashi Toshiki, who gave me suggestions on the kinematics aspect of gait analysis. I wish to thank Mr. Hok-Sum Man, Miss Meng Huang, Miss Shuzhe Wang, Mr. Xinguang Wang, Dr. He Gong, Miss Xuan Liu and Mr. Jie Yao for their kind support in specific aspects of my studies.

I would like to thank all the research staff and fellow students in the Department of Health Technology & Informatics for giving me a warm and supporting research environment throughout my studies.

I need to thank Dr. Hector Ma and colleagues from the Scanning Department of St. Teresa’s Hospital, Kowloon, Hong Kong for facilitating the MR scanning and the Industrial Centre of The Hong Kong Polytechnic University for providing the MIMICS software.

Last but not the least, I must extend my graceful thanks to my parents for their loving support and patience during my study.

Finally, I would like to acknowledge the Research Grant Council of Hong Kong (Project Nos. PolyU 5249/ 04E, PolyU 5317/05E) and HTI department support in the form of a PhD studentship.

TABLE OF CONTENTS

LIST OF FIGURES

LIST OF TABLES

LIST OF ABBREVIATIONS

1D: One-dimensional

2D: Two-dimensional

3D: Three-dimensional

AFO: Ankle foot orthosis

A-P: Anterior – posterior

BW: Body weight

COP: Center of pressure

CT: Computed tomography

E: Young's modulus

EDL: Extensor digitorum longus

EHL: Extensor hallucis longus

EMG: Electromyography

EVA: Ethylvinyl acetate

FDL: Flexor digitorum longus

FE: Finite element

FEA: Finite element analysis

FEM: Finite element method

FHL: Flexor hallucis longus

G: Shear modulus

GRF: Ground reaction force

HDPE : High-density polyethylene

HHS: High-heeled shoe(s)

M-L: Medial-lateral

MR: Magnetic resonance

MTP: Metatarsophalangeal

MTJ: Midtarsal joint

OA: Osteoarthritis

PB: Peroneus brevis

PCSA: Physiological cross sectional area

PIP: Interphalangeal

PL: Peroneus longus

PU: Polyurethane

ROM: Range of motion

STJ: Subtalar joint

TA: Tibialis anterior

TMJ: Tarsometatarsal joint

TP: Tibialis posterior

TPR: Thermoplastic

ν: Posson’s ratio

CHAPTER I INTRODUCTION

1.1 History of High-heeled Shoes

The term “high-heeled shoe” (HHS) indicates the shoe is constructed such that the heel of the wearer's foot is significantly elevated higher than the toes. Both the heel and the toes raised is generally not treated as a HHS but a platform shoe.

1.1.1 The Advent of High-heeled Shoes

The elevated shoe in style called the chopine originated in Turkey in about 1400. These shoes were typically 7-8 inches (18-20 cm) high, and in the extreme case, as much as 18 inches (46 cm) tall, helping to keep the wearer’s skirts out of mud (Linder and Saltzman, 1998). Women loved the attention and the additional height, but chopines were so restrictive that ladies had to stay at home, forced by their footwear.

According to Schlager (1994) statement, Catherine de Medici (1519-1589), the diminutive wife of Duke of Orleans, was credited with wearing the first true high heels and with taking the style to France in 1533. She had commissioned the Italian designers to create the high heel by modifying the chopine’s to eliminate its awkwardness, while still increasing her stature. But unlike previous construction, this heel was higher than the toes and the "platform" was made to bend in the middle with the foot. These high heels served vanity in another way, by making the feet appear smaller and the arch of the foot higher. Both of these physical attributes were considered signs of nobility.

Catherine's Italian style was quickly adopted by the French court. From then on shoe height has historically reflected nobility, authority and wealth. Gentlemen as well as ladies continued to wear high heels as a matter of noble fashion throughout the 17th and 18th centuries. However, by the late 18th century, high heels were almost exclusively worn by women.

After World War II, the high heels regained popularity primarily because of the growth in consumer spending and the variety and availability of designs produced. Stiletto heels became fashion in the 1950s. In the 1960s, stiletto heels were attached to 'wet-look' boots that enhanced the effects of miniskirts. Today's designers experiment with every material and type of ornamentation, to create and embellish high heels.

1.1.2 The Reason for Popularity

Optical Sensuousness

There are many reasons why ladies want to wear high heels. The primary reason for adding heel height to the shoe is sensuous. No matter whether women are standing or walking, wearing HHS creates an optical illusion of a smaller foot, shapes the contour of ankle and leg, contributes to a long-legged look, thrusts the buttocks backwards and increases height to generate the sensation and appearance of power and status. While walking, the high heel shortens the stride, accentuates the shape and movement of lower limbs, buttocks, abdomen and bosom, and increases the curve of the back and the sway of pelvis, which make the stride appear sensuous.

Anthropological Perspective

When basic biology and culture seem to run counter to each other, a pattern of human behavior arises that is of considerable anthropological interest. The anthropologist Smith and Helms (1999) comprehensively analyzed how high heels provide a good example of an evolved cultural display directed by sexual selection. Conforming to culturally prescribed patterns of dress must have some positive fitness-enhancing aspects. A woman wearing high heels sends a variety of messages that reveal her receptivity, sexuality, confidence and power. High heels go well beyond sexual symbolism and actually enhance the sexual attractiveness of a woman. The advantages in mate selection gained by women wearing may far outweigh the physical trauma that high heels incur. Clearly, women are engaging in a behavior that pits major short-term fitness payoffs against long-term fitness costs. High heels are a cultural trait that continues in populations in spite of its potentially fitness-reducing properties. High heels offer an extraordinary example of the interaction of biology and culture in shaping behavior.

1.1.3 The Adverse Effects of High-heeled Shoes

Gallup organization reported that 59% of women wore HHS for one to eight hours per day (The Gallup Organization Inc., 1986). Medical scientists have documented the adverse effects of HHS, its adverse effects could be traced back four centuries ago (Linder and Saltzman, 1998).

Many researchers reported that overworked or injured leg muscles, lower back pain and knee osteoarthritis (OA) may be linked to the abnormal posture that high heels induce (Kerrigan et al., 2005). In study of the relationship between posture and heel inclination (2 inches), it is found that lower back pain may be affected by usage high heels because of the reduction of normal lumbar lordosis (Franklin, 1995). On this basis, these researchers have proposed that high heels might lead to the development and progression of Knee OA (Cimmino, 2004, Kerrigan et al., 2005).

It is important that high heels do cause cumulative damage to the feet. The Mayo Clinic Foundation (Mayo Clinic, 2006) listed the most common foot problems associated with high heels, such as corn, callus, hammer, mallet and claw toes, hallux valgus, Morton's neuroma, metatarsalgia, pump bump and tight heel cords. If women frequently wear HHS that are too narrow or too short for their feet, they could be setting themselves up for one or more of these foot problems.

Toe Pain

Mallet, hammer and claw toes are the most common toe problems caused by wearing shoes that have too small size or have too high heel (Fig. 1-1). This jams the toes against the front of the shoe and causes one or more joints to bend. The toes may press against the top of the toe box of the shoe, causing pressure and pain. Constant pressure on the toes and nail beds can lead to nail fungus and ingrown toenails.

Corns and calluses are thick and hardened layers of skin caused by high friction areas between shoe and foot (Fig. 1-1). Painful rubbing can occur from wearing HHS. This slides the foot forward in the shoe. A narrow toe box can create uncomfortable pressure points on the foot.

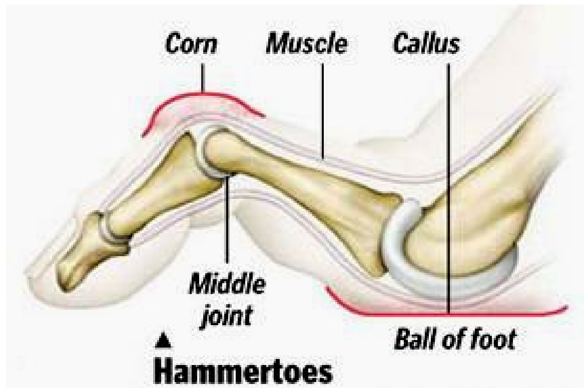

Figure 1-1. Hammertoes, corn and callus (Brenna Maloney, 2008).

Hallux valgus (Bunion) is a deformity of the foot in which the hallux deviates laterally and the first metatarsal deviates medially (Fig. 1-2). When the hallux deviates laterally, it rotates, and the surrounding muscles pull it even more laterally. This is caused by improper alignment of the bones in the foot during walking. Bunions can also occur on the joint of little toe (bunionettes). It was reported that there was a significant increase in the number of surgical procedures performed for hallux valgus in Japan, after the adoption of westernized footwear in preference to the traditional sandal (Kato and Watanabe, 1981). This condition is 99% preventable and 1% hereditary. About 98% of the people who have this problem are women between the ages of 48 and 60 years old. This is often due to the wearing of pointed high heels.

Figure 1-2. Bunion and bunionette (Footsolutions Inc., 2007).

Morton's neuroma (also known as Morton's metatarsalgia) is a benign neuroma of an intermetatarsal plantar nerve, which occurs at the base of the third and fourth intermetatarsal spaces. Neuroma is often the result of compression and irritation of the nerve. Wearing tight shoes or HHS can lead to Morton's neuroma because high heels put extra pressure on the ends of the bones. The bones, squeezed together by narrow or pointed shoes, pinch the nerve that runs between them.

Forefoot Pain

Metatarsalgia is a painful condition in the metatarsal head region that is often a result of inflammation caused by wearing shoes with thin soles and high heels (Fig. 1-3). Increased pressure on the forefoot, often as a result of HHS, can cause terrible pain. The pain can occur under the regions of any of the five metatarsal heads. Bent or twisted toes and bunions can make the problem worse. Shoes with tight fitting toe boxes can lead to similar discomfort. A stress fracture is a tiny crack in one of the foot bones, often in the area beneath the second or third metatarsal.

Figure 1-3. Metatarsalgia (Footsolutions Inc., 2007).

Rearfoot Pain

Haglund's deformity (Pump bump) is bony enlargement on the back of heel which can become aggravated by the rigid backs or straps of high heels when walking (Fig. 1-4). The deformity could lead to painful bursitis, which is an inflammation of the bursa (a fluid-filled sac between the tendon and bone). The deformity is most common in young women who wear pumps, although heredity may play a role in developing the deformity (Stephens, 1992).

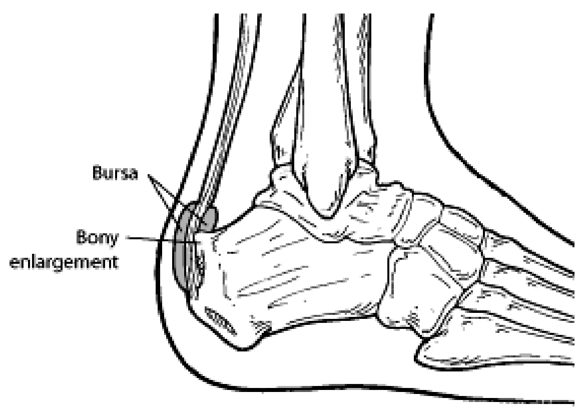

Figure 1-4. Haglund's deformity (American College of Foot and Ankle Surgeons, 2008).

Finally, wearing high heels keeps the Achilles tendon from fully stretching during walking. Over time, the Achilles tendon contracts to the point that the wearers no longer feel comfortable wearing flat shoes. This may indicate tight heel cords. High heels may impair the balance and increase the risk of falling, which could lead to ankle sprain or fracture.

Although the above mentioned foot problems caused, HHS could also be used as an alternative therapeutic measure in the treatment of tendinitis and partial ruptures of the Achilles tendon (Kogler et al., 2001). The conservative treatment strategy for plantar fasciitis can reduce the strain in plantar fascia (Gordon, 1984; Cole et al., 2005; Marshall, 1988).

Cost of Improper Fitting of Shoes and High Heels

Based on the survey of the American Orthopaedic Foot and Ankle Society on women's shoes in 1993, 88% wear shoes that were smaller than their feet (average 12 mm), 80% had foot pain or deformity, and 76% had one or more forefoot deformities. It was estimated that in the US, 43 million people had foot complaints every year and one third of these would eventually seek medical care (Coughlin, 1995). A conservative estimation of physician and hospital fees and time lost from work following forefoot surgical reconstruction was \$2 to \$3 billion per year (Thompson and Coughlin, 1994). The review of the number of surgical treatments done over a 15-year period showed that 87% of the forefoot treatments were for women (Thompson and Coughlin, 1994).

However, there was an equal incidence rate in both men and women surgical treatments such as ankle fusions and ankle fractures. Obviously some problems are not related to constricting shoe wear (Coughlin, 1995). In regard to specific diagnoses, women again had a much higher frequency of surgical treatments: 94% for hallux valgus procedures, 81% for hammertoe repairs, 89% for neuroma excisions, and 90% for bunionette corrections. With increasing age, the frequency of surgical correction increased as well.

1.2 Objective of Study

Foot problems such as corn, callus, ulceration, bunion and bone fracture may result from improperly or incorrectly fitted footwear. Wearing high-heeled shoes may cause discomfort and eventually lead to foot problems such as hallux valgus, metatarsalgia, knee OA and lower back pain. Fit and comfort are complex and multifaceted. Many experimental techniques have been developed and employed to quantify the biomechanical interactions of foot and footwear. These techniques include in-shoe pressure measurement, motion analysis, in-shoe thermal measurement and skin blood flow measurement. However, direct biomechanical measurement of internal stress and strain on bony, ligamentous and intramuscular structures of the foot remains unavailable or highly invasive. Our understanding and quantification of HHS design from biomechanical aspects are still far from complete.

Computational modelling, such as the finite element (FE) method, provides an opportunity to efficiently investigate footwear design parameters from biomechanical aspects. The purposes of this study are:

1) To develop a comprehensive FE model of the female foot with HHS, using the real three-dimensional (3D) foot geometry and incorporating nonlinear material properties, large deformations and interfacial slip/friction conditions to more accurately simulate the biomechanical interaction between foot and HHS, and

2) To evaluate the effects of different parameters, such as heel height, material properties and friction of HHS from biomechanical aspects, through FE analyses and experimental measurement. The results of the computational model will be validated / compared by comprising pressure distributions and the shape changes from computational model results and experimental measurements including human subject testing and cadaveric experiments.

The biomechanical information on the effects of different parameters of HHS obtained from this study will be useful for better understanding HHS related foot problems and designing proper footwear.

1.3 Outline of the Dissertation

Following this introductory chapter, chapter II is the literature review, which is divided into four sections. The chapter begins with an introduction of the musculoskeletal system of human foot. The research on general shoe designs for fit and comfort is then reviewed. After that, biomechanical studies of gait on wearing HHS are summarized. Finally, the advantages of the FE method are briefly introduced and followed by a detailed review of FE studies on foot and footwear biomechanical research.

In chapter III, the development of the FE model of the foot. This includes material properties, loading and boundary conditions prescribed is presented in details. The parametrical studies investigating the effects of varying heel height, coefficient of friction and outsole stiffness are described. The loading conditions for simulating mid-stance phase are presented. The experimental procedures for balanced standing and gait on different heel height shoes/foot supports and cadaveric experiments are presented.

Chapter IV presents the results of the FE analysis and experimental studies. This chapter reports the findings of the parametrical analyses using the FE foot model developed in this study. The results of static balanced standing measurement, cadaveric experiment and gait analysis for FE model validation are included.

Chapter V is the discussion of the findings and limitations of this study. The FE predictions and experimental measurements are compared. Relevant clinical implications of the parametrical analyses performed on the FE foot model are presented.

Chapter VI summarizes the findings in this study and presents clinical implications regarding different simulated conditions of the foot. Suggestions on future research directions are presented.

CHAPTER II LITERATURE REVIEW

The literature review is divided into four sections. This chapter begins with a brief introduction of the musculoskeletal system of human foot from biomechanical aspects. Then, the research on general shoe designs for fit and comfort is reviewed. After that, the postural change and gait biomechanics studies on wearing HHS are summarized. The advantages of FEM are introduced and followed by a detailed review on the FE studies on foot and footwear biomechanical research. A critical summary of existing FE models is presented at last.

2.1 Musculoskeletal System of the Human Foot

Human foot is a complex structure containing 26 bones and 33 joints, layered with an intertwining web of over 120 muscles and ligaments. It serves the following four major functions:

- Supporting body weight (BW)
- Acting as a shock absorber
- Serving as a lever to propel the leg forward, and
- Maintaining balance by adjusting the body to uneven surfaces.

Human foot combines mechanical complexity and structural strength. The foot can sustain large pressure and provides flexibility and resiliency.

2.1.1 Joints and Ligaments of the Foot and Ankle

Structurally, the foot consists of three main portions, which are forefoot, midfoot and rearfoot (Fig. 2-1). The forefoot is composed of five phalanges and their connecting five metatarsals. The midfoot has five irregularly shaped tarsal bones, forming the foot longitudinal arch, and serves as a shock absorber. The rearfoot is composed of several joints and links the midfoot to the ankle (talus). The top of the talus is connected to two long bones of the lower leg (tibia and fibula), forming a uniaxial hinge joint. The calcaneus is the largest bone in the foot. The calcaneus joins the talus to form the subtalar joint, which allows inversion and eversion of the foot. The bottom of calcaneus is cushioned by fat pad.

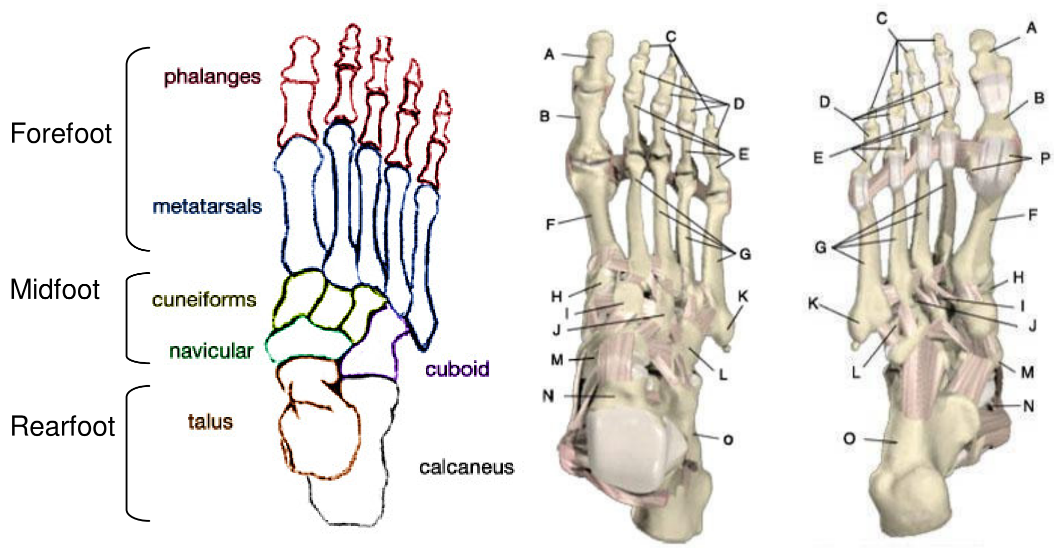

Figure 2-1. The top and bottom views of the bones of the human foot: A. distal phalanx of the hallux, B. proximal phalanx of the hallux, C. distal phalanges, D. intermediate phalanges, E. proximal phalanges, F. first metatarsal, G. lesser metatarsals, H. medial cuneiform, I. intermediate cuneiform, J. lateral cuneiform, K. styloid process, L. cuboid, M. navicular, N. talus, O. calcaneus, P. sesamoids. (www.orthcoastfootcare.com; Interactive Foot and Ankle, 1999).

Tendons in the foot connect muscles to bones and joints. Ligaments stabilize the joints. The largest and strongest tendon is the Achilles tendon, which extends from the calf muscle to the heel.

Plantar Fascia

Plantar fascia has a long ligament-type structure which supports the longitudinal arch when walking. Plantar fascia has three bands, which are medial, central and lateral band. Its central component is known as the plantar aponeurosis (Fig. 2-2). The plantar fascia contributes to the support of the arch of the foot by acting as a tie-rod, where it undergoes tension when the foot bears weight. The plantar fascia has an important role in static standing and dynamic function during gait (Aquino and Payne, 1999).

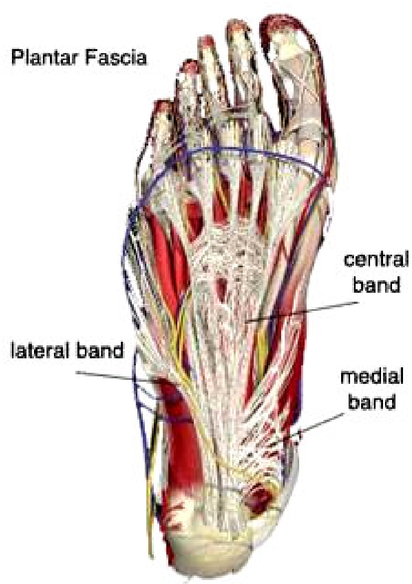

Figure 2-2. Plantar fascia (Interactive Foot and Ankle, 1999).

Talocrual Joint

Talocrual joint (ankle joint) is a triplanar joint although its basic motion is in the sagittal plane. The complex interplays among the tibia, fibula and talus and their associated ligamentous connections allow rotation and a small amount of translation. The ligaments of the ankle joint are grouped into two categories, the deltoid ligament group and the lateral collateral ligaments group. Four ligaments make up the deltoid ligament, which are posterior tibiotalar ligament, tibiocalcaneal ligament, tibionavicular ligament, anterior tibiotalar ligament (Fig. 2-3). These ligaments give support to the medial side of ankle joint. The tibiocalcaneal and tibionavicular ligaments resist abduction. The other two deltoid ligaments limit plantar flexion and dorsiflexion respectively. There are three ligaments on the lateral aspect of the ankle joint, which are anterior talofibular ligament, calcaneofibular ligament and posterior talofibular ligament. The anterior talofibular ligament limits plantar flexion of the joint. The left ligaments limit dorsiflexion.

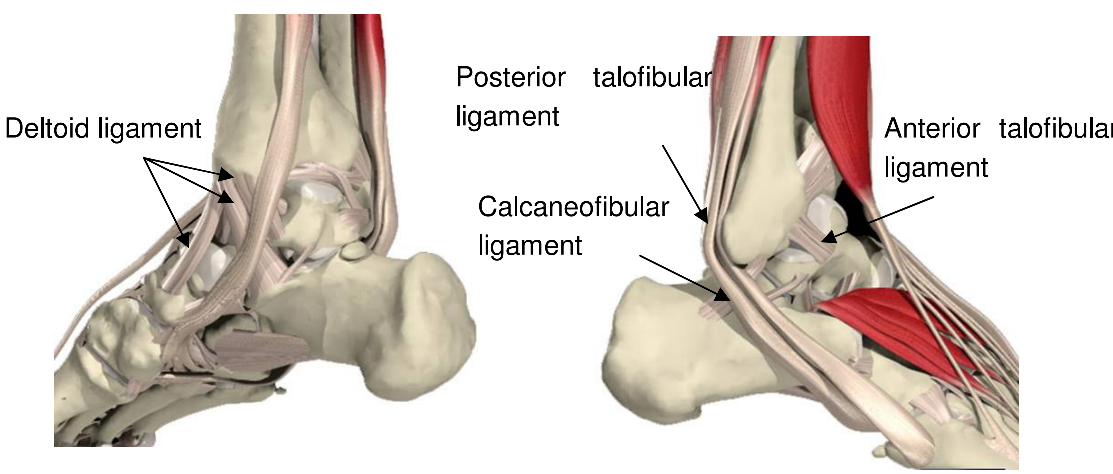

Figure 2-3. The deltoid and lateral collateral ligaments of the ankle joint (Interactive Foot and Ankle, 1999).

Subtalar Joint (STJ)

The articulation between calcaneus and talus is the subtalar joint. The articulation contains two joint surfaces, which are posterior and anterior. This structurally based articular geometry, along with the interosseous talocalcaneal ligament, limits the amount and type of motion at the STJ (Fig. 2-4). Other four additional ligamentous structures that offer support to the STJ are the medial, lateral, anterior and posterior parts of talocalcaneal ligaments. At the STJ, the triplanar axis of rotation is directed in an anterosuperior to posteroinferior direction. Based on *in vivo* computed tomography, the range of subtalar joint rotation about the helical axis was from 26.6 to 50.4 degrees (Beimers et al., 2008).

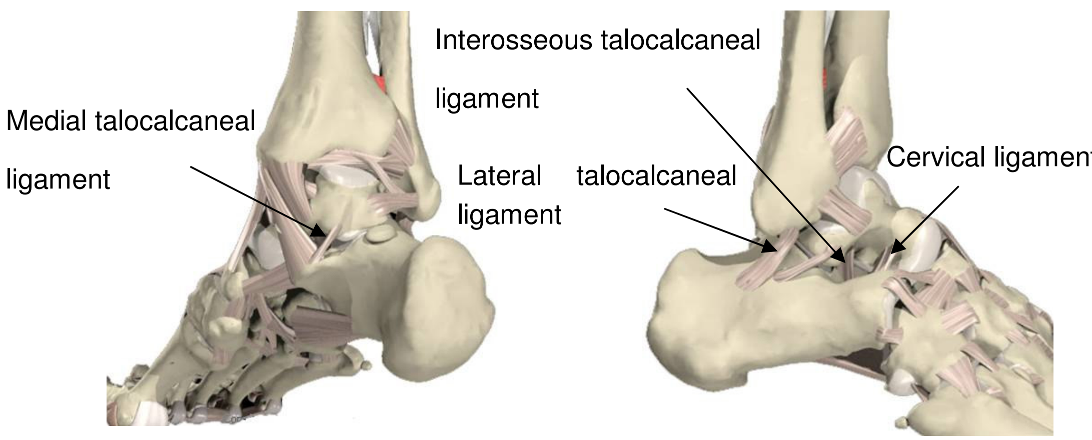

Figure 2-4. Talocalcaneal ligaments supporting the subtalar joint (Interactive Foot and Ankle, 1999).

Tarsometatarsal Joint (TMJ) and Midtarsal Joint (MTJ)

The tarsometatarsal joint which is also known as Lisfranc joint, this joint is located between the metatarsals and the cuneiforms (Fig. 2-5). While there is no soft tissue connection between the first and second metatarsal bases, the lateral four metatarsal bases are attached to each other by transverse metatarsal ligaments.

Two articulations between midfoot and rearfoot (talonavicular and calcaneocuboid) form an important composite joint：the midtarsal joint (Fig. 2-5). MTJ movement is supported and restricted by the bifurcate ligament, short and long plantar ligament and plantar calcaneonavicular (spring) ligaments. The short and long plantar ligaments and the plantar calcaneonavicular ligaments support the longitudinal and transverse plantar arches of foot as well. Since the MTJ is a composite joint, its motion occurs in about two separate triplanar joint axes, which are longitudinal axis and oblique axis. Functionally, movement of the forefoot of each joint axis can occur independently of the other. The combination of these two joint axes motion produces supination & pronation of the MTJ.

The amount of motion possible at the two MTJ axes depends on the position of the STJ. In STJ supination, the two joint axes are nearly perpendicular so that MTJ mobility is restricted. This mechanism helps to convert the forefoot into a rigid structure for propulsion during the push off phase of gait. When the STJ is pronated, the joint axes are more parallel and allow a greater degree of MTJ mobility.

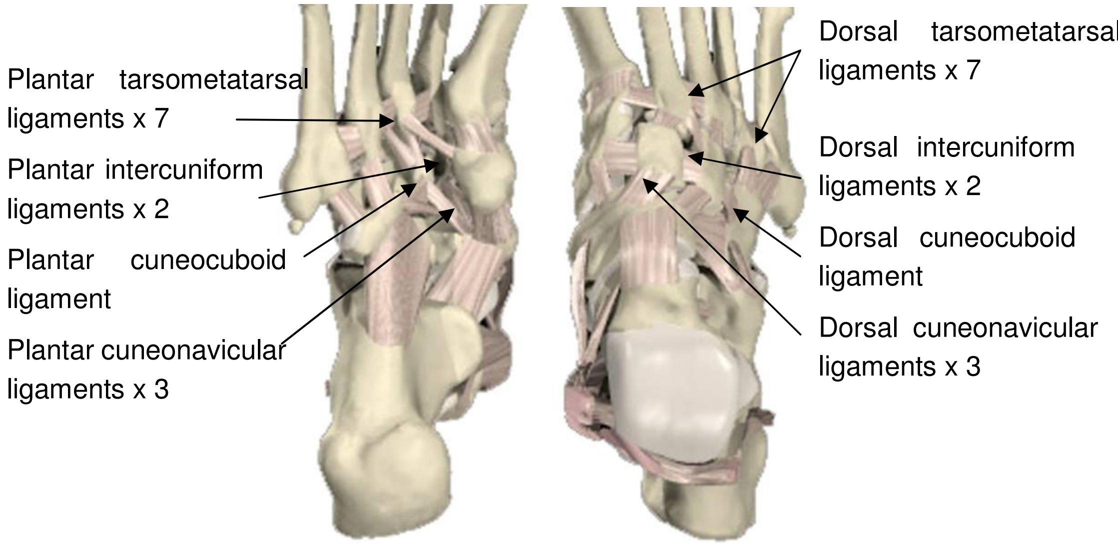

Figure 2-5. Ligaments supporting the distal intertarsal and tarsometatarsal joints (Interactive Foot and Ankle, 1999).

Metatarsophalangeal (MTP) Joint and Interphalangeal (PIP) Joint

The forefoot is comprised of structures that are distal to navicular and cuboid bones. It is subdivided into five rays and toes. The MTP joints are ball-and-socket articulations between the metatarsal head, the base of the proximal phalanges and the plantar plate (Fig. 2-6). The PIP joints are hinge joints that permit phalanges flexion and extension (Fig. 2-6). It was observed that the MTP joint limited plantar flexion and the PIP joint limited dorsiflexion (Joseph, 1963).

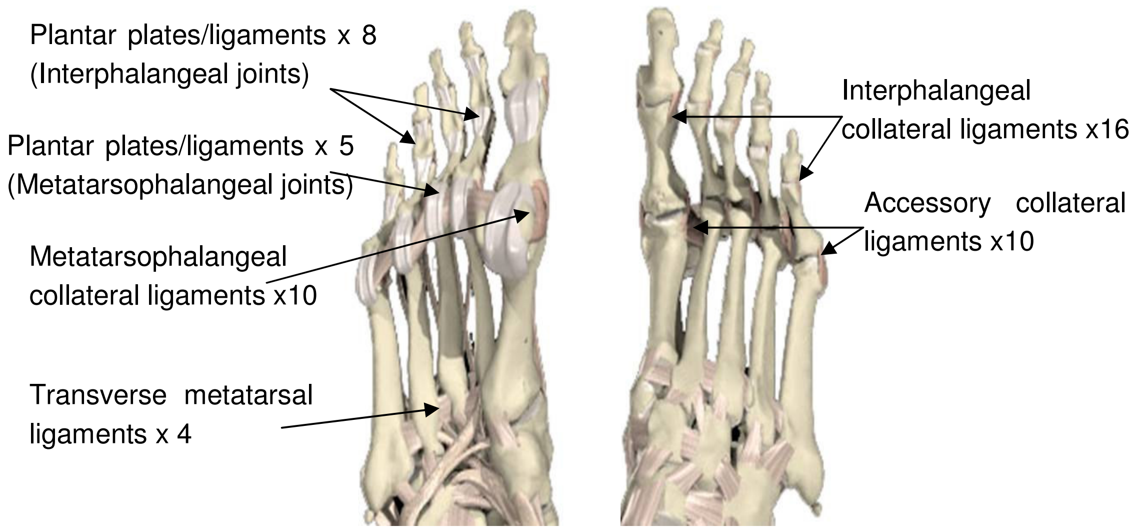

Figure 2-6. Ligaments supporting the metatarsophalangeal and interphalangeal joints (Interactive Foot and Ankle, 1999).

2.1.2 Muscles of the Foot and Ankle

A network of muscles, tendons and ligaments supports the bones and joints in foot. Muscles in foot give the foot its shape by holding the bones in position as well as allowing expansion and contraction to impart movement. Most of the motions of the foot are initialized by the major muscles in the lower leg whose tendons are connected in the foot. The main muscles of the foot are the tibialis anterior, which dorsiflexes and inverts the foot; the tibialis posterior, which inverts and plantarflexes the foot and supports the arch; the peroneus, which controls inversion and plantarflexion movement of the ankle; the extensors, which help the ankle raise the toes to initiate the act of stepping forward; and the flexors, which help stabilize the toes against the ground.

There are numerous small muscles in the foot. Smaller muscles enable the toes to lift and curl. While these muscles are not nearly as important as the small muscles in hand, they do affect the way that the toes work. Most of the muscles of the foot are arranged in layers on the sole of the foot. They control the movement of toes as well as provide padding underneath the sole of the foot.

Muscles within the Foot (Fig. 2-7):

1. Extensor digitorum brevis and the dorsal interossei are on the dorsum foot; the former muscle extends the PIP joints and the latter muscles abduct and flex the PIP joints.
2. Flexor digitorum brevis, abductor hallucis and abductor digiti minimi form the superficial layer of the sole of the foot; they flex the PIP joint and abduct the first PIP joint and the fifth PIP joint, respectively.
3. Flexor accessories, flexor hallucis brevis and flexor digiti minimi brevis form an intermediate layer in the sole of foot; they flex the PIP joints.
4. The adductor hallucis has two parts – the oblique and transverse heads. It adducts the big toe.
5. The plantar interossei and the lumbricals lie in the deepest layer of the foot; the former adduct and flex the PIP joints; the latter flex the proximal phalanges and extend the distal phalanges.

The above five groups of muscles are known as the intrinsic muscles of the foot. These intrinsic muscles help to contribute to the stability of the arch and position of the toes.

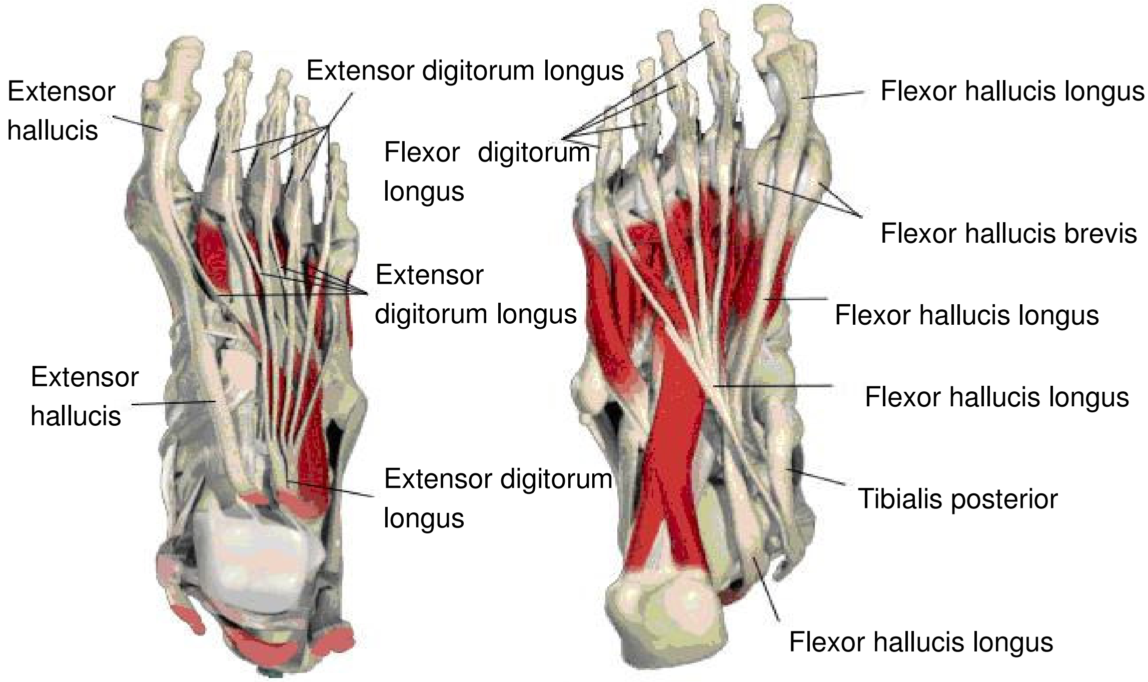

Figure 2-7. The main tendons in the top and bottom in human foot (Interactive Foot and Ankle, 1999).

Muscles Acting across the Ankle and Subtalar Joints (Fig. 2-8):

The function of the extrinsic muscles should be understood in relation to the axes of the ankle and subtalar joints. Those muscles that are posterior to the ankle axis bring about the plantar flexion motion and those anterior to the ankle axis muscles lead to dorsiflexion motion. The further the muscle is located from the axis of motion, the greater is the degree of leverage exerted by it on the axis.

1. Soleus joints with that of the gastrocnemius and sometimes plantaris to plantarflex the ankle. The soleus and gastrocnemius together also known as the triceps surae which terminates at Achilles tendon, are the most powerful plantar flexors of the ankle joint.
2. Extensor hallucis longus, entensor digitorum longus, tibialis anterior and peroneus tertius form the anterior aspect of tibia and fibula and the interosseous membrane.

Tibialis anterior is the main ankle dorsiflexor while the others are weaker dorsiflexors.

3. Flexor hallucis longus, flexor digitorum longus, tibialis posterior, peroneus longus and peroneus brevis are the deep calf muscles. The former two are flexors of the toes; the peroneus are on the lateral side and evert the foot; tibialis posterior is on the medial side and inverts it. Compared to soleus, all five muscles are weaker ankle plantarflexors.

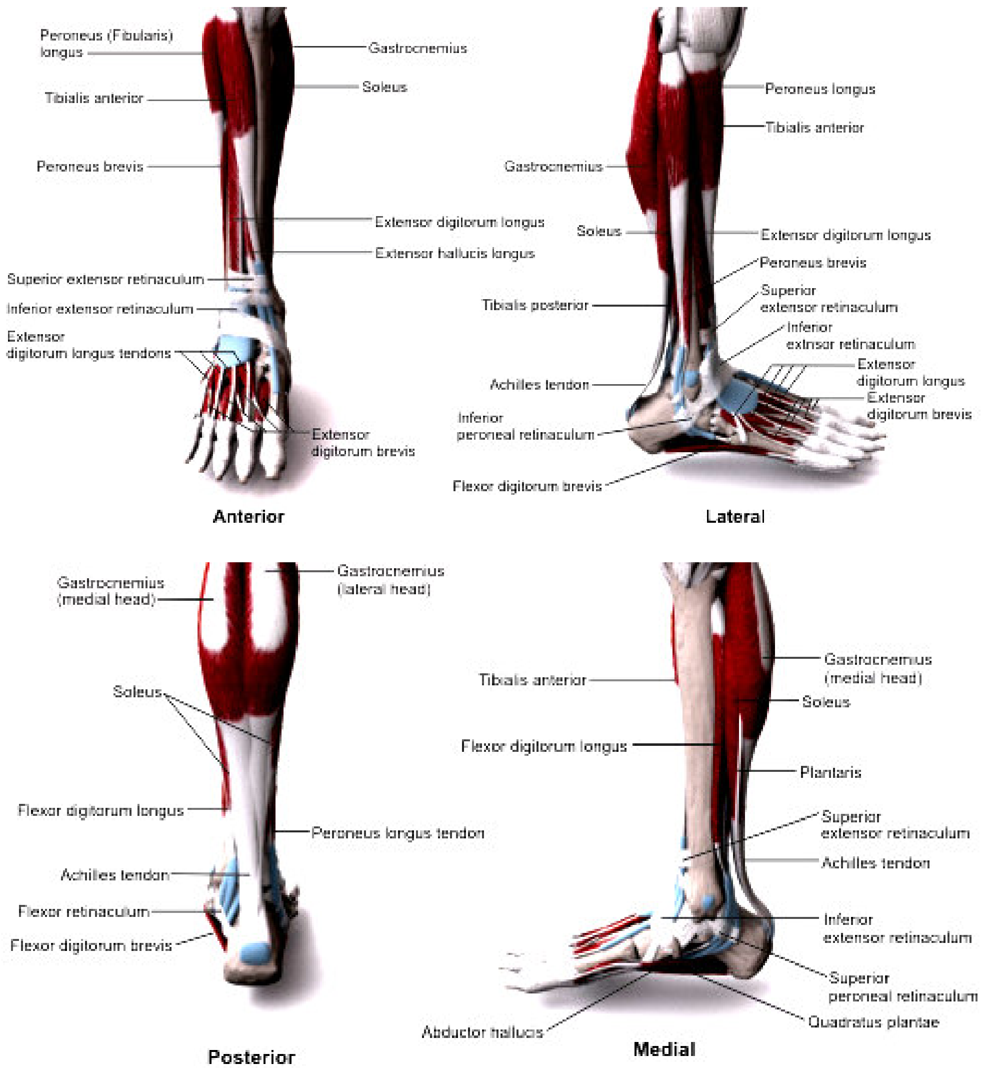

Figure 2-8. The anterior, posterior and side views of the right foot muscles (CD Media Studio Inc., 2003).

2.2 Shoe Designs for Fit and Comfort

Footwear serves to protect the foot from hard and rough surfaces, as well as climate and environmental exposure; to enhance performance and function of foot; and in many cases, to serve a cosmetic function. However, when the foot becomes restricted by shoes, the natural form of the foot becomes altered and deformities develop (Lam et al., 1958). It is generally agreed that ill-fitting footwear can cause many foot problems.

2.2.1 Shoe Construction

The basic construction of a shoe, no matter men's and women's, has the same design features, although the proportions are different. A shoe can be divided in two parts, which are upper part and bottom part (McPhoil, 1988). The upper part includes vamp, quarter, toe box, throat and topline. Shoe upper is made up of several 2D patches, which are derived from a 3D shoe last surface (Tam et al., 2007). The sections of the lower shoe consist of an outsole, shank and heel (Fig. 2-9).

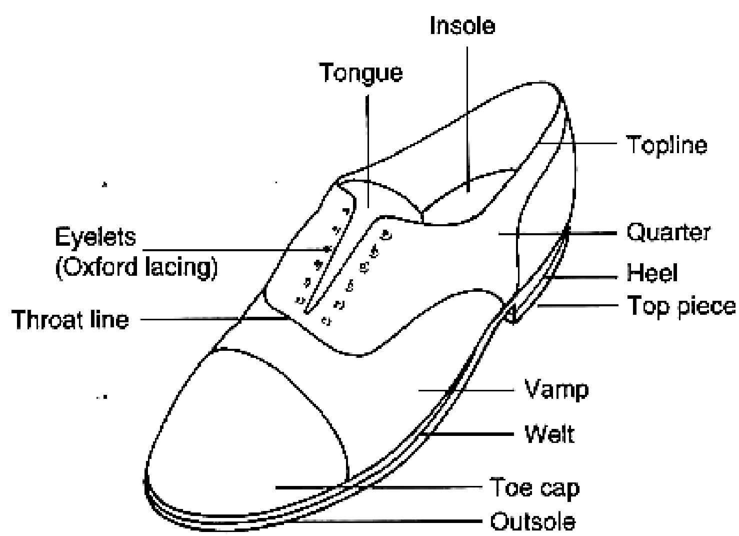

Figure 2-9. The construction of a shoe (McPhoil, 1988).

The toe box is the anterior portion of a shoe upper which retains the contour of a shoe toe. A narrow, pointed toe box gives the illusion of a smaller foot, often for sake of fashion desire. However, this type of toe box often compresses the toes from the sides and applies pressure on the dorsum of toes. The pointed narrow toe box can push the hallux into valgus position, and the lesser toes may be pushed up into a flexed posture, which can lead to hammertoes. In contrast, wide high toe box allows ample room for the toes to maintain a natural position without compressing or abrading the foot skin. With toe spring, the toes of the foot are constantly angled upward, depending upon the amount of shoe toe spring. The toe spring is to compensate for lack or absence of shoe flexibility at the ball, and creates a rocker effect on the shoe sole.

Behind the toe box is the vamp which covers the dorsum of foot, and superior aspects over the instep. In a women's fashion pump, there is very little vamp and no tongue. The minimization of the vamp is another fashion illusion to make the foot appear smaller. However, the reduced vamp size requires the shoe to fit tightly in order to hold the foot securely. Behind the vamp, the portion of upper comprising the posterior part of the shoe upper is called the quarter. The counter is a component of the quarter that stabilises the rearfoot in the shoe.

The insole is inside the shoe. The function of insole is to provide cushioning, moisture regulation, hygiene and motion control. The bottom portion of the shoe that contacts the ground is the outsole. This is important for friction, insulation and shock absorption. The outsole is constructed in different thickness and degrees of flexibility.

The shank bridges between the heel breast and the ball tread. The shankpiece reinforces the waist of the shoe and prevents it from collapsing or distorting in wear. The contour of the shank is determined by heel height. Shoes with low heels or wedged soles do not require a shank because the torque between the rearfoot and forefoot does not distort the shoe. Steel shankpiece is widely used to maintain shank contour of HHS.

Another feature of the shoe is the heel height, despite the fact that this is generally a fashion consideration. Heel height is measured from the bottom of outsole where the heel begins, to the plantar surface of heel. The pitch of heel is the angle or inclination of the posterior surface of heel, from vertical. Generally, the higher the heel the greater the pitch, which reduces the contact area of the weight-bearing surface with the floor.

2.2.2 Shoe Fit Analysis

Shoe fitting is generally assessed using the two variables of foot length and foot width, even though feet and shoes are 3D objects. A good fitting shoe should ensure complete absence of jamming; correct construction, whose substructure provides stiffness and flexibility in the right place; and proper materials which can provide adequate regulation of heat and moisture and ensure that footwear shape is preserved because of their resistance to wear and form-retainable properties (Snijders, 1987). Proper measurement of shoe size includes the overall foot length, arch length and width. The foot and ankle sourcebook (Tremaine and Award, 1998) states that proper shoe fit requires "shape or last design with proper toe depth and shape, proper instep (vamp) depth, proper heel width, and proper curve (flare) of the shoe". However, the term proper has not been defined or clarified.

Proper fitting of footwear to feet involves good understanding of feet, shoes, and the selection of shoes to achieve a required fit. The lacking of information in relation to the proper match hinders the progress of design and the selection of footwear (Rossi et al., 2001).

Ill-fitting footwear may be too loose or too tight. Direct, constant deforming pressure is reduced in "over-dimensioned" footwear; however, during intensive activities, it will increase relative movement between foot and shoe, resulting in foot problems such as blisters and calluses (Fig. 2-10).

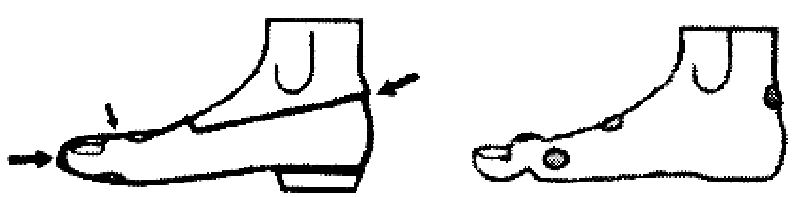

Figure 2-10. Toe pressure and heel counter pressure in the shoe (Philip, 1996).

Wearing "under-dimensioned" footwear, the toes can markedly change the alignment, particularly into flexion and midline deviation (Fig. 2-11).

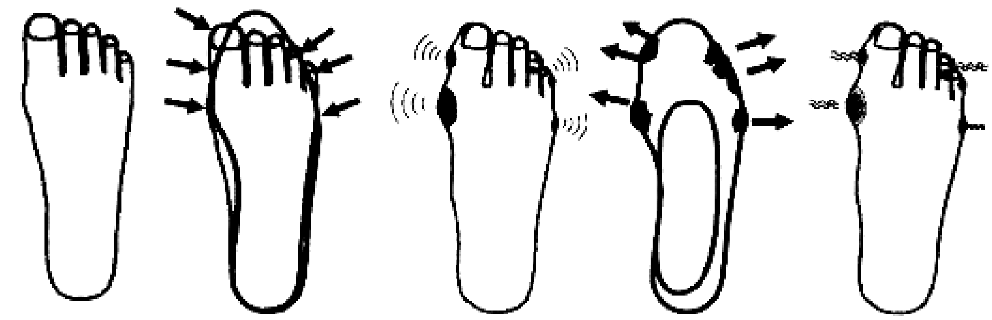

Figure 2-11. Reciprocal changes in both foot and shoe (Philip, 1996).

Anthropometrical Measurements

The anthropometrical measurements are the basis for shoe design. Shoe-makers must be familiar with the 3D form of the foot. Normally, the shoe designer collects basic statistics through sales or systematic two-dimensional foot measurements. The mechanism by which the shape and size of foot alter at weight-bearing condition or in walking is also significant (Rossi, 1983).

Many sources of two-dimensional foot anthropometry are available. Garca-Hernandez et al. (2005) further developed a 3D foot shape database called MORFO3D using INFOOT laser scanner in Spain. The location of foot landmarks could be obtained by simply marking them on the user barefoot with adhesive markers. That database contains 3D foot shapes and footwear fitting reports.

Rossi (1983) conducted a demographic foot measurements survey embracing 6800 adults in 1981-1982 at resting and weight-bearing conditions. It was concluded that probably no two feet are exactly alike in size, shape, or proportions. That finding may explain why the "perfect" shoe fit is virtually impossible.

Manna et al. (2001) measured 300 Indian subjects and found that there was no significant difference in most foot dimensions between right foot and left foot. However, significant difference in all foot dimensions was observed between male and female subjects. It was pointed out that the female feet are not merely scaled-down versions of the male feet but rather differ in a number of shape characteristics (Manna et al., 2001; Wunderlich et al., 2000).

Baba (1975) conducted the anthropometrical measurements of the right foot of 826 male and 1018 female healthy subjects in Japan and compared the results to the male foot study of French. It was found that the Japanese males had relatively larger ball girth and broader foot than the French males of the similar range of foot length, and racial difference between European and Japanese are even more noticeable than the observed gender differences. Thus, different shoe lasts for varied populations are necessary for optimal shoe fit.

A set of 2486 adult male samples collected in Taiwan was used to establish the norm for the foot length and joint girth (Cheng and Perng, 1999). In their study, the shoe last was classified into different classes by considering various incremental intervals of foot length. Each class showed different grading by considering the combination of foot length and joint girth.

In conclusion of findings from previous foot measurements studies, foot length, foot width and joint girth are relatively different, either between races and gender, even the right and left foot of the same person. One direction of designing good shoes fit may start from customized design.

Sizing Scale

The existing shoe sizing systems are primarily based on foot length and have evolved in various parts of the world with a view to assist consumers to select suitable footwear. More importantly, they are the yardsticks for shoemakers to design footwear. Therefore, the mismatched shoes may come from shoe sizing systems. The existing different sizing scale systems to population would significantly influence shoe fit. The different sizing systems are generally developed using two major measurements, which are on last or on bare feet.

The systems using measurements on lasts are the most commonly used systems in the world, e.g. the English sizing, American sizing and Continental sizing. The last is the mould to make shoe, which represents the inside shape of shoe as well as anatomical information of foot. Lasts are developed by accumulating experience about the fit for wearer, the making-up method, the average size, the fashion style and ultimate functions of footwear. In most cases, the length and sometimes the width and girth of a last is varied in order to meet the requirement for a certain style and the specific fitting shape for feet, and a consumer has to try a range of sizes when fitting a shoe. There is a more recent system developed with a view to reflect the actual feet size of wearer. The sizing system of China (PRC) is based on bare feet measurements (ISO 9407:1991).

Continental sizing is commonly used in Western Europe, and widely used as the second reference sizing in size labels for shoes using English or American sizing. Normally, Continental sizes range from 0 to 48 or even larger. A size increment of $\frac{2}{3}$ cm, starts at zero cm and continues up the scale without repetition. Similarly different stick lengths will have corresponding girths. In the Continental sizing scale, the girth increment is 5 mm. Typically, for any increase or decrease of 5 mm girth, the width of the widest part of the bottom of the last has to increase/decrease by 1 $\frac{2}{3}$ mm.

Fitting Survey and Analysis Techniques

Frey et al. (1993) conducted a survey related to the effects of shoe on foot deformity and pain. In that study, 356 American women participated, 80% of whom had foot pain and 76% had one or more forefoot deformities. It was found that 88% were wearing shoes smaller than their feet (average 1.2 cm smaller); 28% of the subjects stated that their shoes were not comfortable. Hallux valgus was the most common deformity noted and occurred in 54% of all women in that study. Frey (1995) continued to evaluate how forefoot and heel width vary with foot length using the same method in 255 healthy women. It was found that forefoot width increased slightly with foot length, but heel width did not significantly increase.

Dimensional differences between foot and footwear, such as length and width, are always employed to qualify shoe fit. With the development of scanning techniques, two-dimensional outline difference analysis and 3D surface matching methods are available. In the 2D dimensional evaluation conducted in heel area, Goonetilleke et al. (2000) found that the dimensional error plots between the unconstrained foot and shoe could indicate the quality of fit. In the 3D shape analysis, the foot is located relative to the shoe, the dimensional differences would be visualised by indicating areas with high pressure and those that had little or no pressure.

Witana et al. (2004) qualified footwear fit by matching the two-dimensional foot outlines and last outlines. The dimensional difference plots provide the designer to determine the critical locations that might affect shoe fit. Three dimensional fitting measurement system based on a method for iterative surface matching was developed by Kos and Duhovnik (2002).

Fitting Factors

Researchers have done plenty of investigations on how to qualify proper shoe fit. A good shoe fit should be free of any high pressure areas (Quimby, 1994), but should have the right 'feel' and support at the same time. If a shoe is too tight, the pressure or force will produce undue tissue compression, making the shoe uncomfortable. If the shoe is too loose, there can be foot slippage relative to shoe resulting in damage or injury to soft tissue. In order to achieve the right fit, the desired clearance between feet and shoes should be known in addition to foot supporting at the most appropriate locations. The proposed methodology consists of four steps, which are (1) 3D scanning and orientation, (2) foot and last alignment, (3) computation of dimensional match or mismatch, and (4) the selection of lasts (Luximon et al., 2001).

However, the concept of shoe fit is largely subjective. Size alone is not the only determining factor. Research from the Battelle Memorial Institute had shown that there were at least 37 individual factors influencing or involved in shoe fit. 37 factors were subjective involving the opinions and attitudes of consumer and fitter alike. In the end, it was the customer who determined whether the shoe fitted or not. Thus the problems are multi-factored.

Jeffery and Thurstone (1955) found that the four key factors, length, flare, width and height among the total ten factors could represent the variations of 29 variables. Studies from Goonetilleke and Luximon (1999) also confirmed that shoe flare plays an important role in terms of foot posture in the shoe.

Rarely if ever are the two feet of a pair exactly the same in size, shape and proportions (Rossi, 1983). All feet stretch or expand on weight-bearing. The two feet do not stretch or expand in the same degree or proportions in their various sections. Foot has one shape at non weight-bearing rest (static fit) and another shape at full weight-bearing. Then, foot changes shapes dramatically in functional fit during walking, running and jumping. No shoe or shoe material can match these changes perfectly. Therefore, Rossi claimed that "perfect shoe fit" was impossible. A perfect fit is not possible even in custom-made shoes because the foot keeps changing.

2.2.3 Shoe Comfort Evaluation

Footwear comfort is complex and multifaceted. Dimensional differences between footwear and foot are attributed to shoe fit (Witana et al., 2004). However, footwear comfort is the result of more complex interactions of several factors that affect the foot function during human activity. Many factors such as size, shape, flexibility, style, weight, inside shoe climate (temperature and humidity), material, tread, foot-sock interface, sock-shoe interface, cushioning and physiological responses all contribute to influence footwear comfort. These factors could be divided into two aspects, which are thermal and mechanical.

Thermal Factors

Thermal comfort is defined by microclimatic characteristics of footwear, which are decisive factors for global comfort, even shortly after wearing the footwear (Kurz et al., 1992). The temperature and humidity on diverse foot and body zones were measured during experiments (Kurz et al., 1992; Kawabata et al., 1993; Purvis et al., 2004) and several laboratory tests were developed. Gonzalez et al. (2001) measured temperature and humidity inside the footwear to evaluate the thermal response over time. Schols et al. (2004) developed a method for assessing thermal comfort of shoes using a "sweating" foot which comprised semi-permeable sock, a heating and stirring system and temperature sensor. Purvis et al. (2004) examined the effects of sock type on foot skin and thermal demand using a rating of perceived exertion scale (Borg et al., 1982) and a rating of thermal perceived scale (Nielsen et al., 1989). Footwear thermal comfort should not only be assessed on physiological parameters but also on subject's perception. Thermal comfort is related to body temperature. The human temperature regulation is a mechanism which is solicited everyday when the body heat balance presents disequilibrium. So footwear thermal comfort is influenced by whole body temperature.

Mechanical Factors

Mechanical aspects were widely studied and different techniques were employed to study footwear comfort. Structural and material changes will significantly alter footwear comfort. Size, shape, style, heel height, arch height, shoe weight, flexibility, stiffness of sole and counter, tread, cushioning and sock all contribute to influence the footwear comfort. It was suggested that comfort could not be measured directly (Slater, 1985). Subjective tests based on the compilation of information by means of so-called "comfort questionnaires" were widely used in ergonomics (Shackel et al., 1969). Recently, this method was used in the study of footwear comfort (Jordan et al., 1996; Mündermann et al., 2002).

Jordan et al. (1996) used perception of comfort questionnaires to investigate perceived comfort of six regions in the plantar foot and two regions in dorsal foot. Plantar and dorsal pressures were collected by Pedar in-shoe system and Mikro-EMD system. It was found that peak pressure was significantly increased in the uncomfortable group both total plantar surface and all the regions measured than comfortable group. Maximum force was significantly increased in the uncomfortable group for the rearfoot and forefoot, but the force was lower in the midfoot region of plantar surface. Contact area was significantly larger in comfortable group in the midfoot region of plantar surface and smaller in the comfort group at dorsal surface than uncomfortable group.

Miller et al. (2000) examined the relationship between foot and leg characteristics, shoe characteristics and short-term comfort. The results implicated that skeletal alignment, shoe torsional stiffness and cushioning seemed to be mechanical variables which might be important for comfort.

Sobel et al. (2001) investigated the relatively long-term effect of customized insoles in relieving post-work foot discomfort in healthy people. The pre-wear and post-wear questionnaires were completed by 122 subjects who were required to wear it on up to five weeks for an average seven hours a day. It was found that 68% of population in this group had less foot discomfort.

Llana et al. (2002) used subjective questionnaires to assess the relationship between perceived discomfort and tennis footwear design characteristics by 146 tennis players sampled from a population of about 4000 players. Among indentified independent design factors, it was found that there was a strong correlation between plantar discomfort and incorrect arch support.

Comfort was proposed as one of the important factors for footwear in physical activities (Nigg et al., 1999). Mündermann et al. (2002) proposed visual analogue scale to determine comfort level. Four different shoe inserts were used in the study. A visual analogue continuous scale was developed, which could be used to provide a reliable measure to assess footwear comfort. Intra-test repeatability was also tested and confirmed to be reliable. In that study, differences in comfort ratings between the insert conditions could be identified and found to be significant.

Lee and Hong (2005) studied the impact of insert and HHS on kinetic changes and perceived discomfort from ten subjects. The results demonstrated that increasing heel height increased impact force, medial forefoot pressure and perceived discomfort during walking. A heel cup insert for HHS effectively reduced the heel pressure and impact force, an arch support insert reduced the medial forefoot pressure, and both improved footwear comfort. A total contact insert reduced heel and medial forefoot pressure significantly, attenuated the impact force, and offered higher perceived comfort.

It is clear that excessive pressure on human interface can lead to discomfort. The tactile sensitivity of feet was considered to be one of the factors influencing shoe comfort. Therefore, the pressure-discomfort relationship may depend on the variability of pressure tolerance with the stimulating area. A study on tactile sensitivity of feet was investigated (Dohi et al., 2002). Tactile sensitivity was quantified by the pressure sensory threshold that was measured using the Semmes-Weinstain monofilament testing method on 17 different regions. It was found that there was a significant gender difference for tactile sensitivity. The order of sensitivity, from the least sensitivity to the most sensitivity was the plantar region excluding the plantar arch, side region and dorsal region. The areas that bear high weight loads tended to be less sensitive than areas that do not bear appreciable weight.

Meanwhile, other related studies may contribute to assessments of footwear fit and comfort. Cobb et al. (2001) developed an in-shoe laser Doppler sensor to assess plantar blood flow in foot. Gao et al. (2004) evaluated slip resistant properties of footwear on ice, reported that sole roughness had positive correlation with coefficient of kinetic friction. Li et al. (2004) studied the effects of coefficient of friction with different soles on the elderly people's walking. High slip resistant properties of shoes can reduce fall rate among elderly adults, thus improve their confidence to take part in more activities. Shear stress measurement between footwear and foot is sparse due to technical difficulties (Hosein and lord, 2000). It was reported that the shoe sole hardness and thickness could influence balance in older men (Robbins et al., 1992). In contrast, Lord et al. (1999) found that there was no relationship between hardness of sole and balance.

Footwear comfort encompasses many characteristics and is defined with varied features. Comfort is difficult to quantify or to be directly measured. The ergonomic analysis of user-oriented products, such as footwear, is a complex process involving several interrelated factors. The first level of the chain will group the objective variables related to the characteristics of the subjects, footwear and the features of the ground being used. The musculoskeletal system is subjected to mechanical forces as a consequence of a combination of the factors on the first level and the characteristics of a match. Consequently, subjects have constantly adapted to the movement of their body segments, which is known as the “kinematic adaptation hypothesis” (Nigg et al., 1984). The kinematic adaptation, which can be measured objectively, is the second level in the chain. Directly related to the adaptation, subjects experience discomfort and fatigue, both physically and mentally. If the mechanical demands are too great, an injury may be sustained. This is the third level of the chain. Therefore, comfort evaluation of footwear is complex and multifaceted.

2. 3 High-heeled Gait Biomechanics

Societal and fashion customs encourage the continued use of HHS despite concerns regarding their detrimental effects on gait and lower-extremity function. Complaints of leg and back pain are common among wearers of HHS, and the development of lower limbs problems such as degenerative joint disease have been noted because of postural alignment and gait pattern alteration in high heels.

2.3.1 Gait Cycle

The walking cycle can classically be broken into 4 distinct segments, which are heel strike, foot flat, toe-off, and swing. The first three segments comprise the period of limb support, or stance phase, and account for approximately 62% of the entire gait cycle for each limb. The stance phase is further divided into a period of double-limb support and a period of single-limb support. The period of double-limb support occurs from 0 to 12% of the cycle, followed by the single-limb support, which occurs until 50% of the cycle, when the opposite leg strikes the ground and double-limb support once again begins. The second period of double-limb support continues until 62% of the cycle, when the stance leg leaves the ground, the swing phase starts.

Stance phase of gait can also be divided into four periods, which are loading response, mid-stance, terminal stance and pre-swing. Loading response begins with initial contact, the instant that the foot contacts on the ground. Loading response ends with contralateral toe off, when the opposite extremity leaves the ground. Thus, loading response corresponds to the gait cycle's first period of double limb support. Mid-stance begins with contralateral toe off and ends when the center of gravity is directed over the supporting foot. Terminal stance begins when the center of gravity is over the supporting foot and ends when the contralateral foot contacts the ground. Thus, pre-swing corresponds to the gait cycle second period of double limb support.

2.3.2 Heel Elevated Standing

Posture is a relative arrangement of the various segments of body. HHS can result in an alteration of the orientation of body segments, and may change muscle activities to counteract the gravitational force. Subjects with lower back pain may be affected by high heel usage because of the decrease of lumbar lordosis inclination. Static postural alignment analysis can reveal compensatory postural changes in HHS.

Golinick et al. (1964) measured the ankle and knee joint angles on high heels (6.4-10.2 cm) during standing and walking using electrogoniometer in 15 female subjects. Results obtained from the study showed that high heels had no definite effect on knee angles, while increase in plantarflexion of the ankle joint was expected.

Bendix et al. (1984) examined lumbar curve, pelvic inclination, truck muscle activity and position of the line of gravity in 18 female subjects standing from minus heels (2.5 cm) to heel-elevated supports (4.5 cm) conditions. In that study, with increasing heel height, the lumbar lordosis and pelvis inclination were decreased, but back and abdominal muscles activities were not altered. The line of gravity kept the distance from the forefoot constantly, and the ankle joint was shifted towards the line of gravity with added heel height.

Franklin et al. (1995) used Metrcom skeletal analysis system, a 3D electrogoniometer, to assess static postural changes in 15 female subjects at heel elevation condition (5.1 cm). They found that lumbar lordosis became flattened and anterior pelvic tilt angle decreased with heel height, that were in consistent with previous studies (Opila et al., 1988).

Shimizu and Andrew (1999) investigated the effect of elevating the heel from 0 to 40 mm at an interval of 5 mm during unilateral standing on the structure of foot, and function of foot in maintaining balance. The results showed that medial longitudinal arch was raised, rearfoot pronation was reduced and the length of displacement of the center of pressure (COP) was increased when the heel was elevated. These results implied that elevating the heel of a shoe have an advantage in reducing the signs of a flat foot. Ricci and Karpovich (1964) found that the height of longitudinal arch increased by 4 mm at the end of day when wearing high heels while decreased 3 mm wearing low heels.

Henderson et al. (2004) employed the force platform to measure the subtalar joint axis orientations and joint moments, and found that in high heels standing, small positive inverting moment was induced compared to larger everting moment in the flat shoes condition. In the high heels condition, results showed that there was a trend toward more active of electromyography (EMG) activity of low limb muscles.

Broch et al. (2004) employed an elementary theoretical model based on schematic sketches to calculate the change in distribution of mechanical stress on the plantar foot with change in foot orientation. It was found that forefoot load increases and heel load decreases with elevated heel height and corresponding changes in shoe shapes.

Static postural analysis from pervious studies demonstrated that heel-elevated stance could significantly reduce lumbar lordosis and pelvic inclination, distance of the knee and ankle from the line of gravity, plantarflex foot position and cause more activity of lower limb muscles. The reduction in the normal lordosis of the spine may cause abnormal stresses on muscles, ligaments and lumbar spine, which may predispose or precipitate lower back pain.

2.3.3 Gait Pattern

Early studies concerning gait pattern in HHS generally used semi-absorbent paper to record gait pattern factors. According to the study by Adrian and Karpovich (1966) concerning with gait pattern, it was found that wearing high heels caused a significant decrease in step length, out-toeing and total range of movement at the talocalcaneal joint, and half of the subjects showed instability during walking. Merrifield (1971) found minimum changes in the stride width and foot angle using a similar method.

With the advance of motion analysis systems based on video cameras and force platform, numerous researchers have investigated the kinematics and kinetics of high-heeled gait (Opila-Correia, 1990 a, 1990b; Ebbeling et al., 1994; Wang et al., 2001; Esenyel et al., 2003 and Stefanyshyn et al., 2000).

Ground Reaction Force (GRF)

Previous studies found inconsistent results concerning GRF. As the center of mass is moved forward, an increased vertical GRF was applied to forefoot during stance phase (Snow and Williams, 1994). Analysis of high-heeled gait revealed that vertical GRF and maximum A-P braking force during low limb loading increased significantly as a function of heel height (Ebbeling et al., 1994; Snow and Williams, 1994), while the accumulated impulse of vertical impact force did not significantly increase (Wang et al., 2001). In contrast, Stefanyshyn et al. (2000) found that the highest high heels among four heel height conditions had the lowest value of the maximal vertical impact force. Esenyel et al. (2003) found that there was no statistically significant increase of GRF during limb stance with HHS. High heels resulted in higher GRF in both the anterior and posterior directions. The increased A-P forces corresponded to the increases in the peak deceleration and acceleration forces in the vertical direction (Stefanyshyn et al., 2000). Time at GRF of the second peak vertical, peaks of A-P were significantly affected by heel height. Time at the second peak vertical GRF occurred later in support in high heels. Time to the first peak A-P GRF occurred earlier in the high heels while at the second peak A-P GRF decreased from the low to high condition.

Plantar Pressure Distribution

Ground reaction forces are transmitted through shoe to foot and can be modulated by the composition of materials that make up the sole, the shape of insole and fitting of shoe to foot. In-shoe pressure measurement systems are widely used to evaluate the shoe-foot interface. Plantar pressure distribution changes caused by HHS have been well documented by the in-shoe pressure measurement systems (Mandato and Nester, 1999; Speksnijder et al., 2005; Nyska et al., 1996). In the condition of wearing HHS, pressure under the forefoot was found to increase significantly; peak pressures increase by 30%-40% in the center of the forefoot (2^{nd} -4^{th} metatarsals) and shifted from the heel region towards the central and the medial forefoot especially the first metatarsal head and the hallux. Pressure-time integral of the heel, central forefoot, medial forefoot and hallux area increased by 12%, 48%, 47% and 20%, respectively, while midfoot decreased by 40%. However, among these studies, few of them controlled the factors of shoe type and shape, since the differences of shoe type and shape may influence the gait pattern and plantar pressure.

Kinematics, Kinetics and Muscle Activities of Lower Limb

The effect of wearing HHS on lower limb joint kinematic and kinetic changes proximal to the ankle as well as muscle EMG has been studied extensively. Previous investigations showed that HHS increased hip and knee flexion during stance and flattened the lumbar spine, thus the EMG of lower limb muscles was altered.

Gollnick et al. (1964) investigated the effect of high heels on the ankle and knee joint angles during standing, walking and running. The results from electrogoniometer measurements showed that the ankle angle increased 10-20 degrees in extension while the knee kept constant during walking. During running, the high heels caused an increased of 10-15 degrees in the plantarflexion and 10 degrees in the dorsiflexion of the ankle.

With the instability and balance problems associated with females wearing HHS, Joseph (1968), in comparing muscles EMG of seven subjects in low heels and high heels, found that the tibialis anterior contracted more continuously and less powerfully and the soleus contracted more powerfully while walking with HHS.

Opila-Correia (1990 a) studied the gait of 14 subjects in flat shoe and HHS. It was reported that the increased plantar flexion of the foot, associated with HHS, caused changes in the normal barefoot pronation and supination of the foot during gait. In high-heeled gait, subjects generally walked slower, had shorter stride lengths, slightly higher stance time percentages and greater knee flexion. At toe-off phase of gait, knee flexion and hip flexion were less in high-heeled gait than those in low-heeled gait. The pelvis had a slightly lower range of motion in sagittal plane in high-heeled gait comparing to its in low-heeled gait. Opila-Correia (1990 b) used the data from previous experiment to further investigate the effects of age and experience factors and found that experienced wearers had pronounced increase in knee flexion during stance phase of high-heeled gait, and exaggerated upper trunk rotation in older and inexperienced subjects groups. However, Ebbeling et al. (1994) found that there were no significant differences in any of the parameters as a function of experience in wearing high heels.

Snow and Williams (1994) investigated the high heel effects with three different heel heights on gait, and reported that the rearfoot supinated significantly at foot strike and less pronated with heel height compared to that of low heeled shoes and foot abduction angle decreased with increased heel height. In addition, the ankle joint angle throughout gait cycle increased significantly in plantarflexion with increased heel height. These findings were consistent with previous findings. However, there was no significant change on the average lumbar curvature or pelvic tilt with shoe height. Knee flexion angle was reduced as heel height increased, which may be due to subject variety and the differences in the study design. That reflected the complexity of human movement to investigate the impact of HHS since it may be affected by many variables.

Esenyel et al. (2003) compared flat sports shoe with high-heeled shoe (6 cm heel height), and found that the use of HHS reduced the self-selected walking speed by 6%. The plantarflexed posture of foot in HHS was associated with a significant reduction in the ankle plantar flexor muscle moment in late stance. Thus plantar flexor muscle walking with HHS was reduced by 29% during late stance. The knee muscular moments were similar throughout the stance phase under these two conditions, except for a larger extensor moment for a longer duration during limb loading when wearing HHS.

The use of a higher heel increased lever arm of the floor-to-knee distance, thereby increased the tibial lever arm through the knee. As a compensatory mechanism, a larger extensor muscle moment was needed to resist this reactive trend to flex at the knee. This finding was similar to that reported by Kerrigan et al. (1998).

Ebbeling et al. (1994) studied the energy cost and the lower extremity mechanics with 15 subjects, and found that the heart rate and oxygen consumption increased with heel height. The foot was placed in a more plantar-flexed position while the ankle was less dorsiflexed as the heel height increased. The calcaneal eversion increased, suggesting larger shock absorption. Maximum knee flexion increased as a function of increased heel height throughout the initial shock-absorbing period of support, which was consistent with previous findings (Opila-Correia, 1990 b).

Stefanyshyn et al. (2000) studied gait patterns in 13 experienced female subjects using four different heel heights. An increase in knee flexion during stance and ankle plantarflexion while wearing high heels was found. Soleus and rectus femoris activity showed increase response as heel height increased, while no difference was found in dorsiflexor moment and activities of gastrocnemius or tibialis anterior muscles.

Gefen et al. (2002) employed contact pressure display platform and surface EMG data to determine the effect of muscular fatigue induced by high-heeled gait. EMG measurements from eight habitual HHS wearers revealed an imbalance of gastrocnemius lateralis versus gastrocnemius medialis activity in fatigue conditions, which correlated with abnormal lateral shifts in the foot-ground COP. The activity of peroneus longus was increased, suggesting an increase command in stabilizing the ankle joint when wearing HHS.

Knee OA

In wearing HHS, increased knee flexion during stance phase occurred as a postural adaptation to plantarflexed foot position and as a potential compensatory mechanism for absorbing impact loads. Such mechanisms have also been suspected as a potential source of knee pain and degeneration. Kerrigan et al. (1998) used the video-based motion analysis system and force platform to calculate knee joint torques and knee joint motion in 20 healthy women. Barefoot and low-heeled shoes served as controls to HHS (> 5 cm). It was found that force across the patellofemoral joint was increased and compressive force on the medial compartment of the joint was increased by 23%. In their further research (Kerrigan et al., 2005), it was found that shoes with moderately heel height (3.8 cm) might also significantly increase knee torques.

In conclusion, many researchers have investigated high-heeled gait biomechanics from static measurement on standing posture and kinematics and kinetics during walking. As the foot was placed at plantarflexed position, the center of mass moved forward, and an increased vertical GRF and contact pressure were applied to forefoot during stance phase. Increased knee flexion during stance phase due to postural adaptation to the foot position was considered as a potential source of development of knee osteoarthritis. Imbalanced muscle activities may contribute to fatigue of lower limb. Age and experience were suggested to influence high-heeled gait. Among these studies, few controlled the style and shape of different heel heights of the shoes which may contribute to the discrepancy of some findings. In addition, few studies investigated the subjective comments on wearing shoes with different heel heights, despite the possibility that the subjective comments may provide insights into the effects of heel height. Meanwhile, internal stress/strain of soft tissue and bony structure during high-heeled gait remain unaddressed due to the difficulty of experimental approaches.

2.4 Review on FEA of Foot and Footwear Research

Finite element methods have been used in engineering for decades, and they have been applied to a variety of biomechanical research fields. Technological advances have made it feasible to simulate different conditions in a computer, and provide an invaluable tool for predicting how musculoskeletal responses to particular loads.

Developing anatomical realistic models of musculoskeletal systems will improve the ability to properly characterize and well quantify experimental observations. It could dramatically reduce the need for experimentation. Both experimentation and modelling are vital in all fields of scientific and industrial endeavours. Applications of FE techniques to the modelling of musculoskeletal systems have provided unique insights that would have not been possible experimentally. Finite element analysis (FEA) may be the most effective, combined with experiments.

2.4.1 Introduction to the FEA

FEA is a computer simulation using numerical technique for obtaining approximate solutions to a wide variety of engineering problems, and is already being applied to many biomechanical research fields. Problems were solved by deriving differential equations relating to the problems.

General Procedure of FEA

FEA includes three major steps, which are pre-processing, analysis and post-processing. In pre-processing, the model of physical problem, including geometrical structures, material properties, loading and boundary conditions are defined. Due to the potential complexity of a problem, the geometrical model is created in the CAD system. Afterwards, analysis is normally run on commercial package such as ABAQUS (Hibbitt, Karlsson and Sorensen Inc, Pawtucket, RI, USA) which solves the problem numerically. This analysis may take days to run depending on the complexity of the problem and the power of computer used. Once a simulation is completed, the variables calculated i.e. the displacement, stress etc. can be viewed by the visualization tools. The assumptions made in the model geometry, material behavior, boundary and loading conditions determine the accuracy between the numerical simulation and the physical problem. Therefore, it is important to take model validation by comparison of the predictions with experimental results as seriously as the development of the model itself.

Sources of Nonlinearity

For structural analysis, there are four sources of nonlinear behavior. The corresponding nonlinear effects are identified by the terms of material, geometry, load conditions and displacement conditions. Relationships between body force and stress (the equilibrium equations) and between strain and displacement (the kinematic equations) are closely linked in a "duality" sense, so the term geometric nonlinearity applies collectively to both sets of relations.

Geometric nonlinearity is the change in geometry as the structure deforms which is taken into account in setting up the strain displacement and equilibrium equations. Material nonlinearity depends on current deformation state and possibly past history of the deformation. Other constitutive variables such as pre-stress, temperature, time, moisture, and electromagnetic field may be involved. Force boundary conditions nonlinearity is that the applied forces depend on deformation. Displacement boundary conditions nonlinearity is that displacement depends on the deformation of the structure.

2.4.2 FEA of Footwear Research

Due to the lack of technology and invasive nature of experimental measurements, experimental studies were often restricted to study the plantar pressure distribution and gross motion of foot, while the evaluation of internal joint movements and load distributions are usually unaddressed. As an alternative, researchers proposed modelling approaches. Computer simulations, such as FEM is the efficiently versatile and appropriate tool and have the potential to provide more biomechanical information of footwear effect, due to its capability of modelling structures with irregular geometry and complex material properties, and the ease of simulating complicated boundary and loading conditions. In terms of footwear designs, the FEM allows prediction of plantar pressure, joint movement as well as contact stress and internal stress/strain of foot under varied loading and supporting conditions. These models can isolate the variable of interest, which is not always possible during experiment.

A number of 2D and 3D FE models have been developed to investigate foot biomechanics (Table 2-1). In recent studies, a few studies explored footwear design (Lemmon et al., 1997; Chen et al., 2003; Verdejo R et al., 2005; Cheung and Zhang, 2008). The earlier models available for stress/strain analyses were either 2D (Nakamura et al., 1981; Lewis, 2003; Lemmon et al., 1997; Erdemir et al., 2005; Verdejo and Mills, 2004; Goske et al., 2005; Spears et al., 2007) or simplified 3D with partial foot skeleton or connected bony structure (Chu et al., 1995; Chen et al., 2003). Recently, more accurate 3D FE models were developed (Gefen et al., 2000; Cheung and Zhang, 2005). It has been shown that FE modelling, if conducted properly, could potentially make significant contributions to the understanding of foot biomechanics and improvement of footwear designs. Successful FE analyses (Chu et al., 1995; Chen et al., 2003; Cheung et al., 2005) have been carried out on insoles and ankle-foot orthosis.

Table 2-1. Configurations and applications of finite element footwear models in the literature

Years	Author(s)	Analysis Type	Geometries	Material Properties	Parameters of Interest	Experimental Validation	FE Software
1981	Nakamura et al.	2D, static, nonlinear	Engineering sketch	Unified foot bones (linearly elastic), plantar soft tissue (nonlinearly elastic), shoe sole (linearly & nonlinearly elastic)	Shoe sole stiffness on stress (principal & shear) in plantar soft tissue	Not mentioned	Custom-written
1995	Chu et al.	3D, static, linear	Engineering sketch	Unified ankle-foot bones, ligaments, soft tissue, AFO (linearly elastic)	Drop foot, stiffness of orthosis & soft tissue on stress distribution in ankle-foot orthosis	Not mentioned	ADINA
1997 1998 2005	Lemmon et al. Shorten Erdemir et al.	2D, static, nonlinear	Video image of specimen	Metatarsal bone, sole plate, thread & stud (linearly elastic), encapsulated tissue, insole, midsole, surface (hyperelastic & nonlinearly elastic)	6 insole thicknesses, 2 tissue thicknesses, 36 plug designs of midsole, soccer shoe stud length & penetration, sole plate stiffness on plantar tissue stress & peak plantar pressure	Peak plantar pressure & plantar pressure distribution	ABAQUS & COSMOS
1997	Shiang	3D, static, nonlinear	Engineering sketch	Insole (linearly elastic),midsole (nonlinearly elastic)	Different cushioning configurations of insole & midsole on plantar pressure relief	Peak plantar pressure	ANSYS & ABAQUS
2000	Syngellakis et al.	3D, static, nonlinear	Engineering sketch	Ankle-foot orthosis (nonlinearly elastic)	Thickness on stiffness characteristics of plastic ankle- foot orthosis	Ankle moment	ANSYS
2003	Chen et al.	3D, static, nonlinear	CT images of subject	Ankle-foot bones, cartilages, ligaments, encapsulated tissue (linearly elastic/hyperelastic), Insole, midsole (hyperform)	Flat & total-contact insoles with different material combinations on plantar pressure distribution	Plantar pressure distribution	MSC. MARC
2003	Lewis	2D, static, linear	Engineering sketch	Unified shoe surface, insole, midsole, rocker outsole (linearly elastic)	Material of midsole & outsole on von Mises stress & displacement of shoe	Not mentioned	ALGOR

Cont' Table 2-1

Years	Author(s)	Analysis Type	Geometries	Materials Properties	Parameters of Interest	Experimental Validation	FE Software
2003	Gefen	2D, static, nonlinear	MR image of subject	Bone (rigid), heel pad (hyperelastic)	plantar soft tissue stiffening	Plantar pressure	ANSYS
2004	Verdejo & Mills	2D, static, nonlinear	Engineering sketch	Heel bone (linearly elastic), heel pad, midsole (hyperform)	Compressive stress distribution in heel pad with & without midsole support	Plantar pressure	ABAQUS
2005 2008 2008	Cheung & Zhang Cheung & Zhang Yu et al.	3D, static, nonlinear	MR images of male & female subjects	Foot bones, cartilages, ligaments, high heeled support (linearly elastic), encapsulated tissue, shoe sole (linearly elastic & hyperelastic & hyperform)	Flat & custom-molded foot orthosis with different combination of material stiffness, arch height & thickness, 2-inch high heeled support on plantar pressure & bone stress	Plantar pressure, plantar contact area, arch deformation	ABAQUS
2007	Budhabhatti et al.	3D, static, nonlinear	MR images of subject	First ray bone (rigid), soft tissue (hyperelastic), Insole (hyperfoam)	5 different insole properties on plantar pressure distribution	Plantar pressure & vertical GRF	ABAQUS
2007	Spears et al.	2D, static, nonlinear	MR images of subject	Heel bone (rigid), heel counter (rigid & linearly elastic), skin, heel fat pad tissue, sole (hyperelastic & hyperform)	Heel counter on tissue stress (shear, compressive and tensile) distribution in skin & fat pad of heel	Vertical strains & plantar pressure distribution	MSC. MARC
2008	Antunes et al.	3D, static, nonlinear	CT images of subject	Bone, cartilage, plantar fascia (linearly elastic), soft tissue, insole (hyperelastic)	3 different materials, 3 thickness of insole on plantar pressure distribution	Not mentioned	ABAQUS & Custom-written
2008	Hsu et al.	3D, static, nonlinear	CT images of subject	Bones, cartilages, ligaments, fascia, insole, encapsulated soft tissue (linearly elastic)	Conformity of insole contour on plantar pressure reduction	Plantar pressure	ANSYS

2D FE Model

In the early 80’s, Nakamura et al. (1981) built a 2D FE foot model, which was considered to be the first known FEA for footwear design. The FE model contained a unified bony structure of foot, plantar soft tissue and a shoe sole. A sensitivity analysis on shoe sole material with twenty different Young’s modulus (0.08-1000 MPa) was conducted. The results demonstrated that compressive and shear stress of plantar soft tissue significantly depended upon the Young’s modulus of shoe sole, suggesting optimal range from 0.1 to 1 MPa for minimization of plantar stress.

Another 2D FE model based on sagittal section through the second metatarsal bone with soft tissue was developed by Lemmon et al. (1997). The model was used to estimate the effects of thickness of insole on plantar pressure reduction at metatarsal head regions. Hyperelastic material model and hyperfoam material model were assigned to plantar soft tissue and insole respectively. The FE predicted results revealed that the incremental reduction in peak plantar pressure decreased as insole thickness increased. Using the similar 2D FE model developed by Lemmon et al. (1997), Erdemir et al. (2005) studied the effects of 36 plug designs of a midsole including a combination of three materials, six geometries, and two locations of placement. It was found that plugs were placed according to the pressure measurement were more effective in plantar pressure reduction than those positioned based on the bony prominences.

Lewis (2003) developed a 2D FE model of highly simplified foot with a two-layered rocker sole. A sensitivity study was performed to investigate the sole material effect on foot, showing that materials choice affected the model response in a noticeable manner. Using high-density polyethylene (HDPE) rather than polyurethane (PU) in the top layer could increase stress up to 62% at interface of foot and insole in the design of therapeutic shoe.

Several studies focused on footwear effects on the plantar heel pad response (Verdejo and Mills, 2004; Goske et al., 2005; Spears et al., 2007). Verdejo and Mills (2004) used geometrically simplified calcaneus bone and heel pad to study stress distribution in the heel pad and running shoe midsole using ethylvinyl acetate (EVA) material. It was found that in the foot/shoe simulation, while force was less than 200N, the majority of deformation was in the lower surface of heel pad. While under higher force, the deformed heel pad did not decrease much in thickness and midsole upper surface became increasingly concave.

Goske et al. (2005) developed 2D FE model of the heel region from magnetic resonance (MR) images, incorporated with heel counter and sole to study the effects of combinations of three insole conformity levels (flat, half-conforming, full-conforming), three insole thickness values (6.3, 9.5 and 12.7 mm) and three insole materials (Poron Cushioning, Microcel Puff Lite and Microcel Puff) during heel strike. It was found that conformity of the insole was the most influential design parameter, whereas peak pressures were relatively insensitive to insole material selection. 24% decrease in pressure compared to barefoot conditions when using flat insoles and the reduction increased up to 44% for full conforming insoles were predicted.

Based on non-weight-bearing MRI data, Spears et al. (2007) created 2D FE model of heel fat pad, skin and sole to simulate heel counter effect on plantar soft tissue during static standing in confined and unconfined conditions. The FE model predicted that the effect of the counter on peak stress was to increase compression (0-50%), reduce tension (22-34%) and shear (22-38%) in the skin while reducing both compressive (20-40%) and shear stress (58-80%) in the fat pad, indicating a well-fitted counter could reduce heel pad stress effectively.

3D FE Model

Several 3D FE models, either based on partial, simplified or geometrically detailed foot structures were reported. A linearly elastic model with simplified geometrical structures of the foot and ankle was developed by Chu et al. (1995). FE predictions found that during toe off, the peak compressive stress and tensile stress occurred in the heel region and neck region of the ankle-foot orthosis (AFO) respectively. Parametric analyses found that the model was sensitive to the elastic modulus of the AFO and soft tissue, whereas relatively insensitive to the ligament stiffness.

Shiang (1997) built a 3D FE model of shoe soles at rearfoot section, including midsole, insole board and insole combinations. The results based on comparison between linear and nonlinear analysis revealed that nonlinear stress strain curve and compressibility offered by the nonlinear hyperfoam approach could correctly describe the shoe material when deformations of footwear were relatively large.

Syngellakis et al. (2000) developed a 3D ankle foot orthosis (AFO) model with large deformation and nonlinear materials. The results revealed that the thickness of AFO did not significantly influence the peak stress of AFO, whereas thickness distribution of AFO based on rational analysis could help to design lighter AFO.

A 3D FE model of the foot and ankle using CT images of 2 mm interval, together with two total contact insoles was developed by Chen et al. (2003). That model was used to estimate the effects of total contact insole on plantar foot stress redistribution. Foot bones and major plantar ligament were created, and the nonlinear material property of insole and frictional interface contact behavior were considered in that model. It was found that the peak and average normal stress decreased in the most regions except the midfoot and hallux regions by wearing total contact insole compared with that of the use of a flat insole.

Linear and nonlinear analyses were conducted by Barani et al. (2005) using a 3D FE model of insole with four different materials during mid-stance phase. The results revealed that most of the materials especially Silicon Gel were effective in plantar stress reduction.

Wang and Lu (2006) developed highly simplified foot model to investigate stress in the second metatarsal with flat shoes and HHS. It was found that the bending of metatarsal due to flat shoes may increase the chance of fracture while compressive stress was predicted at HHS condition.

Dai et al. (2006) developed a 3D FE model for simulating the foot – sock – insole contact interaction to investigate the biomechanical effects of wearing socks with different combinations of frictional properties on the plantar foot contact. Wearing sock with low coefficient of friction against the foot skin was predicted to be more effective in reducing plantar shear force on the skin than the sock with lower friction explicit against the insole.

Cheung and Zhang (2005; 2008) developed a 3D male anatomical based ankle-foot model which consisted of 28 distinct bony segments, 72 ligaments, plantar fascia, and a bulk soft tissue boundary. They reported the first 3D FE simulation considered anatomically detailed ankle-foot structures, relative joint movements, and foot-ground contact as well as nonlinear material properties. That model was used to evaluate the effect of different custom orthotic designs on plantar pressure distribution. Taguchi method was employed to identify the sensitivity of five design factors (arch type, insole and midsole thickness, insole and midsole stiffness) of foot orthosis on reducing peak plantar pressure. It was found that the custom-molded shape was the most important design factor in reducing peak plantar pressure. With the use of an arch-conforming foot orthosis, the insole stiffness was found to be the second most important factor for peak pressure relief.

2.4.3 Summary

For human musculoskeletal joint modelling, the challenge remains to produce geometrically, kinematically and mechanically accurate models that can then be used in fundamental investigation, as well as injury simulation and prediction (Penrose et al., 2002).

The FE model may help to decide footwear design parameters such as material, heel height and sole shape. The development of comprehensive computational models of human foot was suggested to be one of the most important directions for future research in podiatric biomechanics (Kirby et al., 2001). Reviewing the FE models related to foot-footwear developed so far in literature, modelling accuracy of foot-footwear could be improved in the following ways.

1) Limited FEA is available for interaction of assembly footwear and foot under different loading conditions due to FEA simulation complication. Comprehensive 3D foot-footwear model could offer unique insight to footwear design by sensitivity analysis.

2) If the bones are modelled as separate components, the ligamentous connections will play an important role in realistic joint movement simulation in multiple directions. It is necessary to apply more realistic load boundary conditions, including muscle forces, for the gait simulation, because the muscle activity plays an important role in load balance.

3) FEA is a powerful tool that has been extensively used in biomechanics, but it is “easy to do poorly and very hard to do well” (Viceconti et al., 2005). Few models were carefully assigned with physiological based boundary conditions (Speirs et al., 2007) and well validated. Therefore, only validated FE model can be a platform for parametric study.

4) Several male foot models for FEA (Jacob and Patil, 1999; Gefen et al., 2000; Chen et al., 2003; Cheung et al., 2005) were developed in the literature while few FE models of a female foot have been reported. According to the morphological studies, a female foot is not merely a scaled-down version of male foot. Female foot has its own shape characteristics (Manna et al., 2001; Wunderlich and Cavanagh, 2001). A FE model, taking into account the morphological features of a female foot, is a prerequisite for studying the biomechanical behavior of a female foot and the evaluation of HHS.

The FE model may help to decide the effects of HHS design parameters such as heel height and sole stiffness. Few FE analyses are available for interaction of assembly footwear and foot under different loading conditions. Thus developing a FE model of a female foot is essential for investigation of female foot biomechanical response for design of footwear, especially for HHS. The FE analysis could allow systematic evaluation of the parametric design effects of footwear and biomechanical response of foot under different conditions due to shape and material variations, without prerequisite of fabricated footwear and trials to a series of shoes designs.

CHAPTER III METHODS

This chapter describes the methods used in this study. It is divided into two main sections. Firstly, the development of FE model of a female human foot and a high-heeled support is presented. The FE model developing procedures for obtaining the geometries, material properties, loading and boundary conditions are described. The experiments for validating model are presented. In the second section, methods for the parametrical analyses of FE foot-footwear model are presented. The biomechanical effects of heel height, coefficient of friction of foot/shoe interface and outsole stiffness on the weight-bearing foot are reported.

3.1 Development of the FE Model

3.1.1 Geometrical Reconstruction and Mesh Generation

FE Model of Foot

To develop an anatomically detailed FE foot model, coronal MR images of the right foot in a neutral, non-weightbearing condition were obtained at 1-mm interval using a 3.0-T MR scanner (Seimens, Erlangen, Germany). The MR image contained 256×256 pixels (resolution = 0.625 mm). The subject is a healthy female adult of age 28, height 165 cm and mass 54 kg. The subject signed a consent form before participating in the study. The neutral configuration of ankle joint complex followed the definition of "Standardization and Terminology Committee of the International Society of Biomechanics", which proposed a general reporting standard for joint kinematics based on the joint coordinate system (Wu et al., 2002). Foot assessment was carefully done on the subject by an experienced physician and it was found that the subject is free from lower limb disease and pain. Based on the reported normal range from 17 to 32 degrees of calcaneal inclination angle (calcaneal pitch), the calcaneal inclination angle of subject is 25 degrees, which is considered normal (DiGiovanni and Smith, 1976). A custom-made ankle-foot orthosis was used to fix the ankle in a neutral unloaded position during the MR scanning procedure (Fig. 3-1).

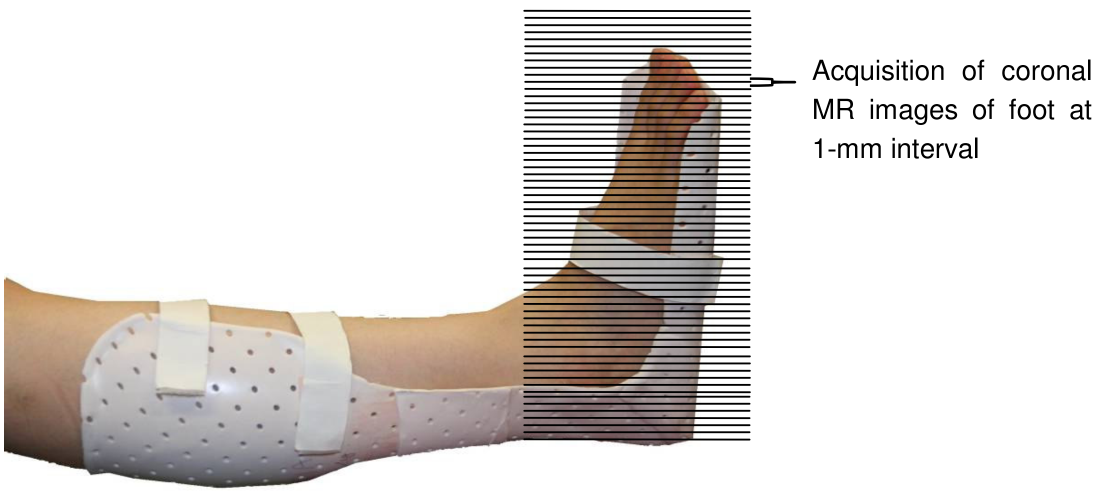

Figure 3-1. Fixing foot and ankle in a neutral foot position by custom-made ankle-foot orthosis.

The MR images were segmented using MIMICS v9.10 (Materialise, Leuven, Belgium) to obtain the boundaries of each bone and skin surface (Fig. 3-2). Afterwards a 3D surface model of bones and skin was generated from the stacked outlines (Fig. 3-3).

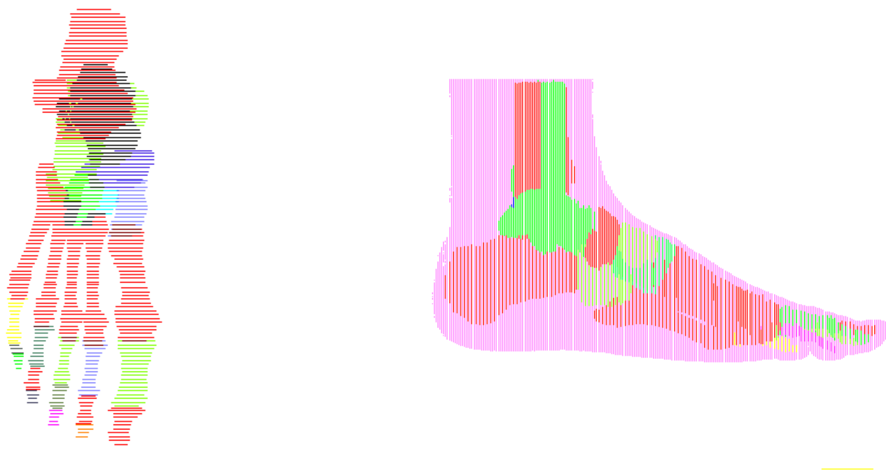

(a) (b)

Figure 3-2. Stacks of closed bounded contours of bones and skin after segmentation of MR images in (a) top and (b) lateral view of bones together with skin.

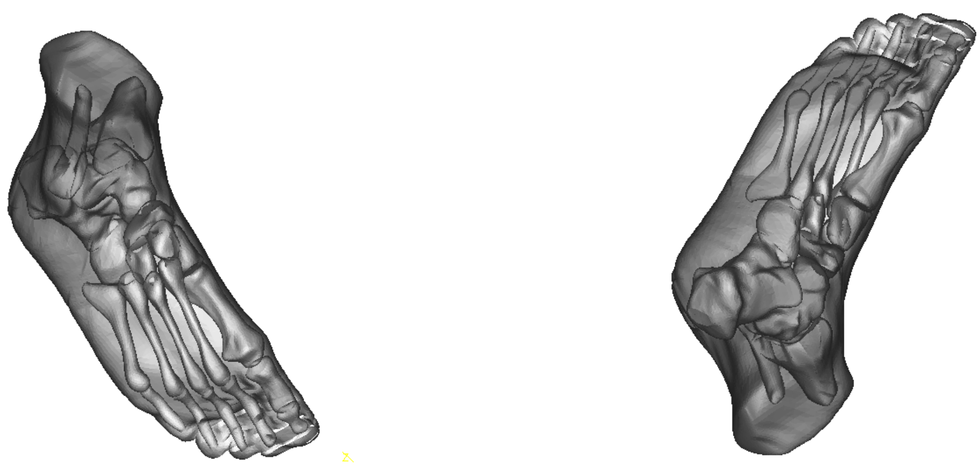

(a) (b)

Figure 3-3. 3D surface model for bony structures and encapsulated soft tissue in (a) lateral and (b) oblique view from bottom.

Only exterior geometrical contours of bones were outlined because the bones were assumed to be of one material. The sesamoids were merged with the first metatarsal. The surface model of the foot structures was imported into SolidWorks 2001 (SolidWorks Corporation, Massachusetts) to create the solid model. The encapsulated soft tissue was subtracted from the whole foot volume by the bony structures. Thereafter, the FE package, ABAQUS v6.7 was used for the creation of FE mesh and subsequent analysis.

Information on the insertion sites of ligamentous structures (Fig. 3-4) was obtained from Interactive Foot and Ankle (Primal Picture Ltd., London, UK, 1999). Except the collateral ligaments of the four lateral phalanges and other connective tissue, a total number of 78 ligaments and the plantar fascia were included and defined by connecting the corresponding attachment points on the bones (Fig. 3-5). All the ligamentous and bony structures were embedded in the bulk volume of soft tissue. The number of section defined for each individual ligamentous structure was determined by its width. For instance, the plantar fascia was geometrically simplified as five separated sections (rays) connecting the insertions between the calcaneus and the five MTP joints while only one section was defined for small ligaments. The attachment points were defined close to the geometrical centre of the attachment regions of ligamentous structures.

Figure 3-4. Insertion sites of the ligamentous structures (Interactive Foot and Ankle, 1999).

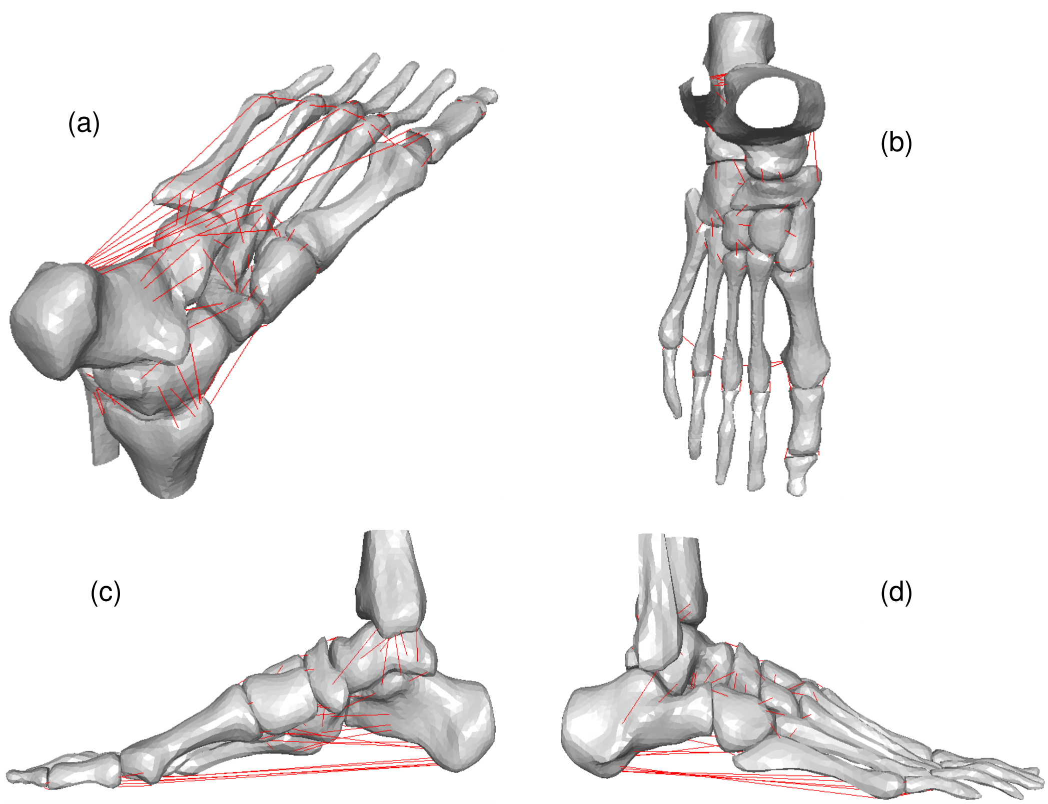

Figure 3-5. The attachment points of the plantar fascia and all major ligaments of the FE model in (a) oblique from bottom, (b) top, (c) medial and (d) lateral view.

The developed FE model consisted of 28 distinct bony segments, including the distal tibia, distal fibula, talus, calcaneus, cuboid, navicular, three cuneiforms, five metatarsals and five phalanges embedded in a volume of encapsulated foot soft tissue (Fig. 3-6). To simplify the model, the four lateral PIP joints were fused using 2-mm thick soft solid elements (Fig. 3-7), which could allow bending and deformations at PIP joints.

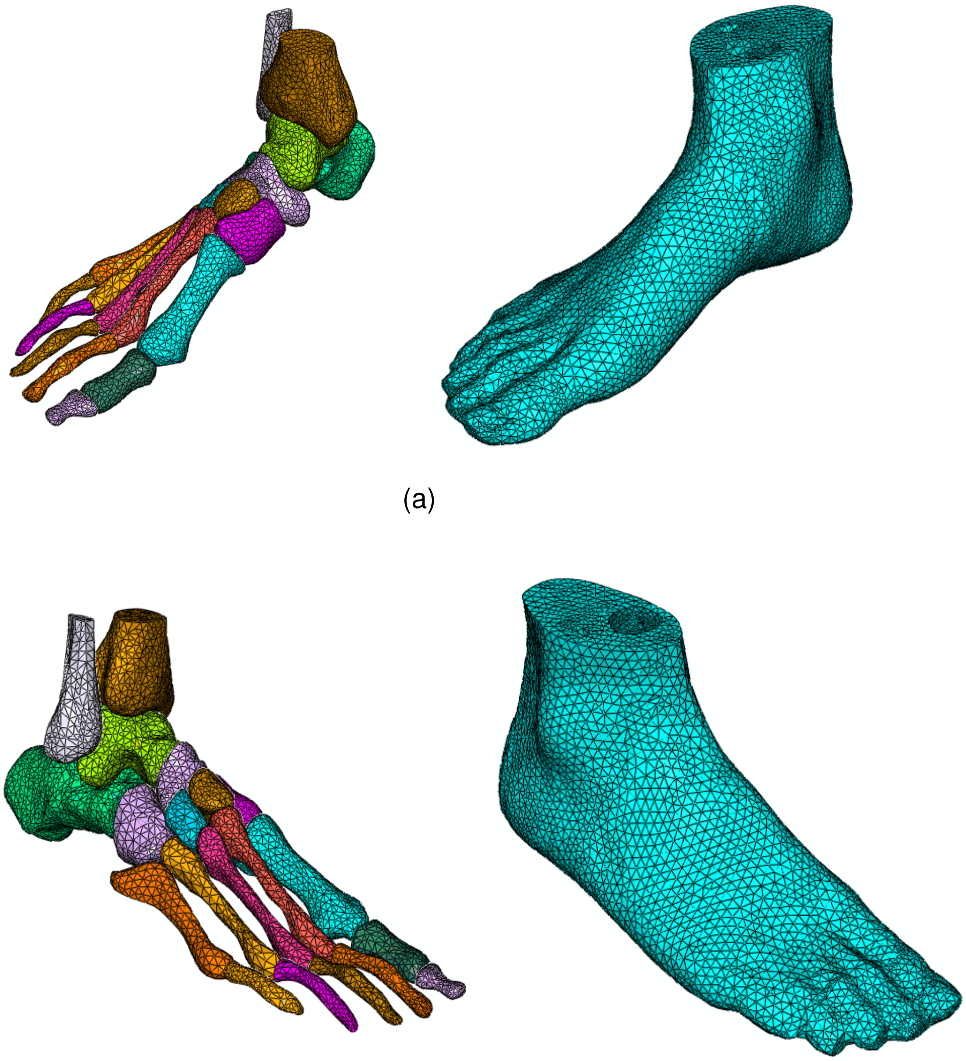

(a)

(b)

Figure 3-6. The FE meshes of the encapsulated soft tissue and foot bones in (a) lateral and (b) medial view.

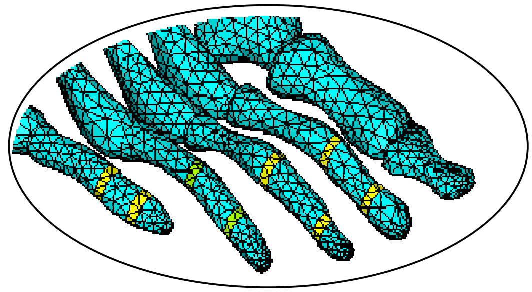

Figure 3-7. The FE meshes of four lateral fused PIP joints.

The plantar fascia and foot ligaments, excluding those ligaments at fused PIP joints were modelled as tension-only truss elements, connecting their corresponding attachment points on the bony surfaces. The tension-only truss element was used to reflect the tensile-resistive but non-compression resistive mechanical characteristics of ligaments.

Information on the insertion sites of extrinsic muscles (Fig. 3-8) was obtained from 3D anatomical model and its corresponding description (Interactive Foot and Ankle, 1999). Nine major extrinsic muscle groups related to controlling foot movement were defined, which included the tricep surae (Achilles tendon), extensor hallucis longus (EHL), extensor digitorum longus (EDL), flexor hallucis longus (FHL), flexor digitorum longus (FDL), tibialis posterior (TP), tibialis anterior (TA), peroneus brevis (PB), peroneus longus (PL). Musculotendon forces were applied at their corresponding sites of insertion by defining contraction forces via axial connector elements (Fig. 3-9).

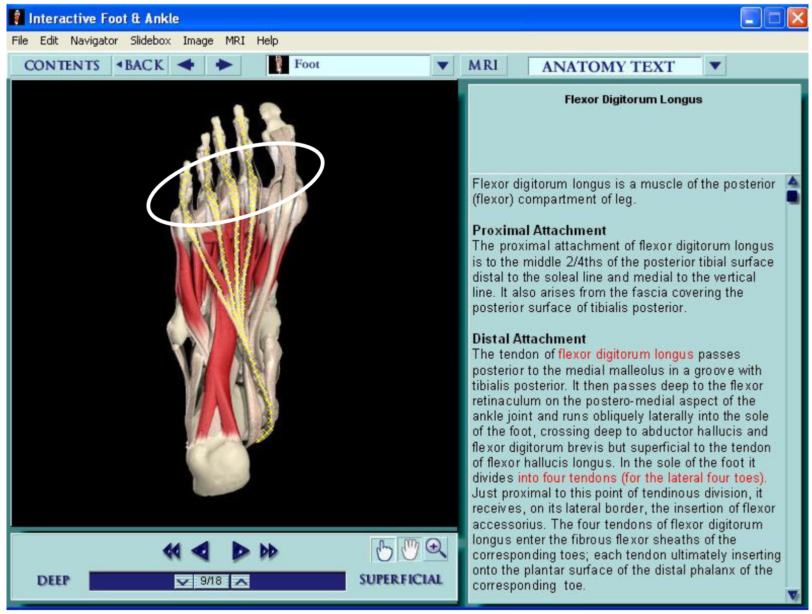

Figure 3-8. Insertion sites of the extrinsic muscles (Interactive Foot and Ankle, 1999).

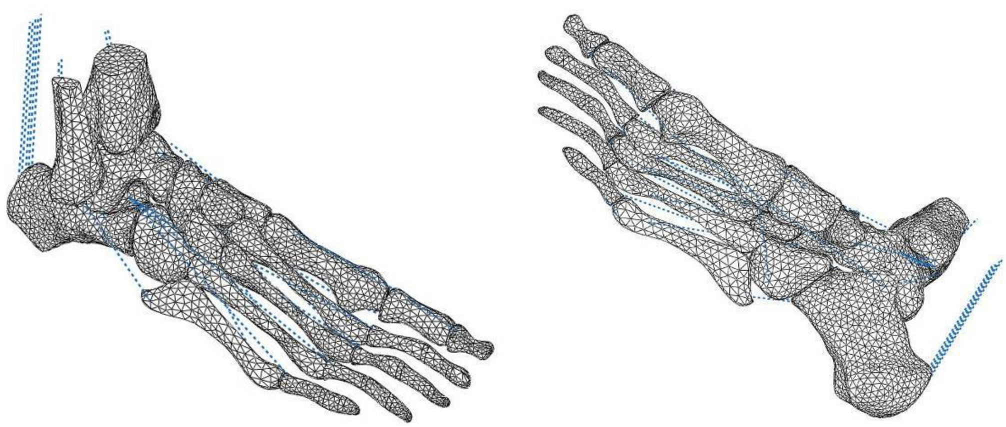

(a) (b)

Figure 3-9. The FE meshes of the encapsulated soft tissue and bones in (a) lateral and (b) oblique view from bottom.

To simulate the surface interactions among joint contact pairs, automated surface-to-surface contact algorithm in ABAQUS was used. Because of the lubricating nature of articulating surfaces, the contact behavior between the contacting bony segments was idealized as frictionless. The overall joint stiffness was governed by the related ligaments and encapsulated soft tissue. Contact stiffness in normal direction was prescribed between each joint contact pair to simulate the loading response of covering layers of articular cartilage (Athanasiou et al., 1998).

The same contact modeling algorithm was used to simulate the contact between the foot and supporting interface. During the contact phase, sliding was invoked when the shear stress exceeded the critical shear stress value ($\tau > \tau_{crit} = \mu p$, where p is the value of normal stress). During the sliding phase, should the shear stress reduce and lower than the critical shear stress value, sliding stops. The surface interaction between the plantar foot and external foot supporting surface was assigned with a coefficient of friction of 0.6 (Zhang and Mak, 1999). The surface interaction between the HHS and ground support was assigned with the coefficient of friction of 0.5 (Hanson et al., 1999).

FE Model of High-heeled Foot Supports and High-heeled Shoe

In order to investigate the biomechanical effects of heel height on foot and to isolate the influences of other design variables of HHS, heel elevated supports with different heel heights were employed. The wider and shoe-upper-free heel elevated supports allow efficient configuration of the testing equipment and measurements of foot deformations and plantar pressure distributions. Customized shoe design software (ShoeCAD, Excel-Last, Hong Kong) was used to develop solid models of high-heeled supports according to the American last design (Adrian, 1991). The shoe size was chosen according to the subject's foot size (Continental size 38) who underwent the MR scanning. The top surfaces of the foot supports were taken from the extended 2D profiles of three standard commercial lady shoe lasts. Therefore, the top foot supports shared the same shank curve with the high-heeled shoe used in the FE simulation and gait analysis experiments. Because of the high rigidity of Pedilen® foam 300 cellular solid material, the box liked shape of high-heeled foot supports were simplified as 10 mm rigid plates. The typical plantar and shank profiles with 1-inch, 2-inch and 3-inch supports were used to simulate high-heeled conditions (Fig. 3-10). The elevated angle at toe spring of 1-inch, 2-inch and 3-inch is 3.4 degrees, 2.1 degrees and 2.0 degrees, respectively.

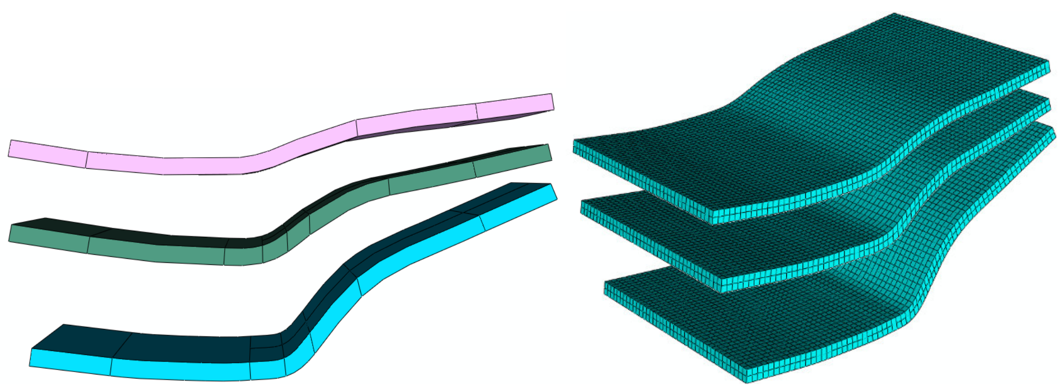

(a) (b)

Figure 3-10. High-heeled foot supports of 1-inch, 2-inch and 3-inch; (a) CAD model and (b) mesh model.

The 2-inch HHS was employed in this study to investigate the effect of HHS design parameters on the foot since 2-inch HHS is commonly worn in nowadays society. The predicted tissue deformation and stress with simulation of 2-inch heel elevation was well within physiological and computational limits of the current FE model. The HHS model consisted of a 4-mm thick outsole, 2-inch heel, 2-mm thick shankpiece and 5-mm thick toplift, which was the hard base of the heel, as shown in figure 3-11. The shankpiece started from the central heel region to the forefoot region with 15 mm in width and 2 mm in thickness. In this study, the shoe upper of the HHS was not modelled. The solid model of high-heeled foot supports and high-heeled shoe were then imported into ABAQUS for the creation of FE mesh and subsequent analysis.

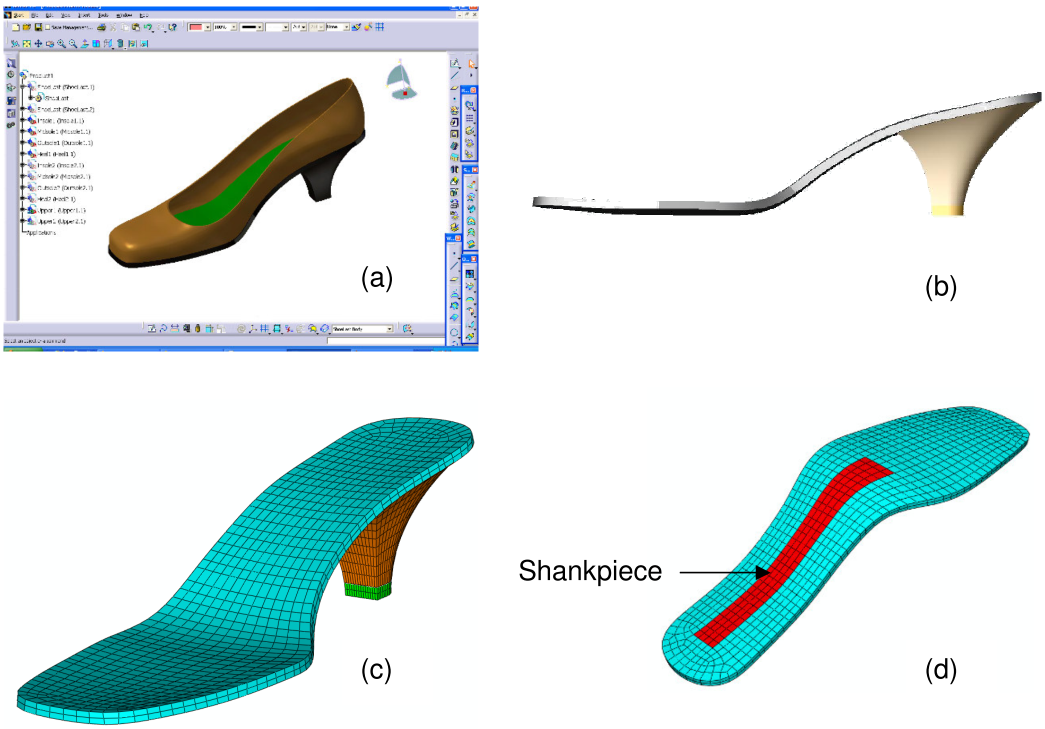

Figure 3-11. 2-inch high-heeled shoe model: (a) designed in ShoeCAD software, (b) CAD model, (c) mesh model and (d) shankpiece embedded in the outsole.

Mesh Element Selection

Numerous mesh elements in ABAQUS element library are available to model the structures, which are appropriate for many different types of analyses. The continuum (solid) element library includes first-order (linear) interpolation elements and quadratic (second-order) interpolation elements. Proper selected second-order elements could usually provide higher accuracy than first-order elements for problems that do not involve complex contact conditions. However, due to the complex joint contact conditions in foot structures, only linear interpolation elements were used.

Among the 3D continuum elements, hexahedral elements usually provide a solution of equivalent accuracy at less computational cost. It is convenient to mesh a complex shape with geometrically versatile tetrahedral elements, for which there are efficient automatic meshing algorithms. No suitable automatic-meshing algorithm is available in ABAQUS to produce hexahedral elements for those irregularly shaped structures. Thus 4-noded tetrahedral elements were chosen for meshing foot bones and encapsulated soft tissue while 8-noded hexahedral elements were used for meshing the high-heeled foot supports and shoe.

Several types of elements were considered to model the ligament in previous studies, such as truss, bar, beam, and shell elements. Because of the large number of ligaments in foot structures and performance of truss element, one-dimensional (1D) truss elements were chosen to model the ligaments. Truss elements are used to model slender, line-like structures that support loading only along the axis or the center line of the element, so no moment or force perpendicular to the center line could be supported by truss element. Truss element allowed load transfer to bones at single or multiple points. This approach has proved useful for predicting joint kinematics under the application of external loads. ABAQUS provides a 2-node straight truss element, which uses linear interpolation of position and displacement and produces constant stress. The length of ligaments was defined by connecting two nodes of truss element. A total number of 109 tension-only truss elements were used to model the ligaments and the plantar fascia of the FE foot model. Connector elements in ABAQUS package provide an easy and versatile way to model many other types of physical mechanisms whose geometry is discrete, yet the kinematic and kinetic relationships describing the connection are complex. Axial connector elements were used to apply extrinsic muscle forces at the insertion sites. In order to better simulate the band of fibrous connective tissue, five connector equivalent forces were used to represent Achilles tendon force at the posterior calcaneus. A total of 28 connector elements were defined to represent the 9 musculotendon forces of the FE foot model.

3.1.2 Material Properties Assignments

In order to reduce the complexity of the FE model, except the bulk soft tissue, the foot bones, cartilages and ligaments were idealized as homogenous, isotropic and linearly elastic (Table 3-1). The Young's modulus (E) and the Poisson's ratio (ν) determine the linearly elastic properties. Since the shear modulus (G) can be calculated by the formulation $G = E / 2(1 + \nu)$, only two distinct constants are needed to be defined.

The Young's modulus and Poisson's ratio of the bony structures were defined as 7300 MPa and 0.3, respectively (Nakamura et al., 1981). The Young's modulus and Poisson's ratio for the bony structures were selected by weighing cortical and trabecular elasticity values in terms of their volumetric contribution (Gefen, 2002). The mechanical properties of cartilage (Athanasiou et al., 1998), plantar fascia (Wright and Rennels, 1964) and ligaments (Siegler et al., 1998) were selected from literature. The foot support was made of Pedilen® rigid foam 300 with material properties adopted from Shiina et al. (2006). High-density polyethylene is a common material for outsole. The outsole material was referred from Lewis (2003). Long thin steel shankpiece is widely used to embed within the middle of outsole to reinforce the shank of HHS. The shankpiece was assigned with material properties of steel. A flat support with its upper layer assigned with properties of rigid foam (Shiina et al., 2006) and lower layer as rigid body was used to simulate the ground support.

Table 3-1. The material properties and element types in current FE model

Component	Element Type	Young's Modulus E (MPa)	Poisson's Ratio v	Cross-sectional Area (mm^2)
Bony structures	3D-Tetrahedra	7,300	0.30	-
Bulk soft tissue	3D-Tetrahedra	Hyperelastic	-	-
Cartilage	3D-Tetrahedra	1	0.40	-
Fascia	1D- Truss	350	-	58.6
Ligaments	1D- Truss	260	-	18.4
Outsole (HDPE)	3D-Brick	1,000	0.42	-
Shankpiece	3D-Brick	200,000	0.30	-
Heel	3D-Brick	3,000	0.10	-
Heel toplift	3D-Brick	10,000	0.10	-
High-heeled supports	3D-Brick	3,000	0.10	-
Ground support	3D-Brick	3,000 upper layer; rigid lower layer	0.10	-

Bones (Nakamura et al., 1981); Cartilage (Athanasiou et al., 1998); Ligaments (Siegler et al., 1988); Plantar fascia (Wright and Rennels, 1964); Soles (Lewis, 2003); High-heeled support (Shiina et al., 2006).

The encapsulated bulk soft tissue was defined as nonlinearly elastic based on the in vivo uniaxial stress-strain data (Fig. 3-12) on heel pad (Lemmon et al., 1997).

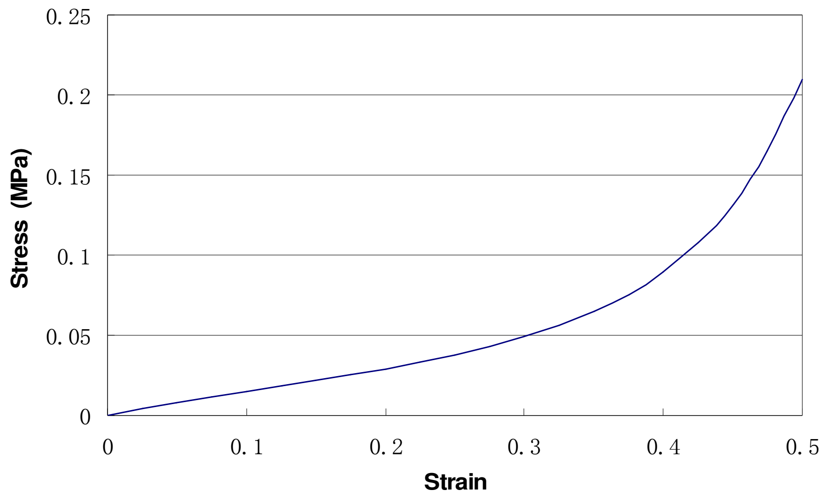

Figure 3-12. Stress-strain curve for bulk soft tissue (Lemmon et al., 1997).

Fitting of Hyperelastic Constants

The constitutive behavior of a hyperelastic material in ABAQUS is defined using a strain energy model. The hyperelastic material model is used to represent the nonlinear and almost incompressible material, especially useful in representing materials that exhibit instantaneous elastic response up to large strains (such as rubber, soft tissue). Given isotropy and additive decomposition of the deviatoric and volumetric strain energy contributions in the presence of incompressible or almost incompressible behavior, polynomial representation of the strain energy in ABAQUS could be derived. A general polynomial strain energy potential (ABAQUS, 2004) is obtained with the form

$$U=\sum_{i+j=1}^{N} C_{ij}(\bar{I}_1-3)^i(\bar{I}_2-3)^j+\sum_{i=1}^{N}\frac{1}{D_i}(J_{el}-1)^{2i} \tag{3-1}$$

The parameter U is the strain energy per unit of reference volume which can take up to six. C_{ij} and D_i are material parameters obtained from the experimental data; the elastic volume strain J_{el}, follows from the total volume strain, J, and the thermal volume strain J_{th}, with the relation

$$J_{el} = J / J_{th} \tag{3-2}$$

J_{th} follows from the linear thermal expansion, ε_{th}, with

$$J_{th} = (1+\varepsilon_{th})^3 \tag{3-3}$$

where ε_{th} follows from the temperature and isotopic thermal expansion coefficient defined in ABAQUS. $\bar{I}_1$ and $\bar{I}_2$ are the first and second deviatoric strain invariants defined as

$$\bar{I}_1 = \bar{\lambda}_1^2 + \bar{\lambda}_2^2 + \bar{\lambda}_3^2 \tag{3-4}$$

$$\bar{I}_2 = \bar{\lambda}_1^{(-2)} + \bar{\lambda}_2^{(-2)} + \bar{\lambda}_3^{(-2)} \tag{3-5}$$

with the deviatoric stretches $\bar{\lambda}_i = J_{el}^{-1/3}\lambda_i$. J_{el} and λ_i are the elastic volume ratio and the principal stretches, respectively.

By setting N =1, so that only the linear terms in the deviatoric strain energy are retained, the Mooney-Rivlin form is recovered:

$$U = C_{10}(\overline{I_1} - 3) + C_{01}(\overline{I_2} - 3) + \frac{1}{D_1}(J_{e\ell} - 1)^2 \tag{3-6}$$

The coefficients of hyperelastic material model of the first-order polynomial form were calculated in ABAQUS (Table 3-2).

Table 3-2. The coefficients of hyperelastic material model of the first-order polynomial form used for the bulk soft tissue calculated by ABAQUS

C_{10}	C_{01}	D_1
0.00398	0.01094	0.00000

By setting N =2, the decoupled second-order energy potential is as follows:

$$U = \begin{array}{l} C_{10}(\bar{I}_1-3)+C_{01}(\bar{I}_2-3)+C_{20}(\bar{I}_1-3)^2+C_{11}(\bar{I}_2-3)(\bar{I}_2-3)+C_{02}(\bar{I}_2-3)^2 \\ +\sum_{i=1}^{2}\frac{1}{D_i}(J_{el}-1)^{2i} \end{array} \qquad (3\text{-}7)$$

The coefficients of hyperelastic material model of the second-order polynomial form were calculated in ABAQUS (Table 3-3).

Table 3-3. The coefficients of hyperelastic material model of the second-order polynomial form used for the bulk soft tissue calculated by ABAQUS

C_{10}	C_{01}	C_{20}	C_{11}	C_{02}	D_1	D_2
0.08556	-0.05841	0.03900	-0.02319	0.00851	3.65273	0.00000

Stress-strain curves based on first-order and second-order polynomial forms were calculated and plotted by ABAQUS (Fig. 3-13). Second-order polynomial form gave more accurate fit to the experimental data than first-order polynomial form, especially at higher strain levels in the stress-strain curve. Therefore, second-order hyperelastic polynomial form was used to represent bulk soft tissue in current FE model.

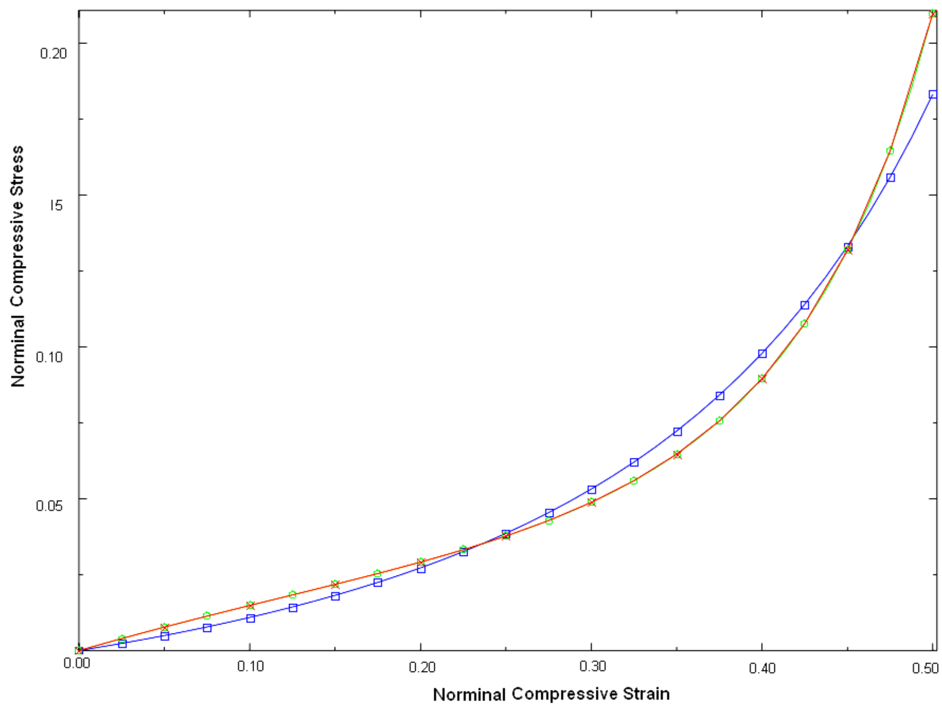

Figure 3-13. Stress-strain curves of experimental data (line with cross mark), first-order polynomial form (line with square mark) and second-order polynomial form (line with circular mark).

3.1.3 Loading and Boundary Conditions

In this study, balanced standing on flat support, heel elevated foot supports and HHS were simulated with the FE model. Physiological muscle forces on the foot and location of GRF of each condition were derived and prescribed. Plantar pressure measurements and motion analysis were conducted to obtain the loading and boundary conditions and validate the FE model response. After the FE model was validated with the balanced standing condition, mid-stance instance on 2-inch HHS was simulated.

To simulate balanced standing on flat support and high-heeled foot supports with different heel heights, a vertical force corresponding to half BW was applied at the bottom of flat support or foot supports of which only vertical movement were allowed. For a subject with body mass of 54 kg, a vertical force of approximately 270 N is applied on each foot during balanced standing. Due to the fact that the line of gravity was in front of the ankle joint during both barefoot and high-heeled standing (Opila et al., 1988), the plantar flexors must act to balance the forward moment of the body on the ankle to achieve a balanced standing position. It was found that the triceps surae played the major stabilization role of the foot during balanced standing on flat support and the reactions of all other intrinsic and extrinsic muscles were minimal (Basmajian and Stecko, 1963). Therefore, only the Achilles tendon tension was considered during simulated balanced standing on flat support while all intrinsic and the rest of the extrinsic muscle forces were neglected. The Achilles tendon force was estimated by matching the FE predictions with the measured plantar pressure distribution and location of COP of the same subject who volunteered for the MR scanning. Foot and ankle are multiplanar. Only Achilles tendon force without muscle forces of PB and PL, the foot has a plantarflexion movement combining with inversion and adduction movement. Thereafter, for balanced standing on high-heeled foot supports and HHS, additional muscle forces of PB and PL were applied to match the foot position according to experimental measurements. .

The superior surfaces of soft tissue, distal tibia and distal fibula were fixed throughout the analysis to serve as the boundary conditions. The loading and boundary conditions for simulating the balanced standing on flat support was shown in figure 3-14.

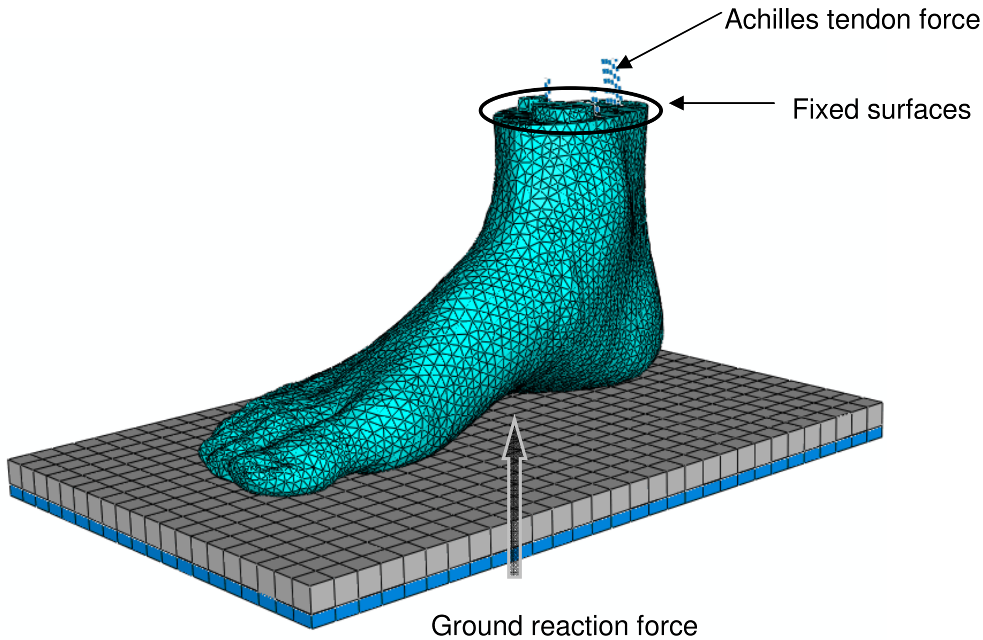

Figure 3-14. Loading and boundary conditions for standing on flat support.

3.2 Parametric Studies of High-heeled Shoe Designs

Before performing parametric analysis of the biomechanical effects of HHS, several validation comparisons were conducted on the FE foot model. Simulation of balanced standing on flat plate and pure compression test were conducted. The results from FE prediction were compared to that from the experimental measurements of the same subject who volunteered for the MR scanning. Moreover, comparison between the FE predictions of this study and previous studies from cadaveric experiments and FE simulations were discussed.

3.2.1 Validation of the FE model of Foot

FE Simulation

For simulated barefoot standing on a flat support, a vertical GRF of approximately half BW (270 N) was applied at the centre of the inferior surface of flat support, which was allowed to move in the vertical direction only. The superior surfaces of soft tissue, distal tibia and distal fibula were fixed throughout the analysis. Before the application of the loading conditions, the flat support was properly aligned such that an initial foot–ground contact was established with minimal induced stress.

Achilles tendon force plays a major stabilization role during balanced standing, so only Achilles tendon force was applied in this simulation. The sensitivity analysis was conducted to verify the physiological loading. To provide a sensitivity analysis of Achilles tendon loading, Achilles tendon force from 135 N to 270 N (50% to 100% of applied loading) was applied while maintaining the GRF at 270 N. The interval of Achilles tendon force was 13.5 N (5% of applied loading). From the sensitivity analysis, the Achilles tendon forces required for simulating the upright, balanced standing posture was estimated by matching the FE predictions with the location of COP and the measured plantar pressure distribution of the same subject. The plantar pressure distribution of the standing subject was measured by the F-scan pressure sensors.

For simulating pure compression, a vertical compressive force from 0 N to 540 N (full BW) was applied to the plantar foot via ground support. The ground support was allowed to move in vertical direction only.

Experimental Validation

Measurements on the right foot of the same subject during balanced standing were done using the F-scan sensor and digitizer (Fig. 3-15). A weight scale was placed under the right foot support in order to monitor the weight-bearing condition. Real time pressure data were recorded for 10 seconds at a sampling frequency of 50 Hz. A pair of F-scan sensors was fixed on top of the flat foot supports. The forthcoming high-heeled foot supports validation employed the same experimental setup. Therefore, on top of the sensor, a piece of plain paper was placed at a fixed position to prevent slippage and for hygienic reason.

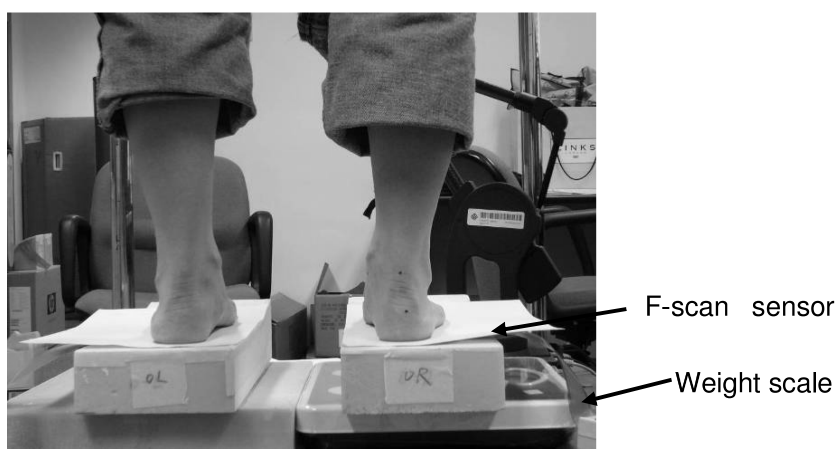

Figure 3-15. Experimental setup for balanced standing measurement.

The F-scan pressure sensor (Sensor model 5100) used in this study has a spatial resolution of 4 sensors per cm^2 (Fig. 3-16). The F-scan sensor is a thin, disposable insoles usually placed in shoes. The sensor is approximately 0.18 mm thick, 20 cm long, containing 960 individual sensors and can be trimmed according to individual subject's foot size. The sensors are created by sandwiching a printed circuit of force-sensitive resistive material in Mylar film. The calibrations and equilibrations of sensing region were done by uniform pressure equipment before the measurement.

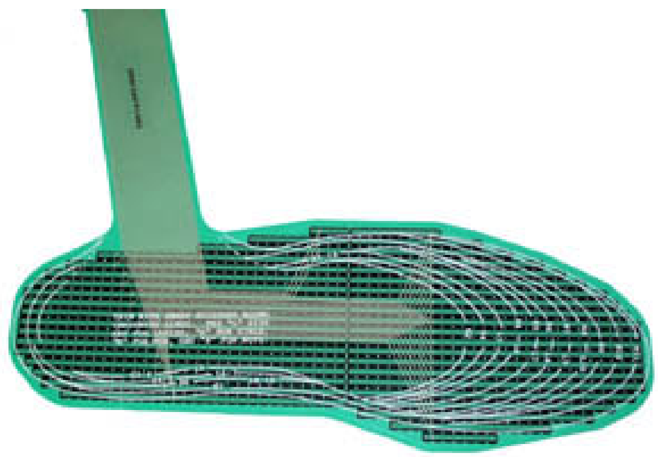

Figure 3-16. F-scan pressure sensor (Tekscan Inc., Boston, USA)

The measured plantar pressures were used to calculate COP on the foot and to compare the FE predicted plantar pressure distribution for the flat and heel elevated foot supports conditions. The plantar foot pressure and contact area were recorded by Tekscan systems. Arch deformations and rearfoot angle of the foot were obtained from the digitizer which measured pointwise spatial coordinate.

3.2.2 Effects of Heel Height on the Foot

FE Simulation

In this study, the high-heeled foot supports with 1-inch, 2-inch and 3-inch heel height were used to simulate high-heeled situations. The loading and boundary conditions for balanced standing on 2-inch HHS was shown in figure 3-17.

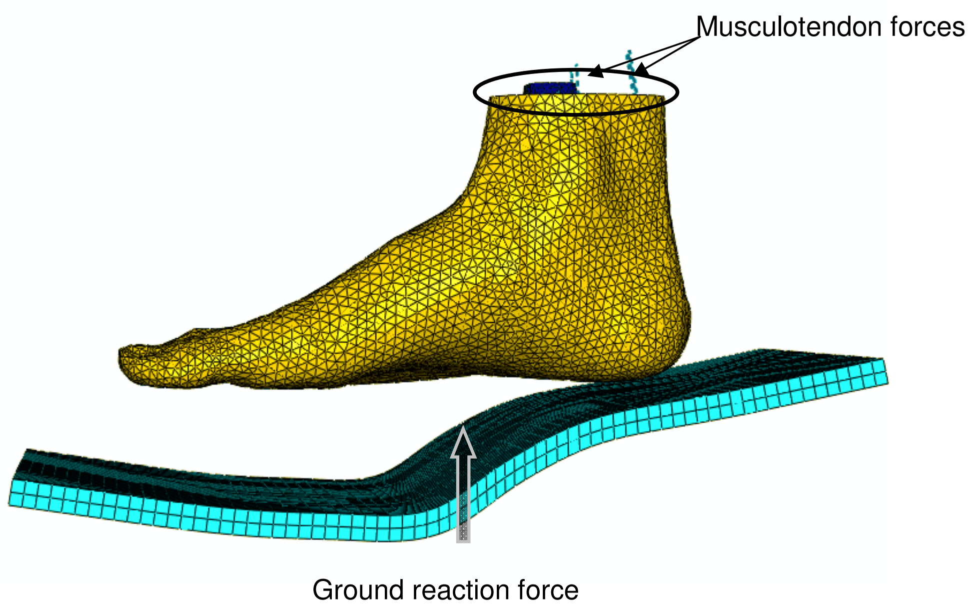

Figure 3-17. Loading and boundary conditions for standing on high-heeled support.

The superior surfaces of soft tissue, distal tibia and distal fibula were fixed throughout the analysis to serve as the boundary conditions in all standing simulations. A vertical GRF of half BW (270 N) was applied at the inferior surface of foot supports. Same sensitivity analyses of Achilles tendon loading as done on the flat support condition were conducted in all balanced standings on high-heeled foot supports. From the sensitivity analysis, the Achilles tendon forces required for simulating the upright, balanced standing posture were estimated by matching the FE predictions with the location of COP and the measured plantar pressure distribution of the same subject.

With high-heeled foot supports, small muscle forces for EHL (10 N) and EDL (5 N) were applied to better accommodate MTP joints upon toe spring. Since the subject stood along the midline of foot supports, muscle forces of PB (20 N) and PL (25 N) were estimated and applied to match foot orientation.

Plantar Pressure Measurement

The foot supports with 1-inch, 2-inch and 3-inch heel height were used for the high-heeled situations. The MTP joint of subject's feet were aligned and positioned according to the profile of the foot supports. As shown in figure 3-18, the F-scan sensors for plantar pressure measurements were placed underneath the plain paper. A pair of F-scan sensors was fixed on the top of each foot support. In order to standardize the foot alignment and foot shape measurements easily for the experimenter, the foot supports were put on top of a platform of 45 cm in height. During balanced standing, real-time plantar contact pressure data was recorded at a sampling frequency of 50 Hz for 10 seconds. The medial longitudinal arch height was determined as the height of navicular tuberosity from a line joining the posterior point of the plantar heel pad and the plantar first metatarsal head (Shimizu and Andrew, 1999). Therefore, the location of navicular tuberosity, the posterior point of the plantar heel pad and the plantar first metatarsal head were marked by the digitizer.

(a)

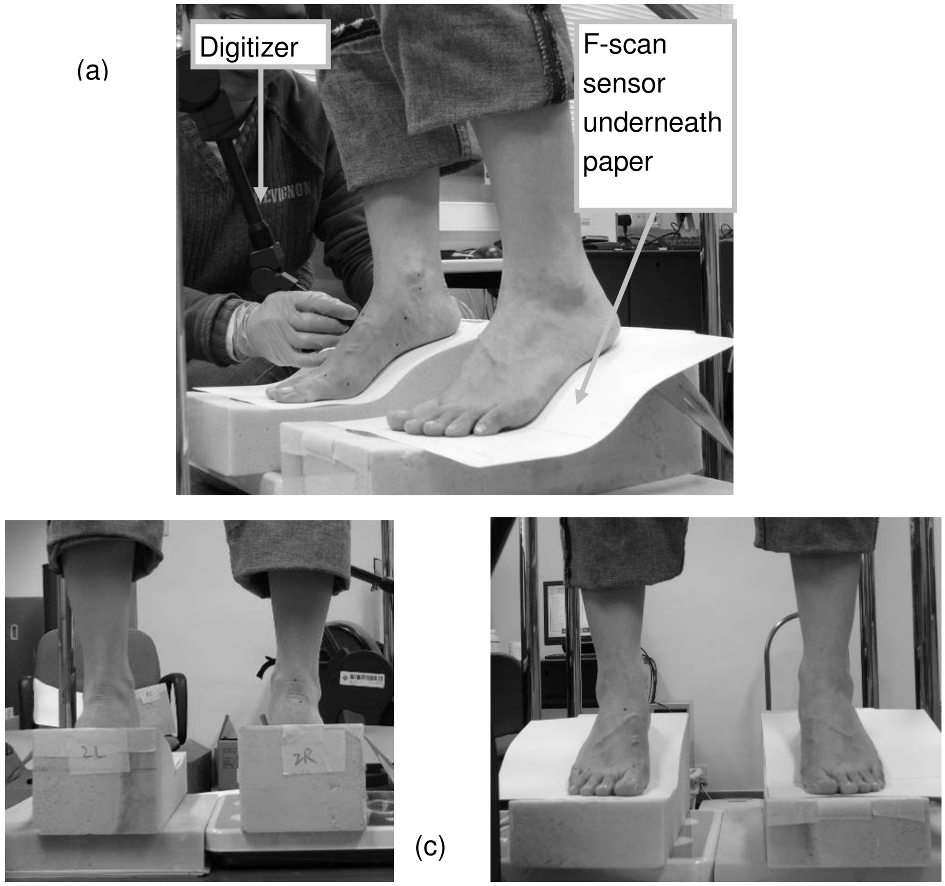

(b) (c)

Figure 3-18. Balanced standing on 2-inch high-heeled foot support: (a) isometric, (b) back and (c) frontal view.

Cadaveric Experiments

In the cadaveric experiments, contact pressure of the first MTP joint, and the foot/ankle kinematics of normal ankles with high-heeled shoe were obtained. The protocol of cadaveric experiments was approved by the IRB/ biospecimens of Mayo Clinic. Two right female ankle-foot specimens amputated at the tibial plateau level with the same foot size (Continental size 38) were used in the study. The specimens were evaluated by both clinical examination and radiography and were free from any observable pathology and deformity. All tissue was preserved at -20 degrees Celsius.

A custom-made multi-axis testing device (Mayo Clinic, USA), was used to generate planar motions of the foot and ankle (Fig. 3-19). This device utilized one motorized rotatory stage (Newport Corporation, Irvine, CA) and two custom-made motorized tilting stages that result in a three axis gimbal. The tilting stages were incorporated with worm gear mechanisms (Rino Mechanical Components Inc, Freeport, NY) that were capable of maneuvering the foot under high axial loading. Unconstrained linear slides in the vertical, AP and ML axis provided a pure moment configuration of the rotations at the ankle and subtalar joint by eliminating the shear forces. The integration of the three rotatory stages resulted in a tilting platform which represented the floor on which the specimen rested. The tibia was rigidly fixed to the testing frame, and an axial load was applied to the tibia. The platform under the foot could be programmed to induce motion in the sagittal plane (plantarflexion-dorsiflexion), coronal plane (inversion-eversion) or transverse plane (internal-external rotation).

Above the fixed tibia, a platform was incorporated with a muscle actuator. Each actuator included a low friction linear pneumatic cylinder (Airpel, Airpot Corporation, Norwalk, CT) and precision potentiometers (Duncan electronics, BEI Technologies Inc, Irvine CA). The applied force would be controlled with a programmable servo-pneumatic regulator (Proportion-Air, McCordsville, IN), and tendon excursions were measured with the potentiometer incorporated in the pulley of the actuator unit.

Figure 3-19. Specimen mounted on multi-axis testing device.

Soft tissue superior to the malleoli was removed. The entire lengths of tendons and muscles crossing the ankle were isolated and preserved. The tibia was rigidly fixed to the testing frame, and an axial load was applied to the tibia. Heavy braided Dacron sutures were sutured to the proximal end of each tendon to enable tendon loading that utilized the pneumatic actuator. Before testing, muscle and tendon lengths were allowed to stabilize for fifteen minutes. The procedure could limit the potential for errors in the measurement from the viscoelastic properties of the soft tissues.

Joint contact area and pressure were obtained with K-Scan System (Sensor model 6900) (Tekscan, Inc., South Boston, MA. USA). The K-scan pressure sensor used in this study had a spatial resolution of 62 sensors per cm^2. The K-scan sensor has four independent sensing regions.

The width and height of one independent sensing region dimension of model 6900 were both 14.0 mm. One sensing region of the sensor of model 6900 was inserted into the first MTP joint from the dorsal surface. The skin incision was sutured after sensor insertion in order to reduce the movement of sensor (Fig. 3-20). The sensing region of sensor calibrations and equilibrations by uniform pressure equipment were done before the measurement.

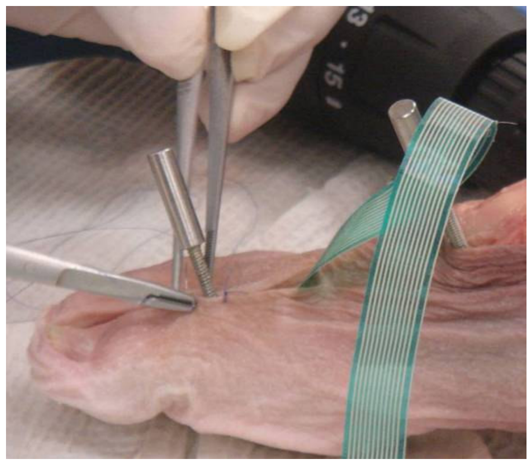

Figure 3-20. Suturing skin incision of the first MTP joint.

Four infrared sensors embedded by rigid bodies were inserted into the tibia, calcaneus, the first metatarsal and the first proximal phalanx of the specimen to measure their motion (Fig. 3-21). An optoelectric tracking device (Optotrak Certus, Northern Digital Inc., Ontario, Canada) was used to measure MTP joint kinematics. Relative angular motion between the bones was calculated with the MotionMonitor software (Innovative Sports Training, Inc., Chicago, IL), and expressed using Euler angles.

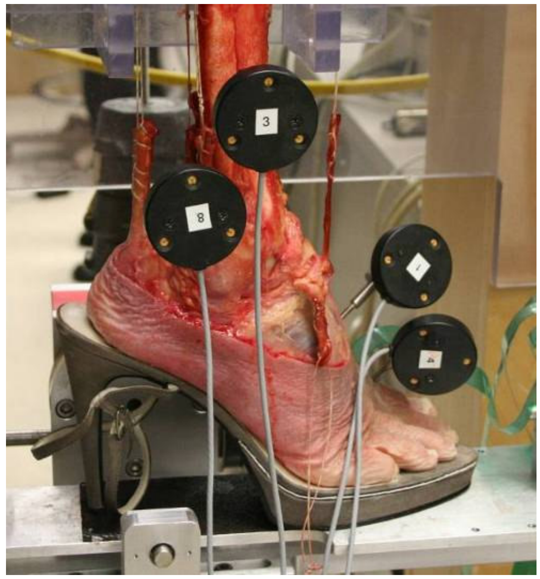

Figure 3-21. Mounting four infrared sensors in the specimen.

An axial load (212N) was applied to the tibia. At first, static loads were applied to the Achilles' tendon, PT, PL, FHL, and EHL. The applied forces were controlled with a programmable servo-pneumatic regulator (Proportion-Air, McCordsville, IN), and tendon excursions were measured with the potentiometer incorporated in the pulley of the actuator unit. An initial preconditioning of each specimen was cyclically loaded at 10 mm/s for 10 cycles at axial load (212 N) to establish a mechanical stabilized state just prior to testing. Measurements were made with each specimen mounted in the testing machine at the end of preconditioning.

Each specimen was subjected to the following three tests, which are a flat support (control) and three different HHS from 1-inch to 4-inch (Fig. 3-22) of the same size (Continental size 38). To follow the HHS used in the FE model and for easy mounting specimens onto the HHS, upper materials of HHS were carefully removed.

Figure 3-22. Photograph of three different high-heeled shoes used in this study. From the left to right: 1-inch, 2-inch and 4-inch.

For each testing condition, five test runs were performed so that an average value could be obtained for data analysis. The protocol for all tests was kept the same for each specimen. Specimens were loaded for 10 seconds for each condition and then data were collected in real time for three seconds.

Static Contact Characteristics of the First MTP with Different HHS

Only one specimen was used in the static condition. Two static weight-bearing conditions with and without tendon load were conducted. Each HHS (1-inch, 2-inch and 4-inch) was placed under the foot. Since upper material of HHS was removed, adhesive strips were used to assist the foot standing on the HHS. An axial compressive load (212N) was applied to the tibia throughout the experiments. In the first step, experimental data were obtained under axial load only. After that, scaled down muscle forces were applied to the Achilles tendon (44 N for 0 and 1-inch heel height, 66 N for 2-inch and 4-inch heel height), TP (12 N), Peroneus (10 N), FHL (5 N), EHL (7.5 N). The peak contact pressure, contact area and force of the first MTP joint were recorded for each run.

Contact Characteristics of the First MTP Joint and Joint Movements with Flat Support and 2-inch HHS during Cyclic Sagittal Movement

Another specimen was used in this dynamic condition. The plate of multi-axis testing device started rotation from 5 degrees in plantarflexion to 15 degrees in dorsiflexion over five rounds. Kinematics of the first MTP segment (the first phalanx relative to the metatarsal) and ankle joint were monitored with an optoelectric tracking system. The specimen was mounted on the plate and then with 2-inch HHS. Axial load and muscle forces were the same as applied in the static condition. Contact characteristics of the first MTP joint were recorded.

3.2.3 Effects of Outsole Stiffness and Coefficient of Friction on the Foot

Before a parametric study of the effects of outsole designs of 2-inch HHS on the foot, validation of simulation of the basic design was conducted under balanced standing.

Effects of Outsole Stiffness

The outsole stiffness is largely determined by the materials of outsole itself and shankpiece. The shankpiece reinforces the waist of the shoe and prevents it from collapsing or distorting in wear. Steel shankpiece embedded into outsole is widely used to maintain the shank contour of HHS.

In this study, effects of outsole stiffness on the foot during balanced standing on 2-inch HHS were investigated. The superior surfaces of soft tissue, distal tibia and distal fibula were fixed throughout the analysis to serve as the boundary conditions. A vertical GRF of half BW (270 N) was applied at the inferior surface of ground support. The ground support was allowed to displace in vertical direction only. While the high-heeled shoe was allowed to move freely after the foot completely stepped on. The magnitude of the muscles loading was the same as the 2-inch high-heeled foot support during balanced standing applied. In the parametric studies, sensitivity test of Achilles tendon force was completed in balanced standing on 2-inch HHS conditions as done in the flat support conditions. The centre of force location relative to the lateral malleolus of right foot was obtained from the force platform and Vicon system during static standing on 2-inch HHS.

The simulation was completed step by step. The first step was to manipulate the foot into plantarflexion position by application of minimal Achilles tendon force and small muscle forces (PB and PL). The HHS was properly aligned such that an initial foot-shoe contact was just established with minimal induced stress in the second step. The ground support was displaced to the bottom of HHS to establish contact in the third step. After that, GRF was applied at the inferior surface of ground support. Finally, Achilles tendon forces estimated according to the magnitude of simulation of balanced standing on 2-inch HHS with steel shankpiece was applied.

Simulations on the outsole without steel shankpiece were compared to the outsole with steel shankpiece design. Four different stiffness materials (specifically, high-density polyethylene, thermoplastic rubber, and polyurethane, ethylvinyl acetate) were used to investigate the effect of change in the outsole materials (Lewis, 2003). All these materials were widely used in the outsole of footwear. The initial position of HHS, load and boundary conditions of FE model maintained the same in all simulations. In solid mechanics, Young's modulus (E) is a measure of stiffness of an isotropic elastic material.

Table 3-4. Material properties assigned in the outsole (Lewis, 2003).

Material	Young's modulus (MPa)	Poisson's ratio
High-Density Polyethylene (HDPE)	1000	0.42
Thermoplastic Rubber (TPR)	100	0.42
Polyurethane (PU)	25	0.42
Ethylvinyl Acetate (EVA)	5	0.40

Effects of Coefficient of Friction

In is hypothesized that the coefficient of friction of plantar foot could influence balanced standing and plantar pressure distribution. In this study, several different values of coefficient of friction were assigned to the contact interaction between plantar foot and upper surface of the outsole. The coefficient of friction depends on the pair of surfaces in contact. As an approximation, the frictional property used in this study was viewed as static friction. The coefficient of friction of 0.4 was assigned to mimic interaction between plantar foot and wool. The coefficient of friction of 0.2 was assigned to mimic interaction between plantar foot and Teflon.

Except varying frictional property between plantar foot and outsole, all the other boundary and loading conditions were kept as the previous settings. Moreover, the frictional property between outsole and ground support was maintained the same.

3.2.4 Walking with High-heeled Shoes

FE Simulation on Mid-stance Phase

In the FE simulation of 2-inch high-heeled shoe walking, mid-stance phase was completed by assigning different boundaries and loading conditions.

In the mid-stance phase, it was found that the foot-shank was approximately vertical to the ground support at this frame. The superior surfaces of the soft tissue, distal tibia and distal fibula were kept fixed throughout the analysis. The analysis steps of mid-stance simulation were similar to that of balanced standing on 2-inch HHS.

To conduct a sensitivity analysis of Achilles tendon loading, Achilles tendon force from 270N to 540 N was applied while maintaining the GRF at 513 N (95% of BW). From the sensitivity analysis, the Achilles tendon forces required for simulating the upright, balanced standing posture were estimated by matching the FE predictions with the measured plantar pressure distribution and location of centre of force of the same subject who volunteered for the MR scanning. The extrinsic muscle forces during mid-stance were estimated from the physiological cross sectional area (PCSA) of the muscles (Dul, 1983) and normalized normal walking EMG data (Perry, 1992) assuming a linear muscle force, EMG, and PCSA relationship (Kim et al., 2001). The GRF, which was obtained by the same subject walking from force platform, was applied underneath the ground support.

Average GRF (513N, 95% BW) obtained from force platform in the gait experiment was applied to the ground support. Musculotendon forces were prescribed according to the assumption of linear relationship between PCSA and EMG values (Table 3-5, Table 3-6). Major extrinsic musculotendon forces for FDL (10N), PB (20N), PL (25N) and TP (85N) were applied at the corresponding insertions via axial connector elements.

Table 3-5. Physiological cross-sectional area (PCSA) (Dul, 1983).

Tendon/External Forces	PCSA (cm^2)
Tibialis Anterior	14
Extensor Hallucis Longus	3
Extensor Digitorum Longus	8
Tibialis Posterior	17
Flexor Hallucis Longus	11
Flexor Digitorum Longus	4
Peroneus Brevis	8
Peroneus Longus	11

Table 3-6. Normalized EMG data, GRF and extrinsic muscles forces applied for mid-stance simulation assuming a muscle gain of 25 N/cm^2. (Perry, 1992; Kim et al., 2001).

Muscles	EMG (%)	Applied Forces
Tibialis Anterior	0	-
Extensor Hallucis Longus	0	-
Extensor Digitorum Longus	0	-
Tibialis Posterior	20.2%	85N
Flexor Hallucis Longus	0	-
Flexor Digitorum Longus	11.4%	10N
Peroneus Brevis	9.7%	20N
Peroneus Longus	9.1%	25N
Vertical Ground Reaction	95% BW	513N

Gait Analysis Experiments with HHS

The HHS of three different heel heights used in this study were designed by using the customized shoe design software (ShoeCAD, Excel-Last, Hong Kong). The shoes had the same style of heel and toe box but with different heel heights (0-inch, 2-inch and 4-inch). The shank profiles were the same as the high-heeled foot supports used in static plantar pressure measurement experiment. Three pairs of shoes of 37 size and three pairs of 38 size of 0-inch, 2-inch and 4-inch heel height were used in this study (Fig. 3-23). All shoes had round toe boxes, low vamps and wide heel.

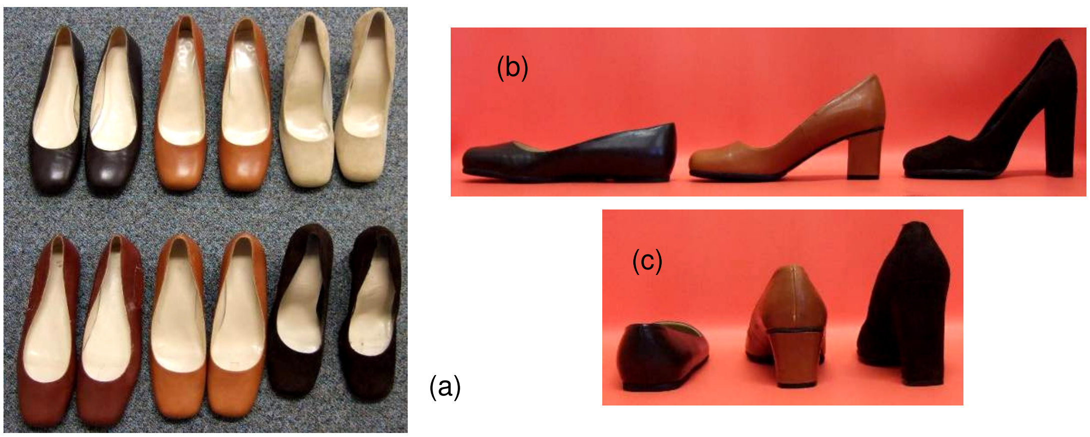

Figure 3-23. The three different pairs of shoes (37 and 38 size) each used in this study. From left to right: 0-inch, 2-inch and 4-inch. a) top, b) medial and c) back view.

Five healthy female subjects took part in this study. All the subjects signed a consent form in accordance with the university policy before participating in the experiment. The subjects ranged in age from 24 to 36 years (29.0 years ±4.7), 1.62 to 1.69 m (1.65 m ±0.03) in height, and 52.3 to 57.8 kg (54.5 kg ±2.1) in body mass. All subjects were healthy and were free of recent injuries that potentially impair gait. Subjects with limb-length discrepancy, foot deformities and skin lesions were excluded from the study.

The subjects had experience of wearing high-heeled shoes and could fit into one of two series HHS, either 37 or 38 (continental).

Kinematic data of complete gait were collected using a set of six-camera 60-Hz Vicon Motion Analysis System (Oxford Metrics Ltd, Oxford, England). As the subjects walked across two force platforms (AMTI Technologies Inc, Oxford, England) embedded in the floor of the walkway, GRF was collected simultaneously sampling at 60-Hz. Reflective markers identifying different body segments were placed on sacrum, pelvis, lateral aspect of thigh, lateral femoral epicondyle, lateral aspect of leg, lateral malleolus, the second MTP joint (Fig. 3-24). To define the heel angle, two markers were placed on the posterior aspect of shoe; one marker at the superior border of the heel counter, the other at the intersection of the inferior border of the heel counter and the shoe heel. To define the leg angle, one marker was placed along the line on the Achilles tendon approximately 2 cm above the heel counter. The other marker was placed in the middle of the line below the calf.

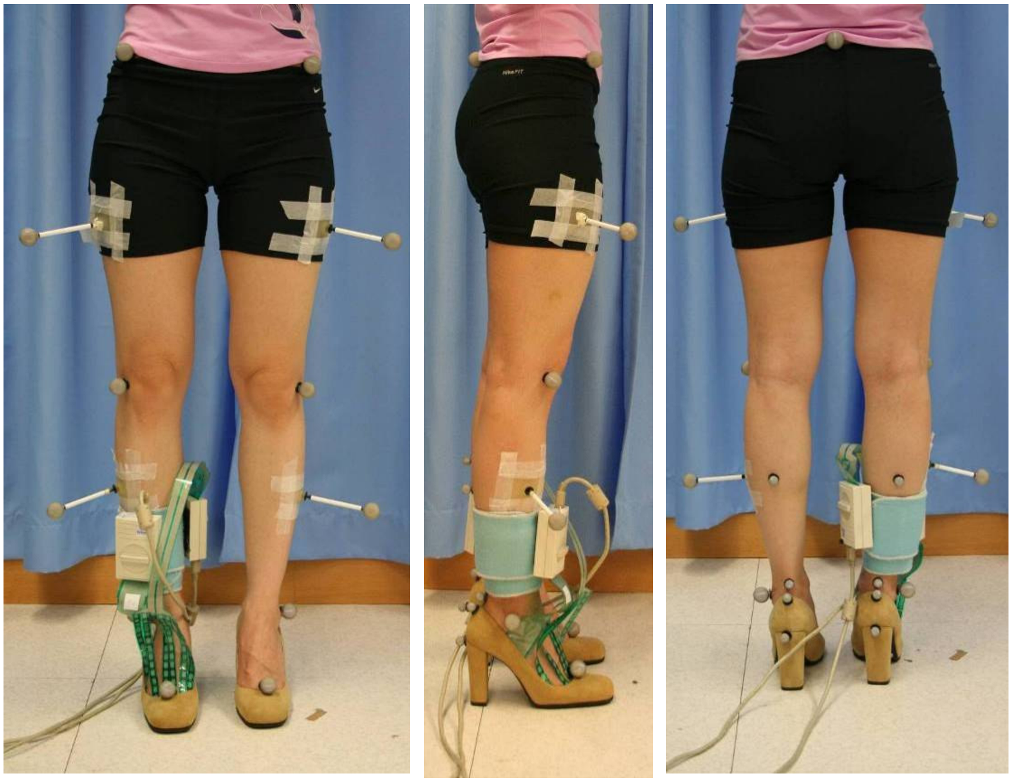

(a) (b) (c)

Figure 3-24. Location of reflective markers: (a) frontal, (b) lateral and(c) posterior view.

Real-time pressures of dorsal and plantar regions of right foot were recorded during walking by Tekscan pressure measurement system with F-scan sensor and F-socket sensor. The F-socket sensor (Sensor model 9811E) used in this study has a spatial resolution of 0.6 sensors per cm^2, and has six independent strips of 16 sensing cells each. The sensor calibrations and equilibrations by uniform pressure equipment were done before the measurement.

The F-scan sensor was trimmed according to the bottom shape of shoes. The F-socket sensor was split into six strips and attached to the medial aspect region of the big toe, dorsal aspect regions of the big toe to fourth toe and lateral aspect region of the fifth toe, respectively (Fig. 3-25).

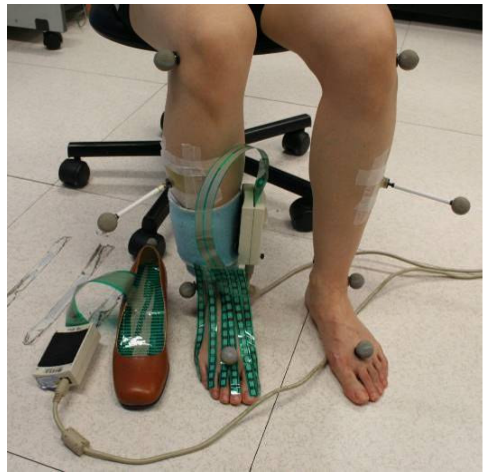

Figure 3-25. Locations of pressure sensors on the dorsal foot and medial side of the big toe.

For each subject, the order of three pairs of shoes was randomly assigned, and five walking trials were collected for each shoe condition because of the recommendation from the literature (Oplia-Correia, 1990 a) that five repeated trials were adequate for analysis of joints motions in all planes from statistical tests of intra-subject variability. The subjects were allowed to walk freely for 10 minutes to warm up, and tried to strike properly on the force platform for each shoes. All subjects are right-dominant, and walk at self controlled comfortable speed.

Static posture trials were recorded at the beginning of experiment for each shoe for 5 seconds. During dynamic trials for kinematics data collection, pressures of foot were recorded and video images connected to the Tekscan system were obtained in real-time from lateral side (Fig. 3-26). Therefore, pressure data could be synchronized with kinematics data.

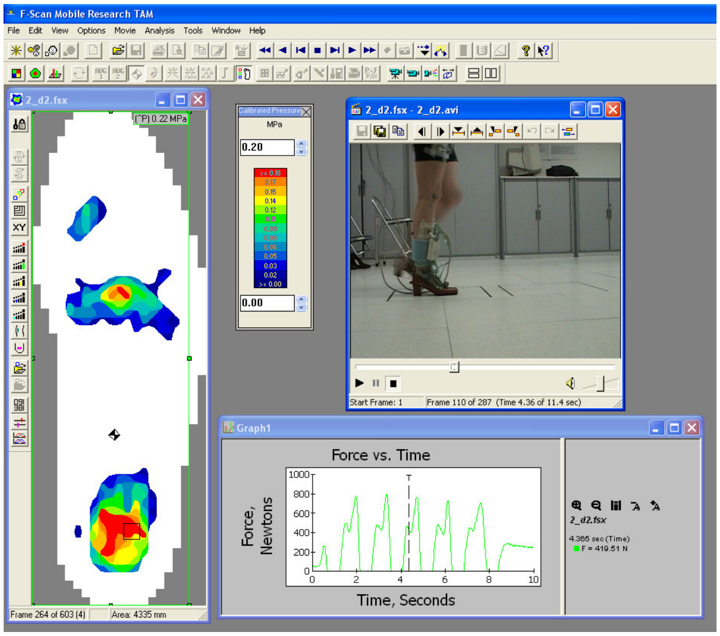

Figure 3-26. Combined Tekscan measurement with Vicon kinematic measurement in gait experiment.

After each heel height condition, subjective questionnaires related to the comfort of body segments were filled by each subject. The content of questionnaires were about the subject’s perception of the following questions, which are easiness in walking, easiness in balancing, total comfort, plantar forefoot comfort, plantar heel comfort, dorsal vamp region comfort, heel counter comfort, toe comfort, knee comfort and lower back comfort (Appendix). The scale was starting from 0 to 6, representing the least to the most by interval of one. The subject answered the questions by ticking the number. The experimenter explained the terminology with anatomical pictures and understandable words if a subject was not familiar with some terms. The subjects had 15 minutes rest for each heel height condition.

In summary, experimental output variables from three series experiments were tabulated (Table 3-7). The values of COP at static condition and GRF at 2-inch dynamic condition were used for FE model input parameters, while the remaining variables were used for validation/comparison to FE predictions.

Table 3-7. Summary of experimental output variables.

Experiment Output	Static					Dynamic				
	0	1	2	3	4	0	1	2	3	4
COP & Plantar Pressure Distribution	✓	✓	✓	✓		✓		✓		✓
GRF						✓		✓		✓
Dorsal Pressure						✓		✓		✓
Arch Deformation	✓	✓	✓	✓						
Rearfoot Pronation Angle	✓	✓	✓	✓						
Contact at 1st MTP	✓	✓	✓		✓	✓		✓		
Rotation of Ankle & 1st MTP						✓		✓		
Subjective Ratings						✓		✓		✓

Prior to the calculation of any variables of kinematics data, Woltring filtering routine was used to filter the kinematic data. Velocity was computed by dividing the distance moved of the sacrum marker during the gait cycle by the cycle time. Stride length was determined by the distance traveled in the direction of progression by the right lateral malleolus marker. Cadence was obtained by dividing two by the cycle time. Stance phase percentage was computed as the time that the foot was in contact with the force platform, divided by the cycle time. One way ANOVA using Student-Newman-Keuls adjustment for post hoc multiple comparisons was performed on the subjective questionnaires.

CHAPTER IV RESULTS

4.1 Validation of FE Model of Foot

4.1.1 Balanced Standing on Flat Support

An anatomically detailed FE model of a female foot with HHS was developed. The model is capable of predicting both plantar pressure/shear stress distribution and internal stresses/strains within bony and soft tissue structures under various loading and supporting conditions.

In this study, the accuracy and reliability of the developed 3D FE model of a female foot to quantify the biomechanical response were preliminarily investigated. Balanced standing on flat support and pure compression with flat support were simulated to validate the FE predictions.

With the total GRF maintained at 270 N (half BW), Achilles tendon force was applied based on the sensitivity study of the effect of Achilles tendon force from 50% to 100% of half BW, at interval of 5%. It was found that Achilles tendon force of 75% of half BW was proper in term of the closest COP. From F-scan measurement of the same subject who volunteered MR scanning, the COP was 65 mm from the posterior extreme of the plantar foot and 20 mm from the medial plantar heel extreme. The predicted COP was less than 0.5 mm medial deviation and 1.5 mm posterior deviation from the experimental measured COP location (Fig. 4-1).

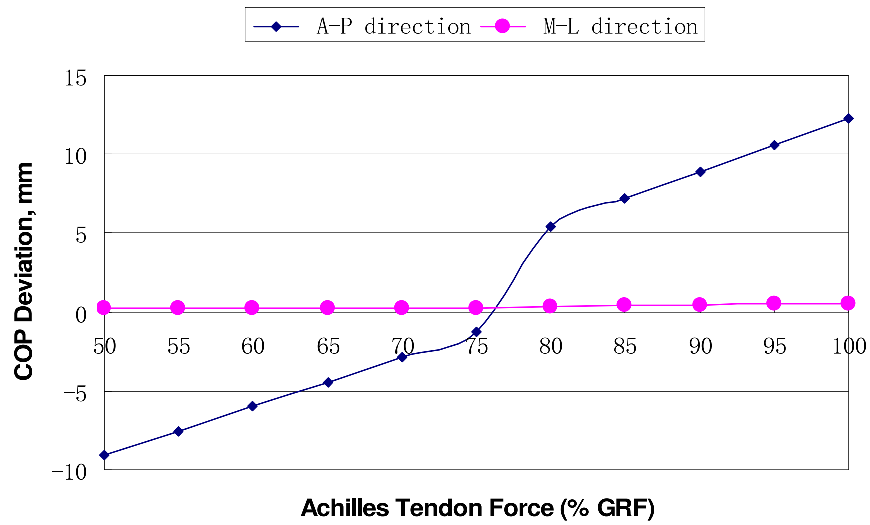

Figure 4-1. The FE predicted COP deviations from F-scan measurement.

The predicted plantar pressure pattern agreed qualitatively with the F-scan measurement shown in figure 4-2. The model predicted peak plantar pressure of 0.23, 0.07, 0.06, 0.07, 0.05 and 0.04 MPa at the heel region and from the first to the fifth metatarsal head regions with flat support, respectively, while the corresponding F-scan measured peak pressure were 0.21, 0.08, 0.06, 0.08, 0.07, and 0.09 MPa, respectively. Both of the measured and predicted values showed high contact pressures at the central heel region and the metatarsal heads.

The contact areas from FE prediction was 61.0 cm^2, compared to 35.6 cm^2 from F-scan measurement during balanced standing.

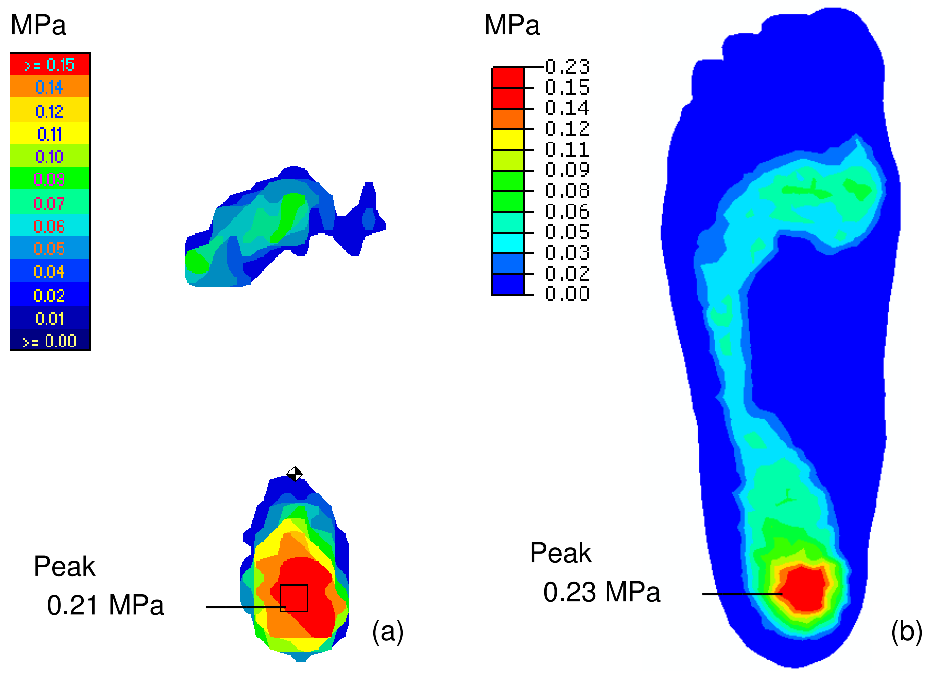

Figure 4-2. Plantar pressure distributions: (a) from F-scan measurement and (b) from FE prediction.

Peak anterior–posterior (A-P) shear stress of 60.3 KPa was predicted at the posterior heel region and peak medial-lateral (M-L) shear stress of 58.8 KPa was predicted at the lateral heel region (Fig. 4-3). Relative high shear stresses of 15 KPa for both directions were concentrated around the soft tissue beneath the medial side of forefoot, especially at the first metatarsal head.

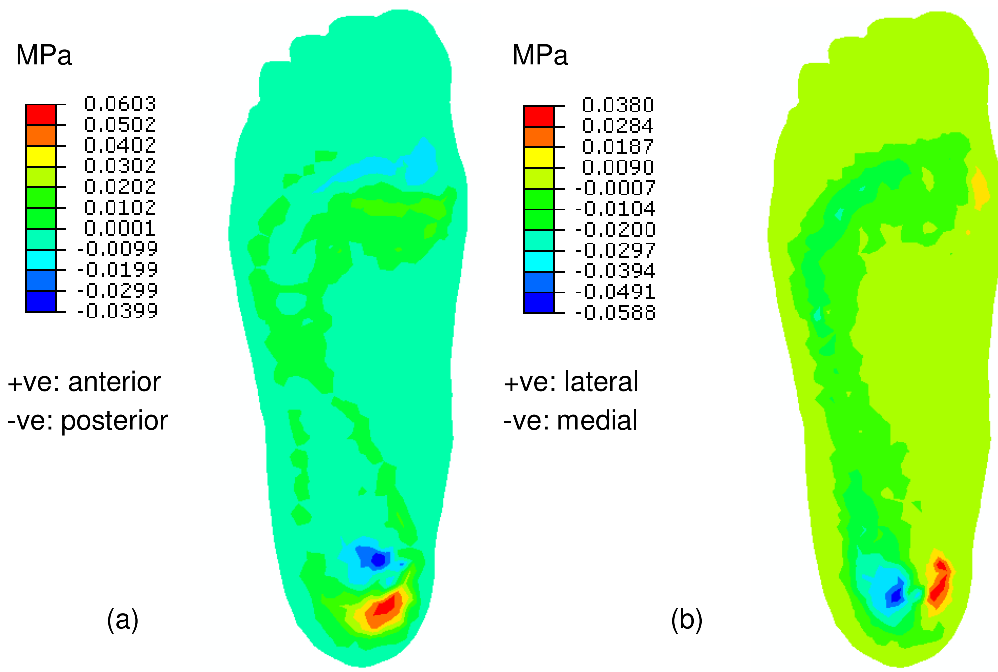

Figure 4-3. FE predicted plantar shear stresses: (a) A-P direction and (b) M-L direction.

Figure 4-4 depicts the von Mises stress of the foot bones during balanced standing with flat support. The von Mises stress (σ_{VM}) is used to predict yielding of material under multiaxial loading conditions using results from simple uniaxial tensile tests. Weighing the effects of principal stresses (σ_1, σ_2 and σ_3), von Mises stress is defined as:

$$\sigma_{VM} = \sqrt{\frac{1}{2}\left[(\sigma_1-\sigma_2)^2+(\sigma_2-\sigma_3)^2+(\sigma_3-\sigma_1)^2\right]} \tag{4-1}$$

From the FE prediction, peak von Mises stress of 13.29 MPa was predicted at the calcaneus, followed by the second metatarsal (6.83 MPa), fourth metatarsal (6.78 MPa), third metatarsal (6.51 MPa), navicular (4.58 MPa), first metatarsal (4.12MPa), lateral cuneiform (3.79 MPa) and talus (3.09 MPa). The plantar junction of calcaneal-cuboid joint sustained the highest stress. The insertion sites of plantar fascia at the inferior calcaneus and the metatarsal heads experienced high stress as a result of tension in the plantar fascia. The insertion site of Achilles tendon at the posterior calcaneus sustained high stress because of applied muscle forces loading. Relatively high von Mises stresses were found at the mid-shaft of metatarsals especially in the second, third and fourth metatarsals.

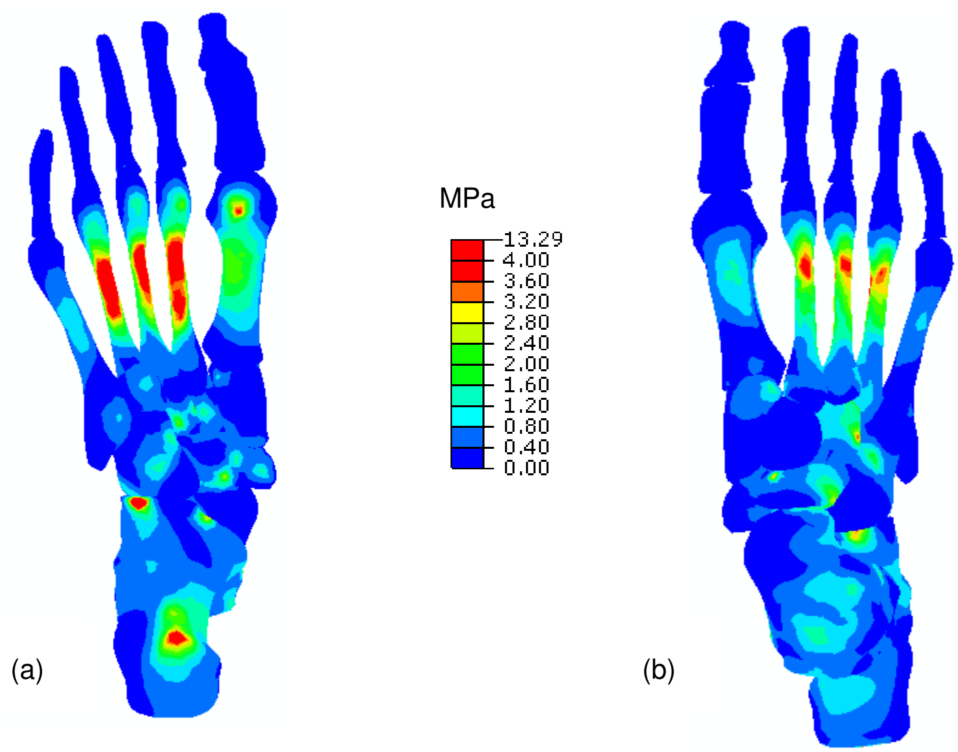

Figure 4-4. FE predicted von Mises stresses of the foot bones under flat plate support: (a) bottom and (b) top view.

The medial longitudinal arch height of the volunteer is 49.5 mm at non-weightbearing condition with 90 degrees knee flexion at during upright sitting. The predicted medial longitudinal arch decreased by 17.8% to 40.7 mm as compared to the experimental measurement with 12.9% to 43.1 mm during balanced standing on flat support. The pronation angle of rearfoot was 2.5 degrees from FE prediction as compared to the experimental measurement of 2.0 degrees. The predicted strain on the five rays of plantar fascia segments ranged from 1.3% to 0.3% with an average strain of 0.7% during balanced standing on flat support. Total tension forces of plantar fascia were 151 N.

4.1.2 Pure Compression

In this study, vertical compression with flat support was applied to the plantar foot to investigate the biomechanical response of GRF on under pure compression without muscle loading. The maximal loading on the standing foot was set to full BW (540 N).

The FE prediction characterised a nonlinear load-deformation response. The medial longitudinal arch decreased nonlinearly by 10.8 mm when pure compressive loading reached from non-weightbearing to full BW from FE prediction (Fig. 4-5). A total contact area of 67.7 cm^2 was predicted under full BW compression (Fig. 4-6).

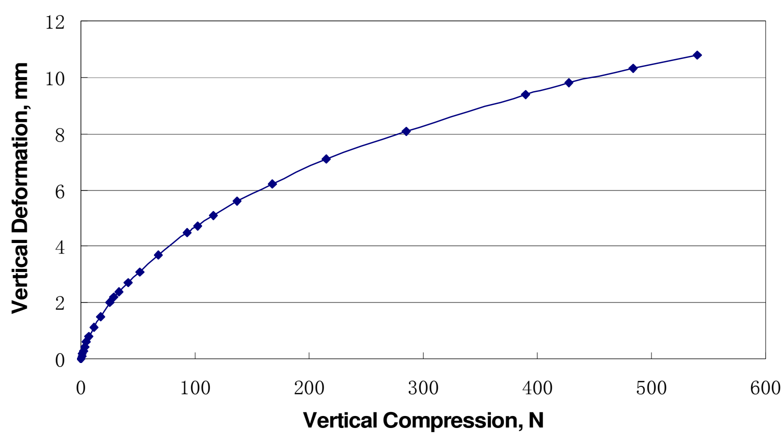

Figure 4-5. FE predicted arch deformations under vertical compression (up to full BW).

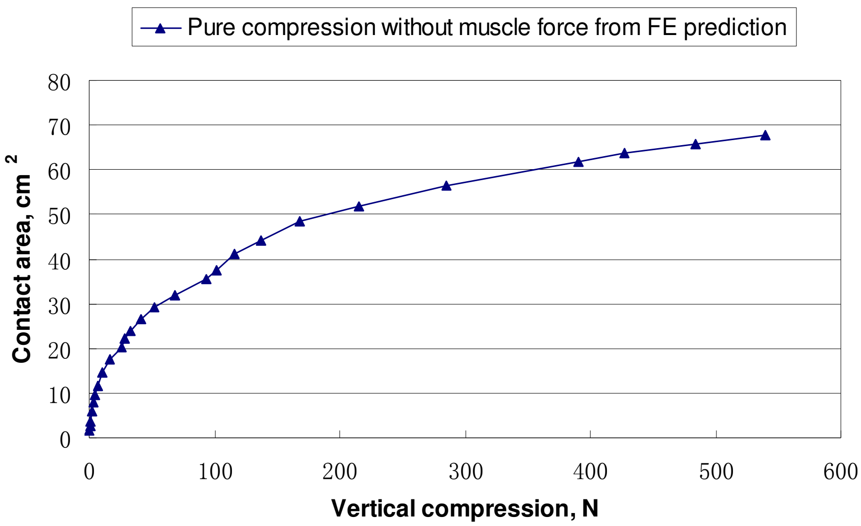

Figure 4-6. FE predicted contact area increment under vertical compressive loading (up to full BW).

The peak and average strain of plantar fascia increased linearly to 1.20 % and 0.64%, respectively (Fig. 4-7). The results of foot and fascia deformation were further compared to the cadaveric experimental data and FE predictions from the literature in the discussion section.

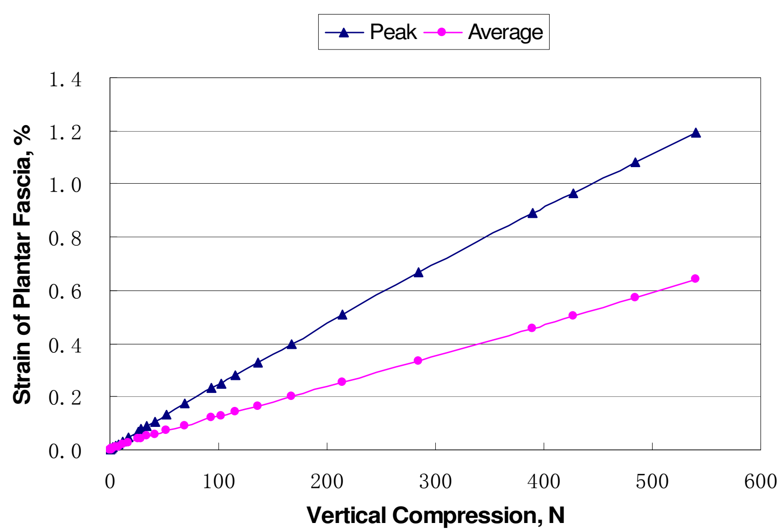

Figure 4-7. The strain of plantar fascia increment under vertical compressive loading (up to full BW) obtained from FE predictions.

The COP shifted 14.8 mm (from 53.6 mm to 68.4 mm) in posterior direction when vertical compression increased from 50 N to 540 N (Fig. 4-8). In medial direction, maximum deviation was less than 2.5 mm throughout pure compression simulation.

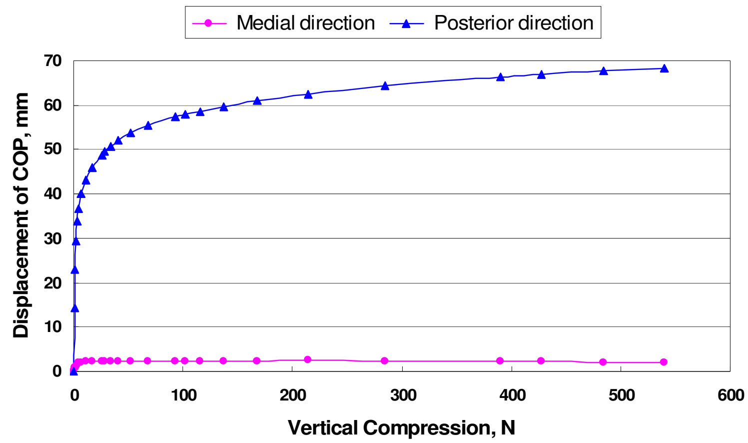

Figure 4-8. FE predicated displacement of COP under vertical compression (up to full BW).

Figure 4-9 depicts the nonlinear relationship between vertical compression and peak pressure. The model predicted peak plantar pressure of 1.13 MPa and 0.07 MPa at the central heel and metatarsal regions under vertical compression of 540 N (Fig. 4-10).

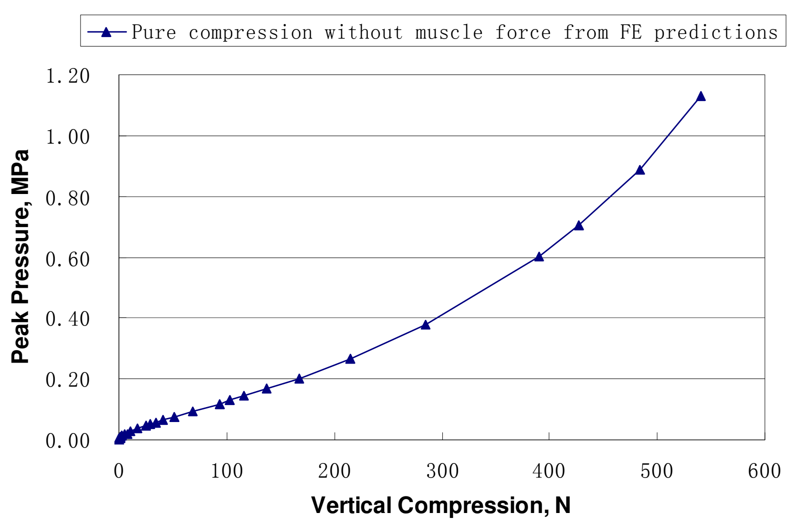

Figure 4-9. FE predicted peak pressure under vertical compressive loading (up to BW).

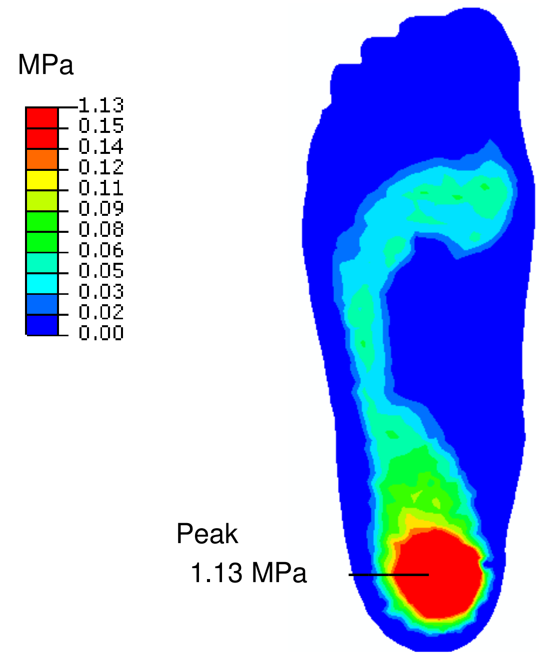

Figure 4-10. FE predicted plantar pressure distribution under full BW pure compression.

The FE predicted results would be compared to that from previous well validated FE studies and cadaveric experiments to further justify FE foot model's reliability.

4.2 Effects of Heel Height on the Foot

In this parametric study, three different high-heeled foot supports (1-inch, 2-inch and 3-inch) were employed to investigate the effects of heel height on standing foot. To simulate balanced standing on each high-heeled support, Achilles tendon force was applied based on the sensitivity study on the effect of Achilles tendon force from 50% to 100% of half BW, at interval of 5%. The Achilles tendon forces were estimated by matching the FE predictions with the measured plantar pressure distributions and locations of COP of the same subject who volunteered for the MR scanning. It was found that Achilles tendon force of 65%, 80%, and 160% of half BW was proper in term of the closest COP, for 1-inch, 2-inch and 3-inch high-heeled foot supports, respectively. During balanced standing on 1-inch, 2-inch and 3-inch, the COP was 59, 41 and 92 mm anterior from the lateral malleolus, respectively. The COP of each condition was about 12 mm lateral from the lateral malleolus. The maximum deviations in all calculated cases between FE predictions and experimental measurements were less than 3 mm in A-P direction and 2 mm in M-L direction.

The foot deformations during balanced standing on four different heel height foot supports are demonstrated in figure 4-11. In all the cases, foot was aligned with the curve of foot support. Maximum foot adduction angle among all conditions was less than 2 degrees.

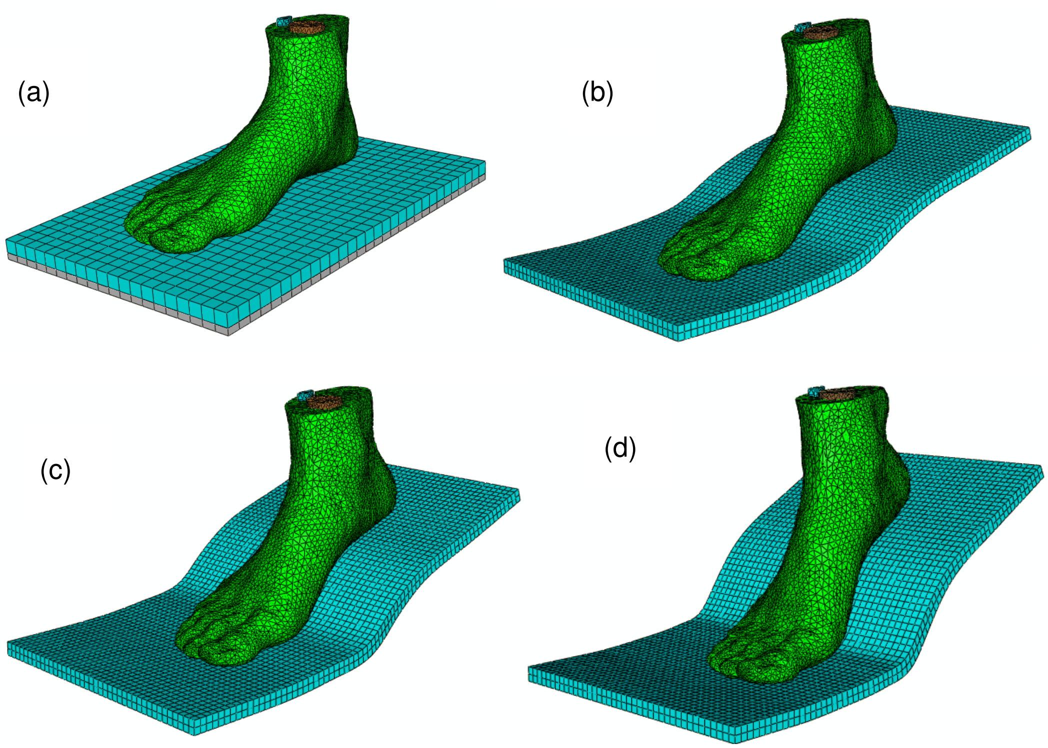

Figure 4-11. Foot deformations during balanced standing on different heel height foot supports: (a) flat, (b) 1-inch, (c) 2-inch and (d) 3-inch.

From the FE predictions, an increase in heel height from 0-inch to 3-inch resulted in a decrease in arch deformation from 8.8 mm to 1.1 mm, which was consistent with measured trend of arch deformation (Fig. 4.12).

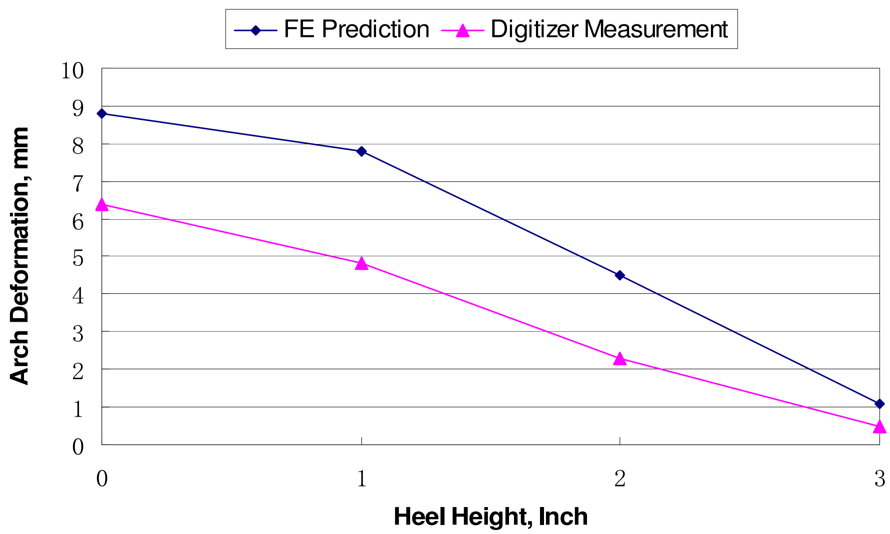

Figure 4-12. Foot medial longitudinal arch deformations during balanced standing on different heel height foot supports: (a) flat, (b) 1-inch, (c) 2-inch and (d) 3-inch.

The plantar pressure distributions during balanced standing on three different high-heeled foot supports from FE predictions and F-scan measurements are compared in figure 4-13. The plantar pressure distribution patterns from FE predictions and F-scan measurements were in general comparable while FE predicted with a slightly larger magnitude. The peak plantar pressure region shifted from the central heel region to the central forefoot region at 3-inch high-heeled foot support condition, both for FE predictions and F-scan measurements.

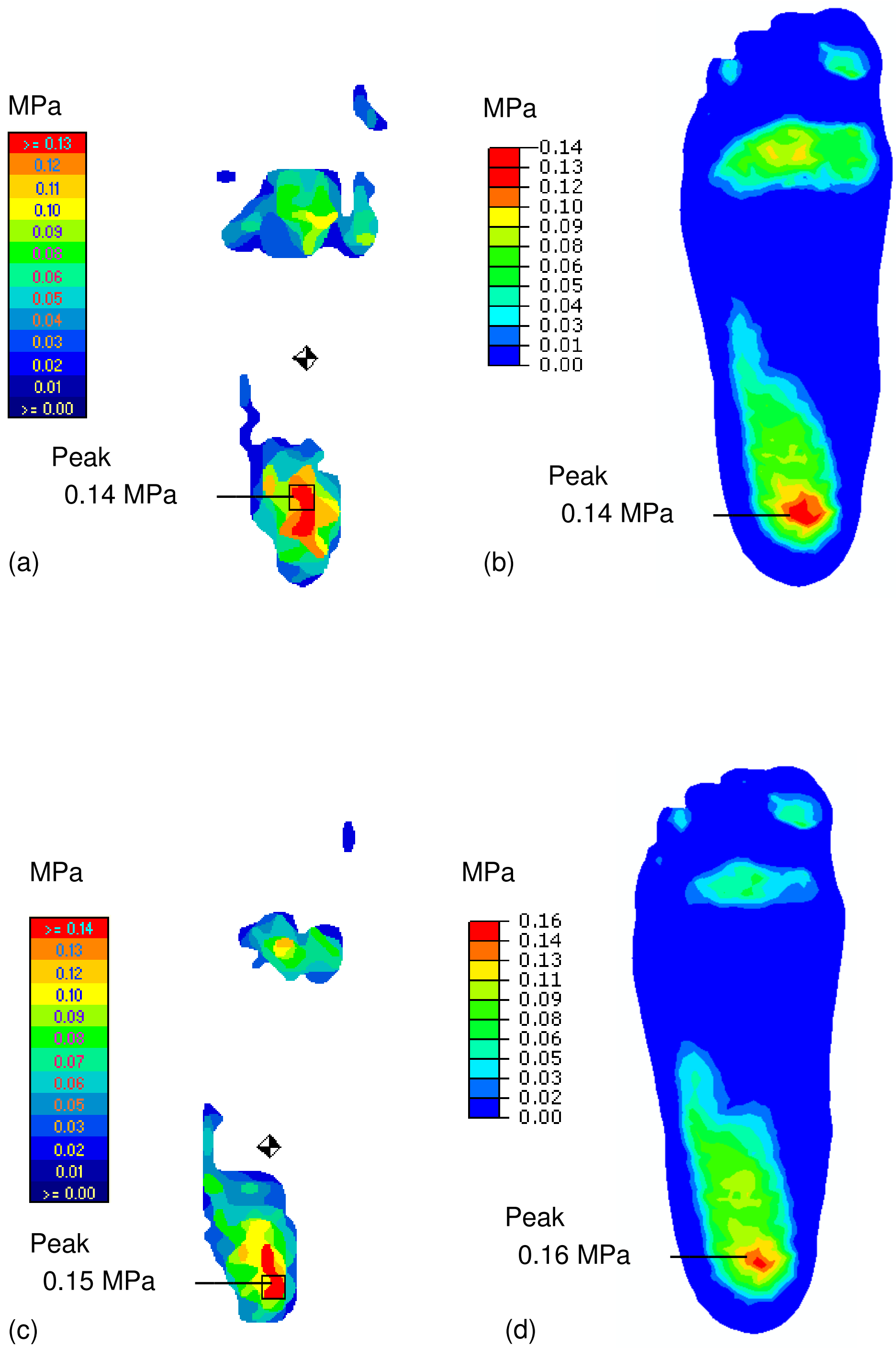
MPa
>= 0.13 0.12 0.11 0.10 0.09 0.08 0.06 0.05 0.04 0.03 0.02 0.01 >= 0.00
Peak
0.14 MPa
(a)
MPa
0.14 0.13 0.12 0.10 0.09 0.08 0.06 0.05 0.04 0.03 0.01 0.00
Peak
0.14 MPa
(b)
MPa
>= 0.14 0.13 0.12 0.10 0.09 0.08 0.07 0.06 0.05 0.03 0.02 0.01 >= 0.00
Peak
0.15 MPa
(c)
MPa
0.16 0.14 0.13 0.11 0.09 0.08 0.06 0.05 0.03 0.02 0.00
Peak
0.16 MPa
(d)

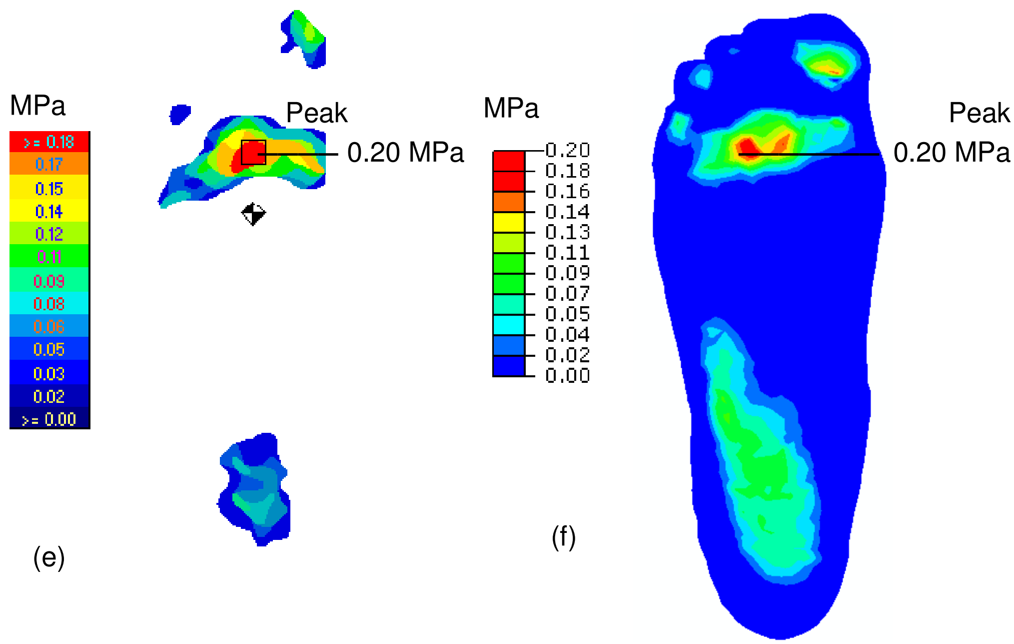

Figure 4-13. Plantar pressure distributions: (a) 1-inch from F-scan measurement, (b) 1-inch from FE prediction, (c) 2-inch from F-scan measurement, (d) 2-inch from FE prediction, (e) 3-inch from F-scan measurement and (f) 3-inch from FE prediction.

The contact area from FE predictions and F-scan measurements both showed slightly reduction with high-heeled foot supports compared to that with flat support, while FE prediction had larger magnitude (Fig. 4-14).

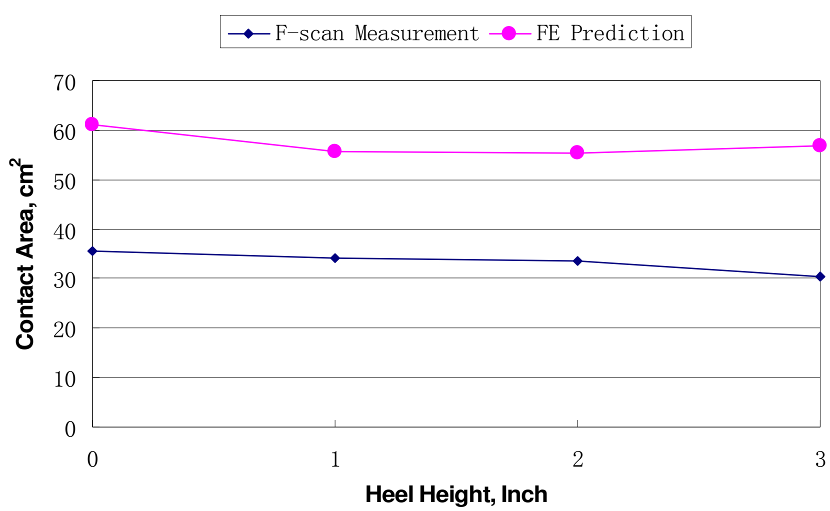

Figure 4-14. Effects of heel height on contact area from FE prediction and F-scan measurement.

There was a general increase in maximum von Mises stress of foot bones with increasing heel height of foot supports from flat to three inches. The peak von Mises stress in major bones with different high-heeled foot supports are compared in figure 4-15. Peak von Mises stress appeared at plantar junction of calcaneal-cuboid joint. In the forefoot region, relatively high von Mises stresses concentrated at the second to the fourth metatarsal shafts as well.

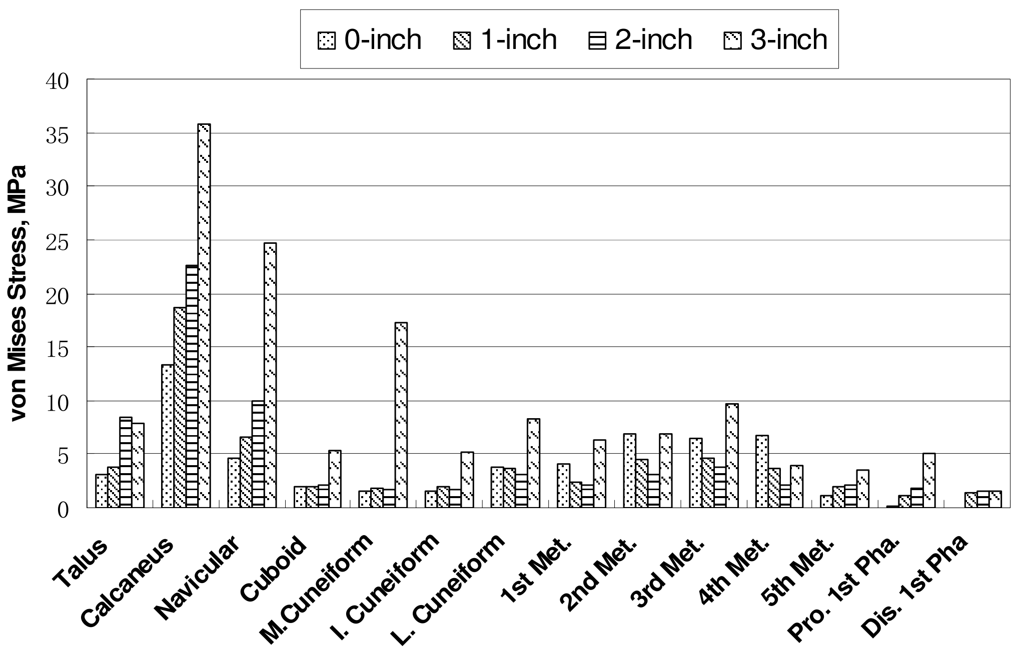

Figure 4-15. FE predicted peak von Mises stress of the foot bones during balanced standing on different high-heeled foot supports.

The FE predicted strain and tension of plantar fascia with different high-heeled foot supports during balanced standing is shown in figure 4-16. At 2-inch high-heeled foot support condition, the strain and total tension force of plantar fascia was minimum in all calculated cases.

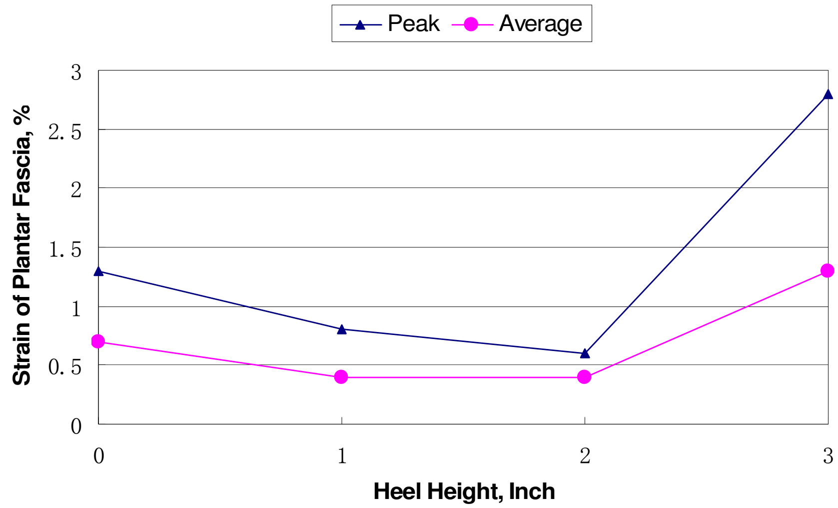

(a)

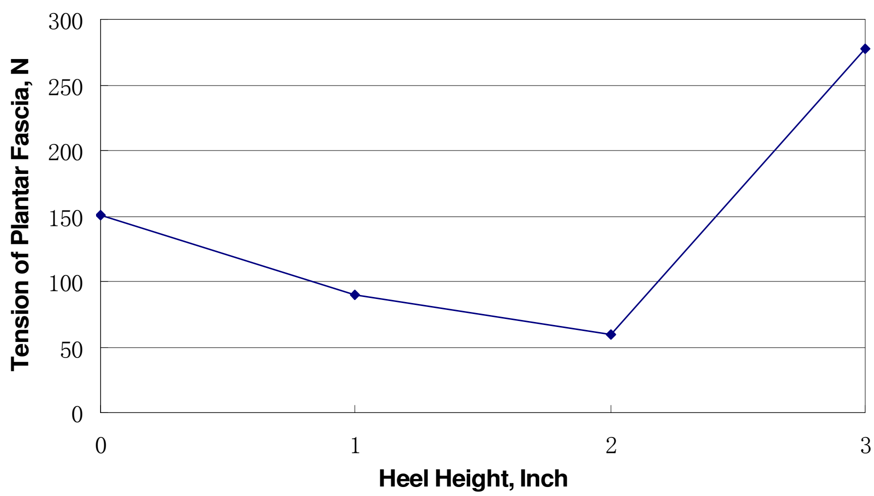

(b)

Figure 4-16. Effects of heel height on plantar fascia: (a) FE predicted peak and average strain and (b) FE predicted total tension force.

Hallux valgus is a common foot problem for the women who wear HHS frequently. Therefore, the effects of heel height on the first MTP joint were investigated. The static weight-bearing contact information like force, area and peak pressure from K-scan measurement and FE prediction was compared in figure 4-17. For peak contact pressure and force, a maximum value was predicted at 2-inch condition while from K-scan measurement the maximum value was at 1-inch condition. With applying

Achilles tendon loading, measured contact peak pressure, force and area increased up to 24%, 13% and 34%, respectively.

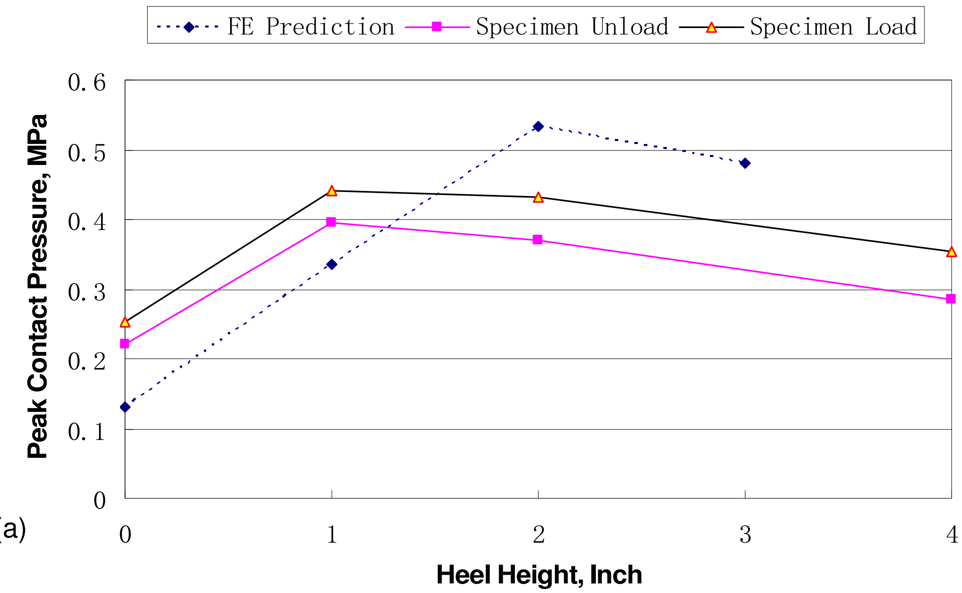

(a)

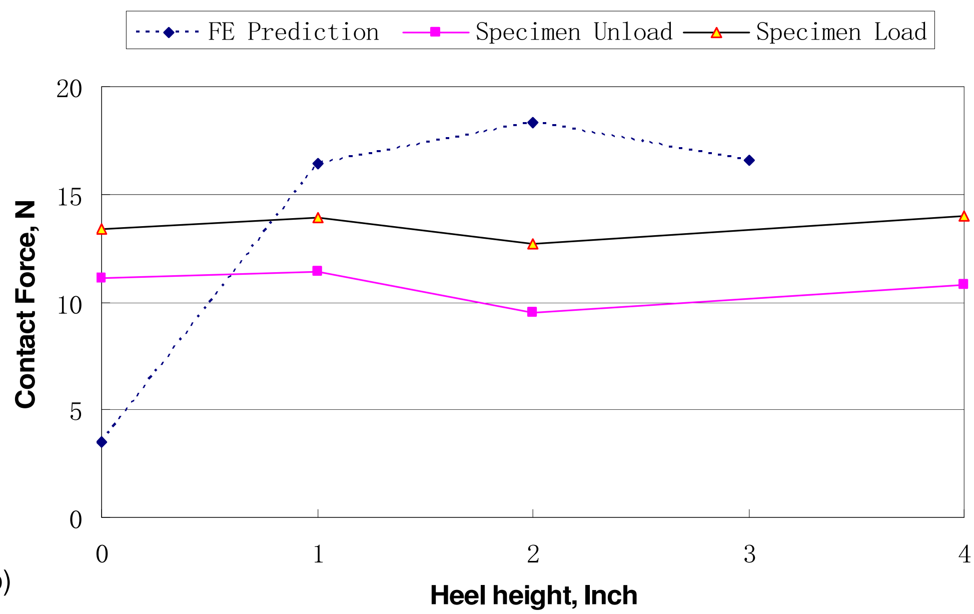

(b)

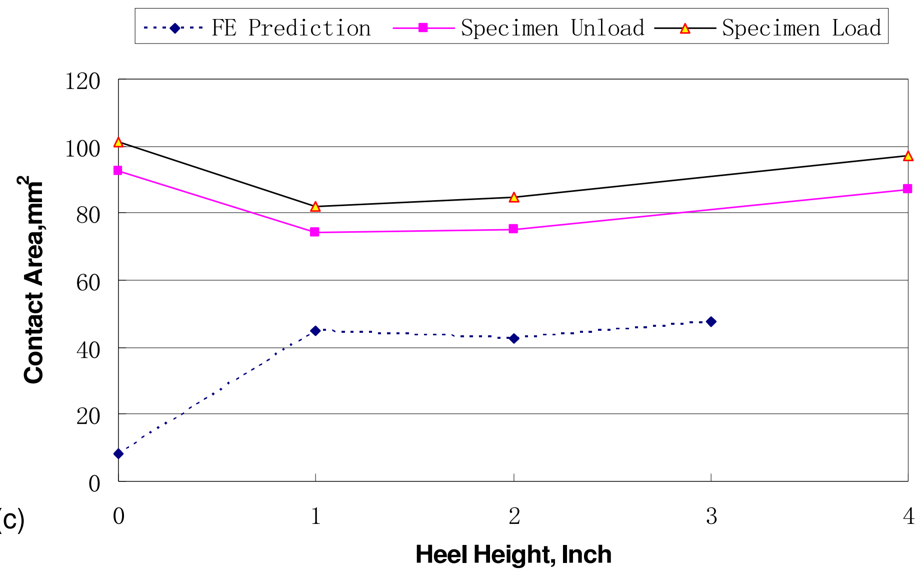

(c)

Figure 4-17. The static weight-bearing contact information comparisons at the first MTP joint between K-scan measurements and FE predictions: (a) peak pressure, (b) contact force and (c) contact area.

During five cyclic sagittal movements with and without 2-inch HHS in cadaveric study, the contact information of the first MTP joint was compared in figure 4-18. A general increase of contact pressure and force was found at with HHS condition.

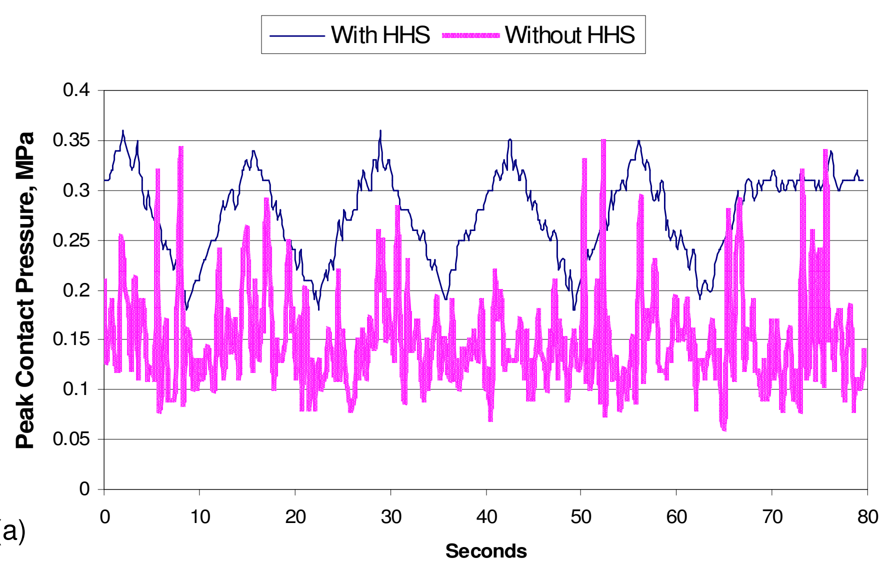

(a)

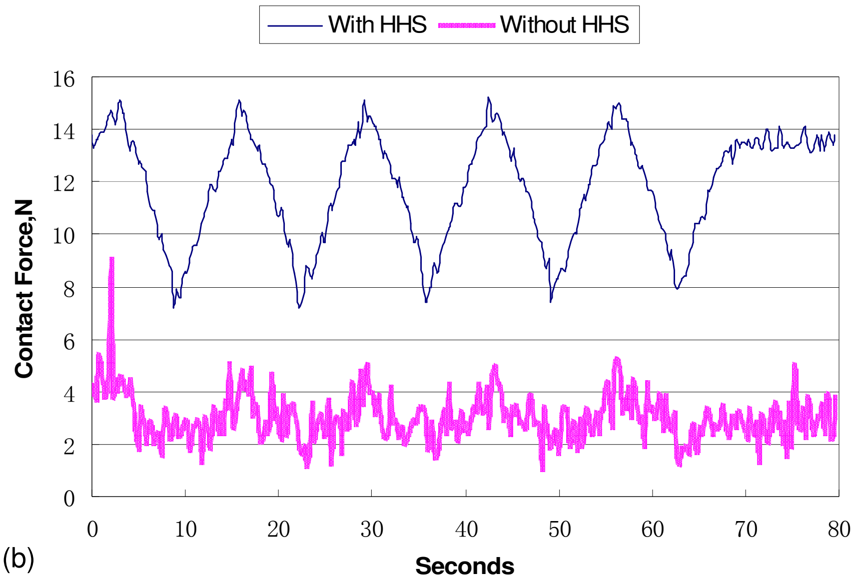

(b)

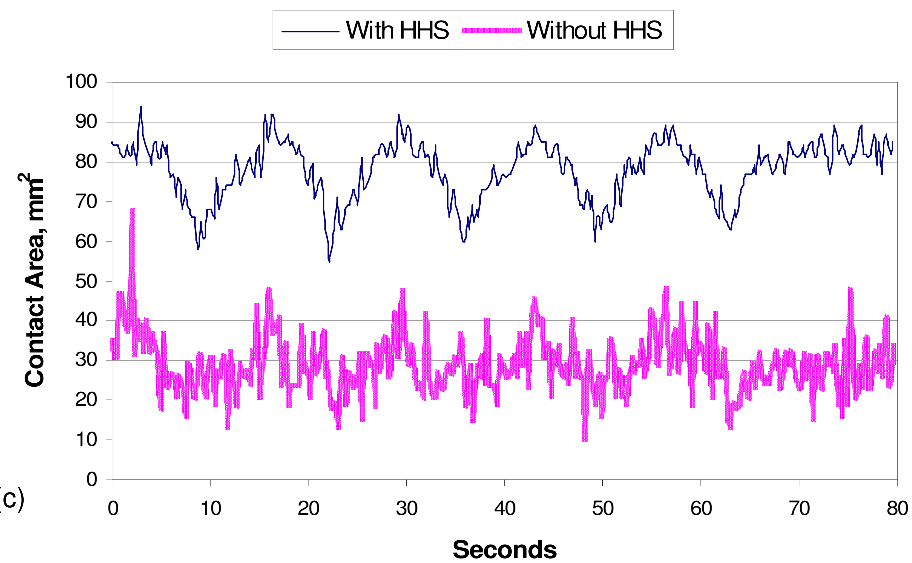

(c)

Figure 4-18. The k-scan measured contact information comparisons at the first MTP joint with and without HHS: (a) peak pressure, (b) contact force and (c) contact area.

During five cyclic sagittal movements with and without 2-inch HHS, the range of motion (ROM) of the first MTP segment (the first phalanx relative to the metatarsal) and ankle joint were monitored at 30 Hz with an optoelectric tracking system (Fig. 4-19). It was found that the first MTP joint had less than 1 degree ROM in the sagittal plane and less than 0.5 degree ROM in the transverse plane (Fig. 4-20). Comparing the FE predictions of static standing on flat support and 2-inch HHS, no noticeable rotation movement in the transverse plane of the first MTP segment was found.

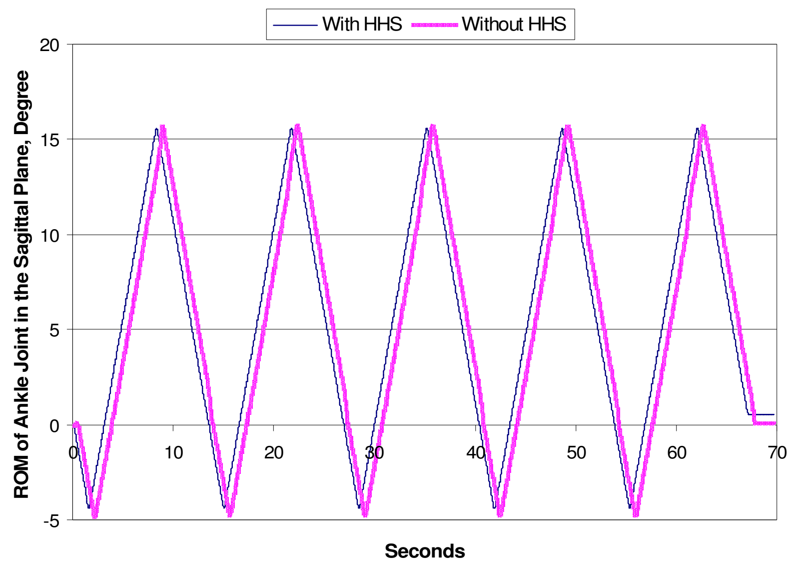

(a)

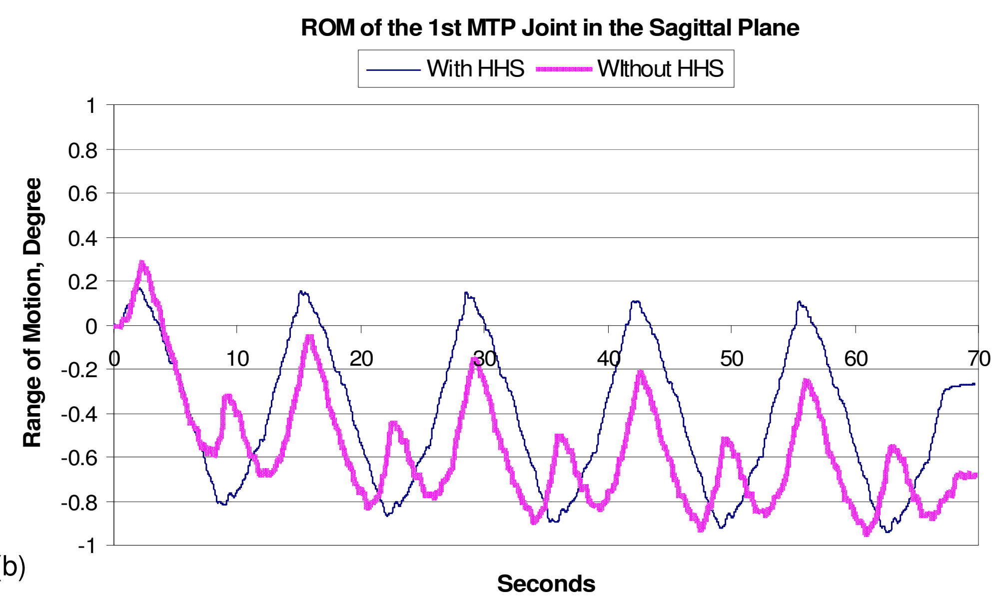

(b)

Figure 4-19. Range of motion in sagittal plane during cyclic sagittal movement: (a) the ankle joint and (b) the first MTP joint.

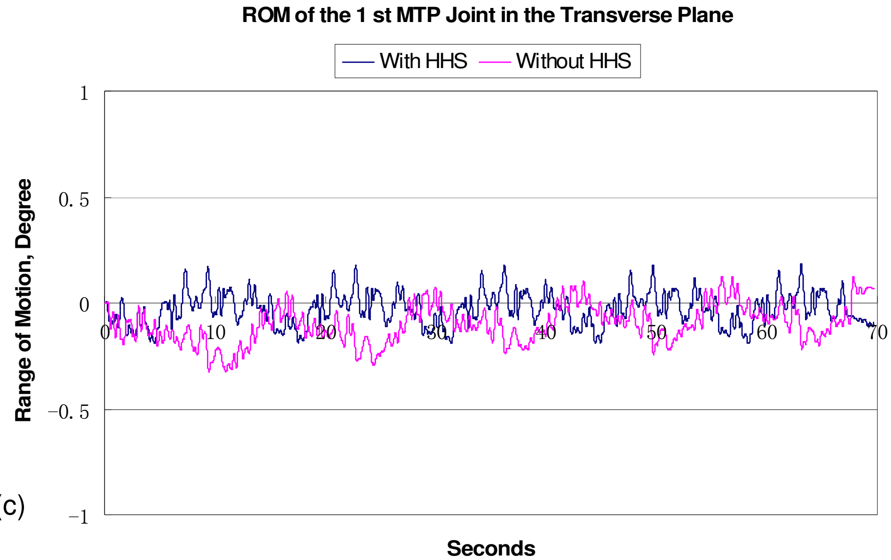

(c)

Figure 4-20. Range of motion in transverse plane of the first MTP joint during cyclic sagittal movement.

4.3 Effects of Outsole Stiffness and Coefficient of Friction on the Foot

4.3.1 Validation of FE Predicted Balanced Standing on HHS

In this study, balanced standing on 2-inch HHS was simulated and validated. The predicted foot deformation with balanced standing on 2-inch HHS is displayed in figure 4-21.

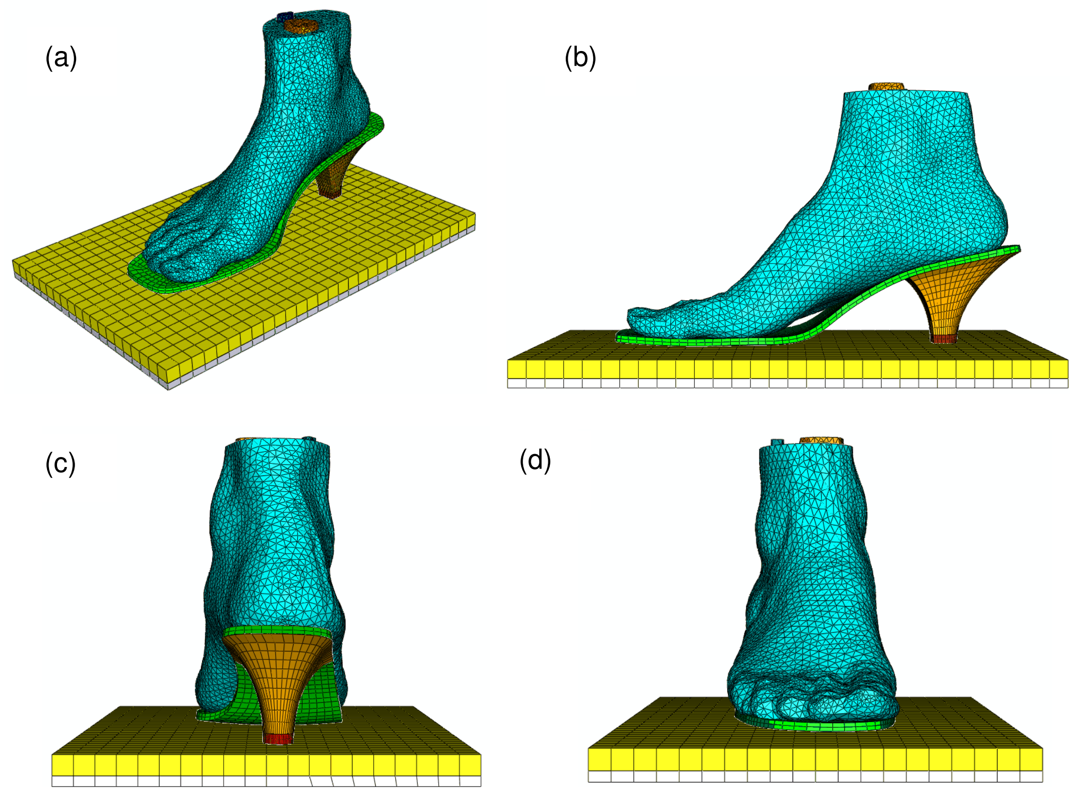

Figure 4-21. Foot on 2-inch HHS: (a) isometric, (b) medial, (c) back and (d) frontal view.

The comparison between plantar pressure distributions obtained from F-scan measurement and FE prediction is shown in figure 4-22. The model had predicted peak plantar pressure of 0.17, 0.07, 0.07, 0.06, 0.06, 0.05, and 0.04 MPa accordingly at the heel region, the first toe region and from the first to the fifth metatarsal head regions, respectively, while the corresponding F-scan measured peak pressure was 0.17, 0.06, 0.05, 0.06, 0.10, 0.07, and 0.02 MPa. The contact areas from FE prediction was 53.7 cm^2, compared to 37.7 cm^2 from F-scan measurement during balanced standing on 2-inch HHS. The COP measured from force platform was 35 mm anterior and 14 mm lateral from the lateral malleolus. Under the same loading condition of 2-inch foot support, the predicted COP was 2 mm anterior deviation and 1 mm medial deviation from the applied GRF location. The predicted arch was decreased by 5.9 mm during balanced standing with high-heeled support.

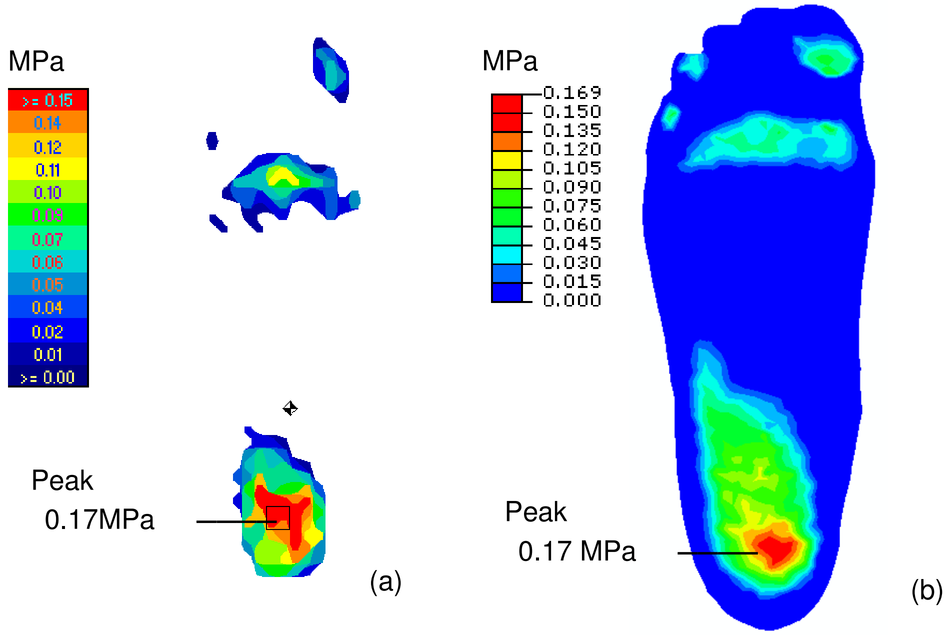

Figure 4-22. Plantar pressure distributions on 2-inch HHS: (a) F-scan measurement, (b) FE prediction.

Figure 4-23 depicts the von Mises stress of the foot bones during balanced standing on 2-inch HHS. The peak von Mises stress occurred at the plantar junction of calcaneal-cuboid joint as well.

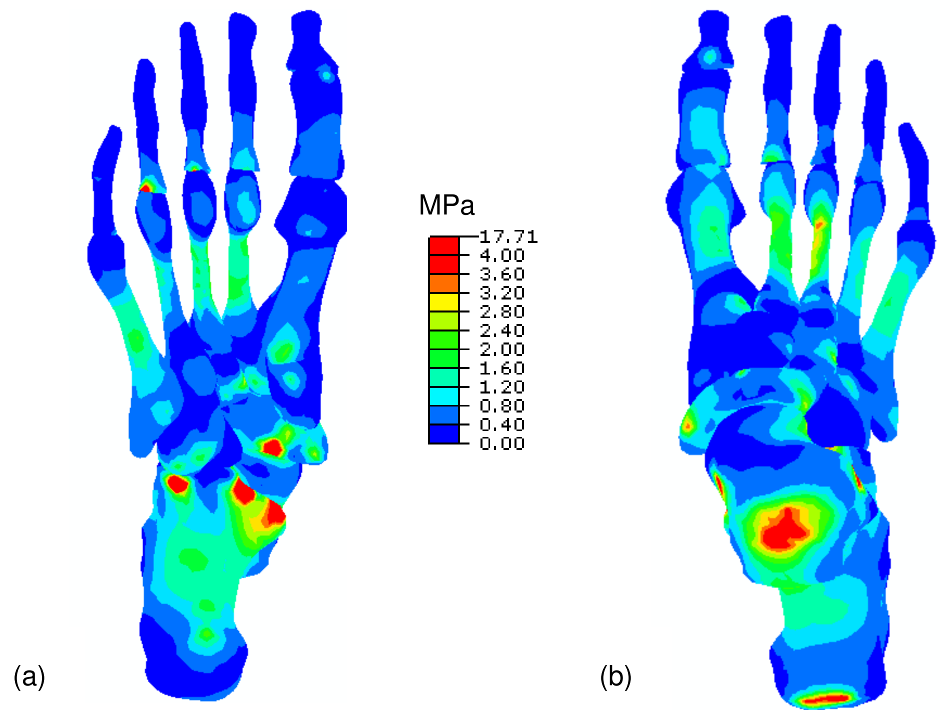

Figure 4-23. FE predicted von Mises stress of the foot bones with 2-inch HHS standing: (a) bottom and (b) top view.

4.3.2 Effects of Outsole Stiffness

Without shankpiece condition, figure 4-24 shows the effects of outsole stiffness on the whole foot/shoe deformations. The heel region of foot was found kept the same position relative to the HHS in all cases calculated from the FE predictions, while deformation of outsole at the connective edge between heel base and outsole was found with softer outsole.

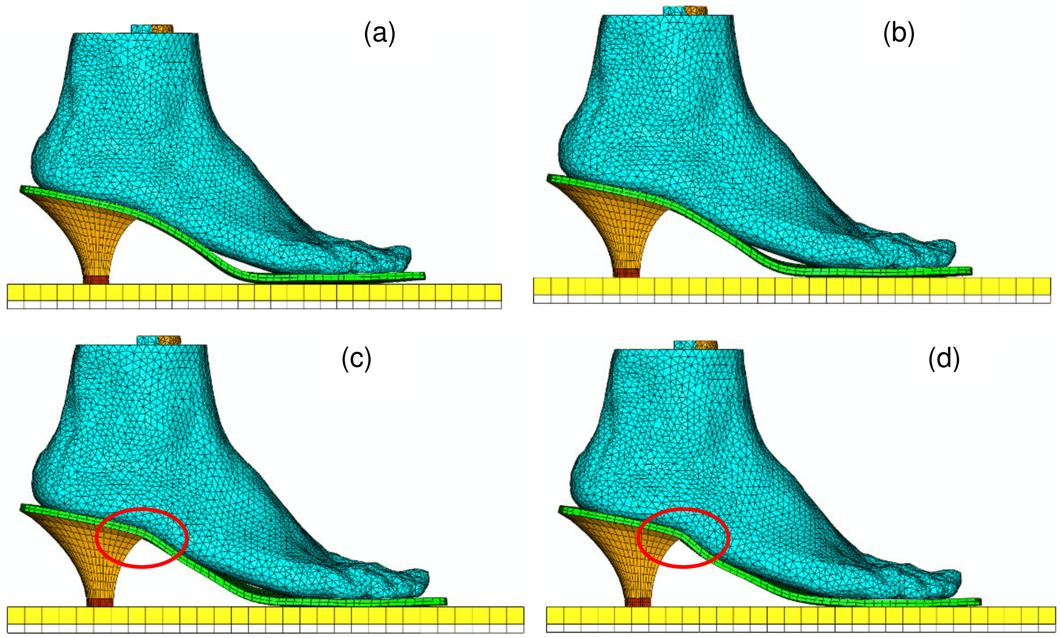

Figure 4-24. Foot deformations with different stiffness outsoles (without shankpiece condition): (a) HDPE outsole, (b) TPR outsole, (c) PU outsole and (d) EVA outsole.

Figure 4-25 shows the effects of the outsole stiffness on the predicted plantar pressure distributions. The peak pressure kept almost the same location with magnitude around 0.16 MPa. The contact areas of plantar foot had no obvious change with different stiffness outsoles conditions (Fig. 4-26).

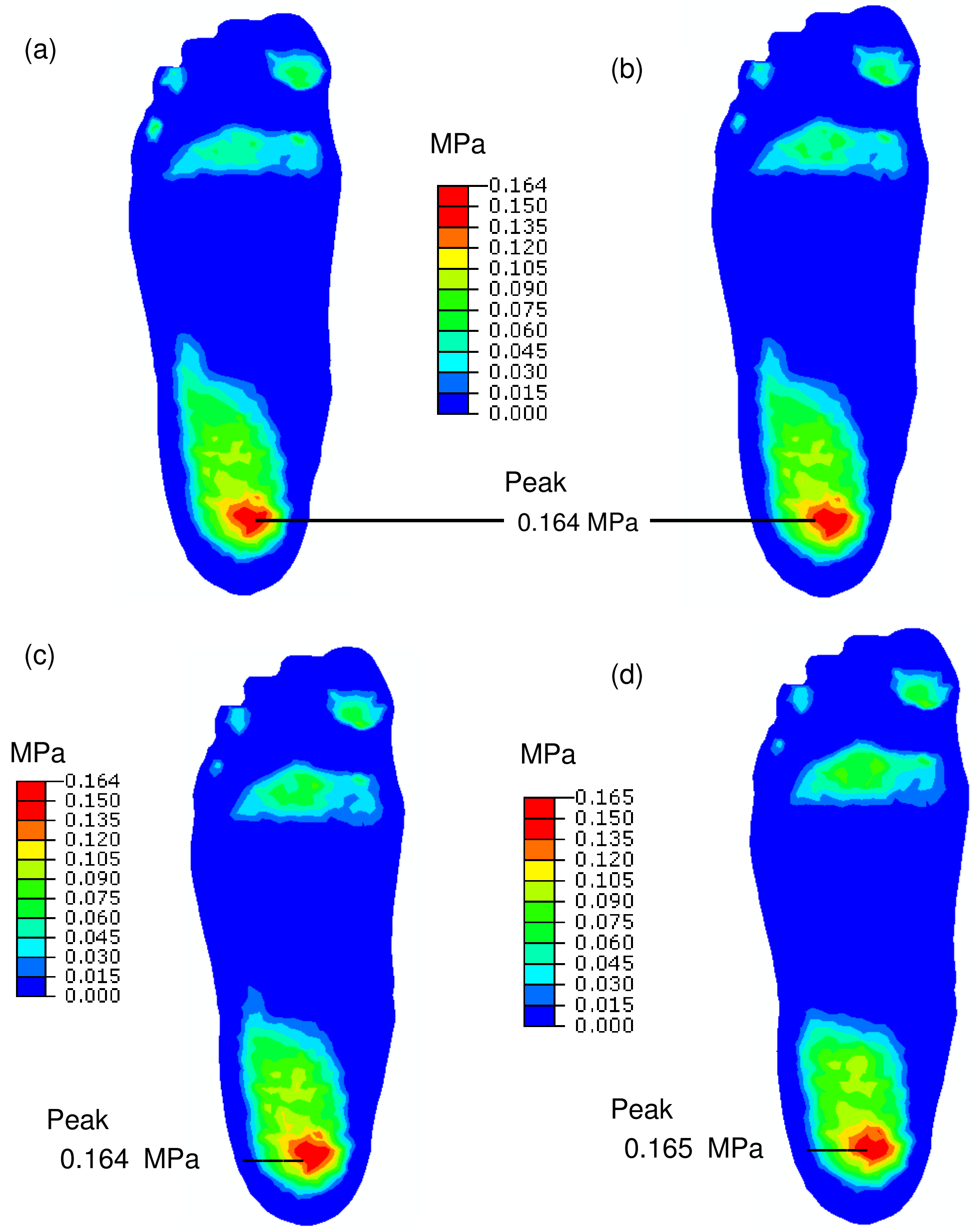

Figure 4-25. Plantar pressure distributions with different outsole stiffness(without shankpiece condition): (a) HDPE outsole, (b) TPR outsole, (c) PU outsole and (d) EVA outsole.

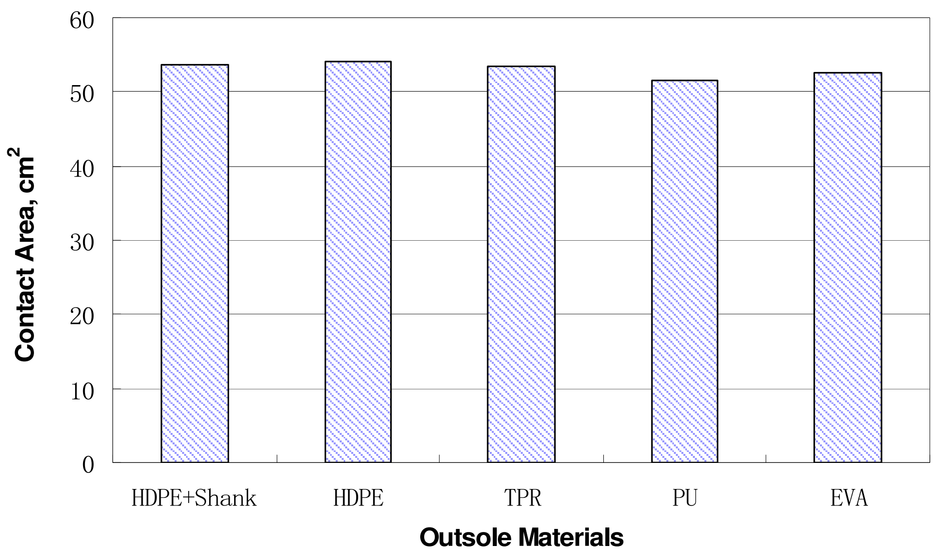

Figure 4-26. Contact area of plantar foot with different outsoles.

The predicted peak and average strain on plantar fascia slightly were reduced for HDPE and TPR outsole conditions, while increased up to 9.9% using much softer outsole (PU and EVA) (Fig. 4-27). Total tension forces of plantar fascia increased significantly up to 16.6% for EVA outsole condition (Fig. 4-28).

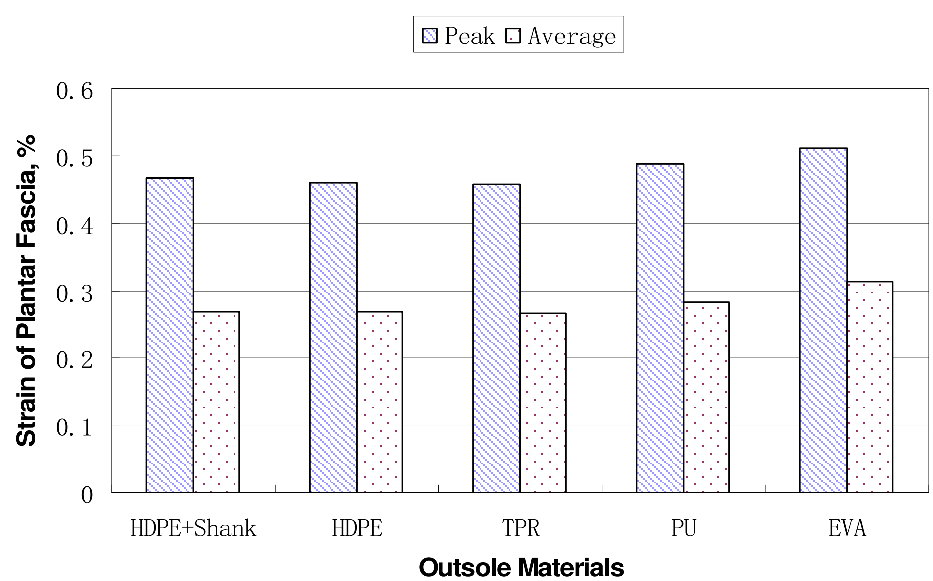

Figure 4-27. Peak and average strain of plantar fascia with different outsoles.

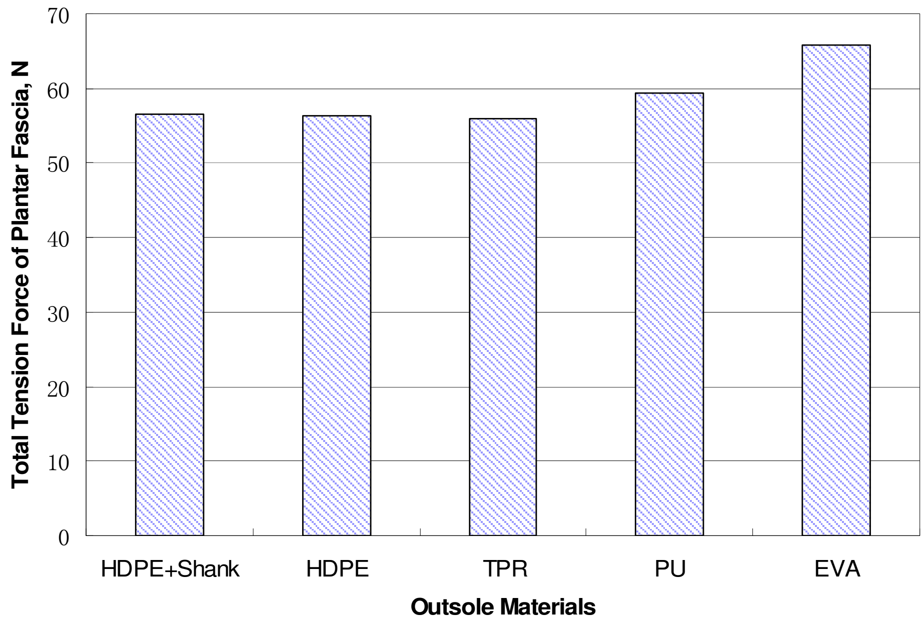

Figure 4-28 Total tension force of plantar fascia with different outsoles.

Figure 4-29 depicts the von Mises stress of the foot bones during balanced standing on HHS with different outsole stiffness. The von Mises stress distributions' patterns of bony structures in all calculated cases were in general similar. The peak von Mises stress in rearfoot bones had decreased trend and central metatarsal bones had increased trend with the reduction of outsole stiffness.

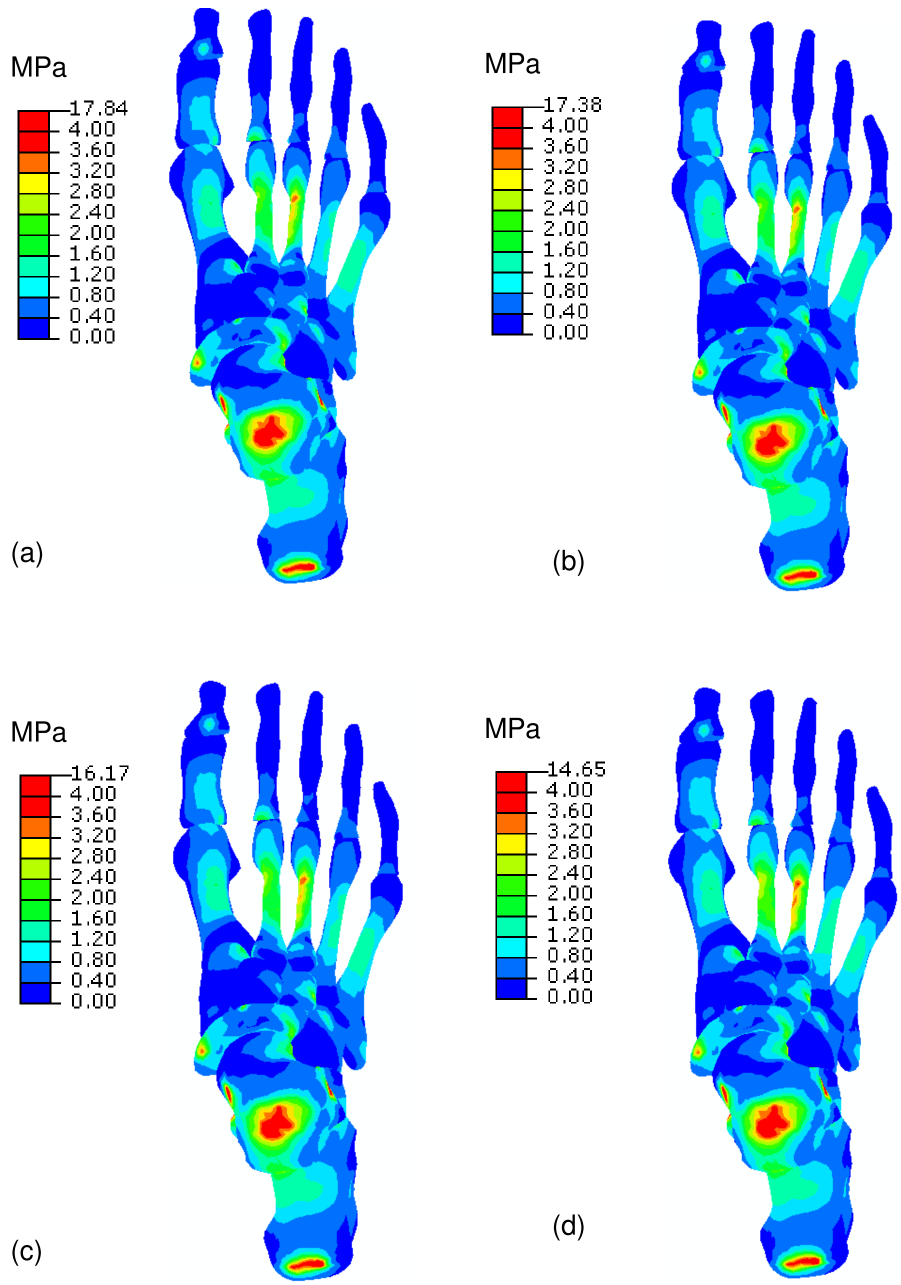

Figure 4-29. FE predicted von Mises stress of the foot bones with different outsole stiffness (without shankpiece condition): (a) HDPE outsole, (b) TPR outsole, (c) PU outsole and (d) EVA outsole.

Figure 4-30 depicts the von Mises stress in the outsole with different stiffness (1000 MPa to 5 MPa) during balanced standing with and without steel shankpiece conditions.

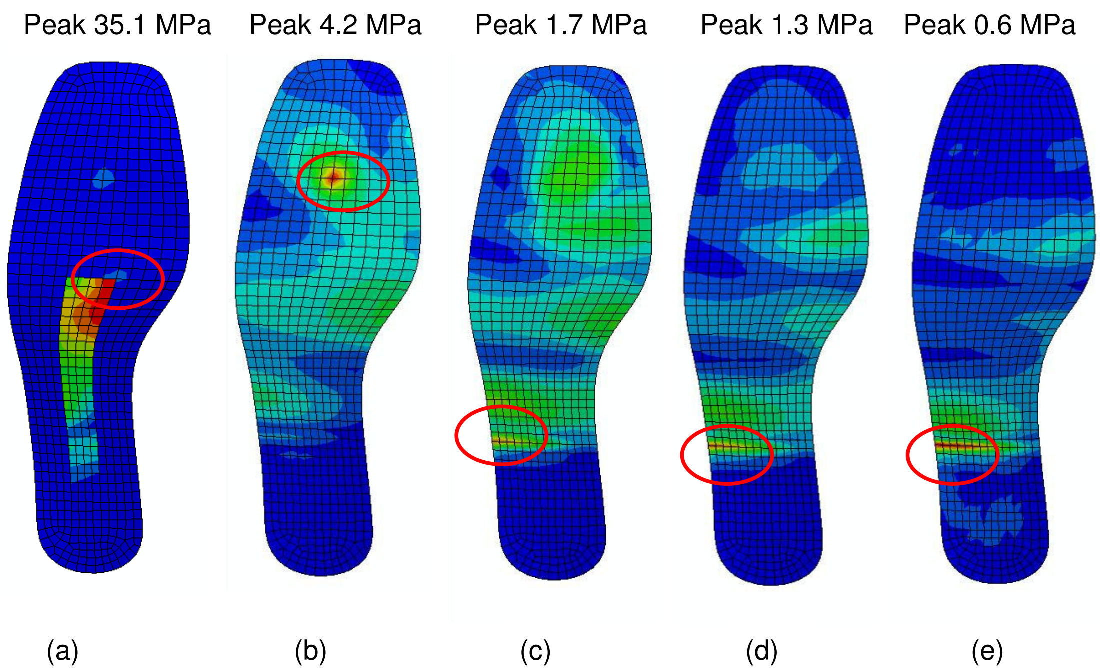

Figure 4-30. FE predicted von Mises stress in the outsole: (a) HDPE with shankpiece, (b) HDPE only, (c) TPR only, (d) PU only and (e) EVA only.

Figure 4-31 depicts the von Mises stress in the outsole with different stiffness (1000 to 5 MPa) during balanced standing with steel shankpiece conditions. It was found that steel shankpiece sustained most of the loading of outsole during balanced standing.

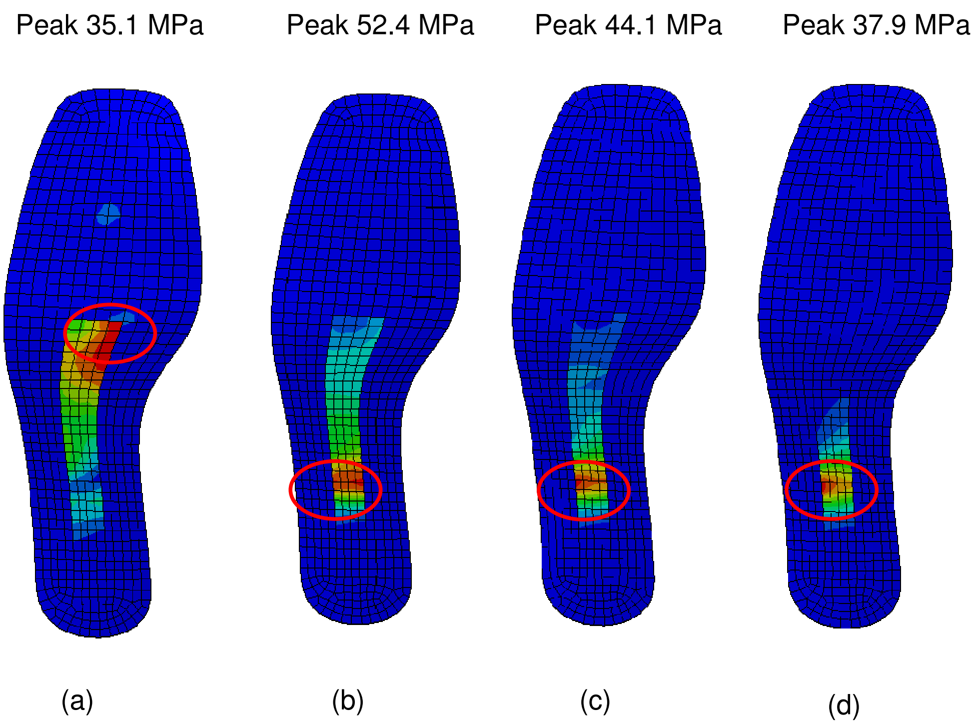

Figure 4-31. FE predicted von Mises stress in the outsole with shankpiece: (a) HDPE, (b) TPR, (c) PU and (d) EVA.

4.3.3 Effects of Coefficient of Friction

In this sensitivity study, the effects of frictional properties were conducted. With assigning different coefficient of friction of 0.6, 0.4 and 0.2, the shear stress distributions of plantar foot in M-L direction and A-P direction are depicted in figure 4-32. With the reduction of coefficient of friction, the peak shear stress reduced, while the peak plantar pressures were the same about 0.17 MPa with less than 1.8% increase.

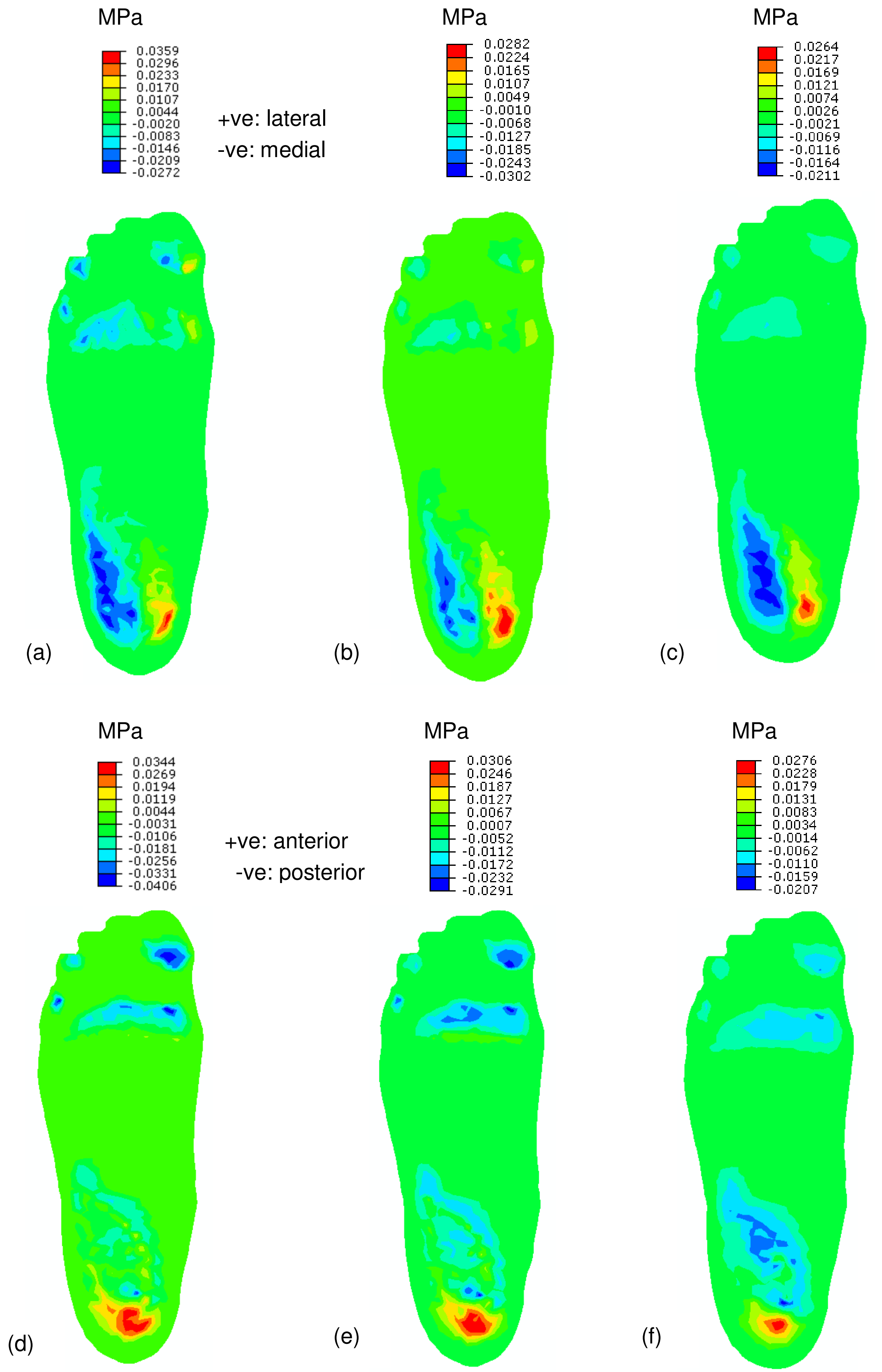
MPa
0.0359
0.0296
0.0233
0.0170
0.0107
0.0044
-0.0020
-0.0083
-0.0146
-0.0209
-0.0272
+ve: lateral
-ve: medial
MPa
0.0282
0.0224
0.0165
0.0107
0.0049
-0.0010
-0.0068
-0.0127
-0.0185
-0.0243
-0.0302
MPa
0.0264
0.0217
0.0169
0.0121
0.0074
0.0026
-0.0021
-0.0069
-0.0116
-0.0164
-0.0211
(a)
(b)
(c)
MPa
0.0344
0.0269
0.0194
0.0119
0.0044
-0.0031
-0.0106
-0.0181
-0.0256
-0.0331
-0.0406
+ve: anterior
-ve: posterior
MPa
0.0306
0.0246
0.0187
0.0127
0.0067
0.0007
-0.0052
-0.0112
-0.0172
-0.0232
-0.0291
MPa
0.0276
0.0228
0.0179
0.0131
0.0083
0.0034
-0.0014
-0.0062
-0.0110
-0.0159
-0.0207
(d)
(e)
(f)

Figure 4-32. Shear stress distributions of plantar foot in M-L direction with different coefficient of friction: (a) 0.6, (b) 0.4 and (c) 0.2; in A-P direction with different coefficient of friction: (d) 0.6, (e) 0.4 and (g) 0.2.

Contact area slightly increased 0.3% from 53.7 cm^2 to 55.2 cm^2 with the reduction of coefficient of friction. No obvious forward slippage (maximum slippage distance <1 mm) was found with the reduction of coefficient of friction. The GRF in A-P direction and M-L direction are shown in figure 4-33. The GRF in A-P direction increased 55.5% with the reduction of coefficient of friction from 0.6 to 0.2.

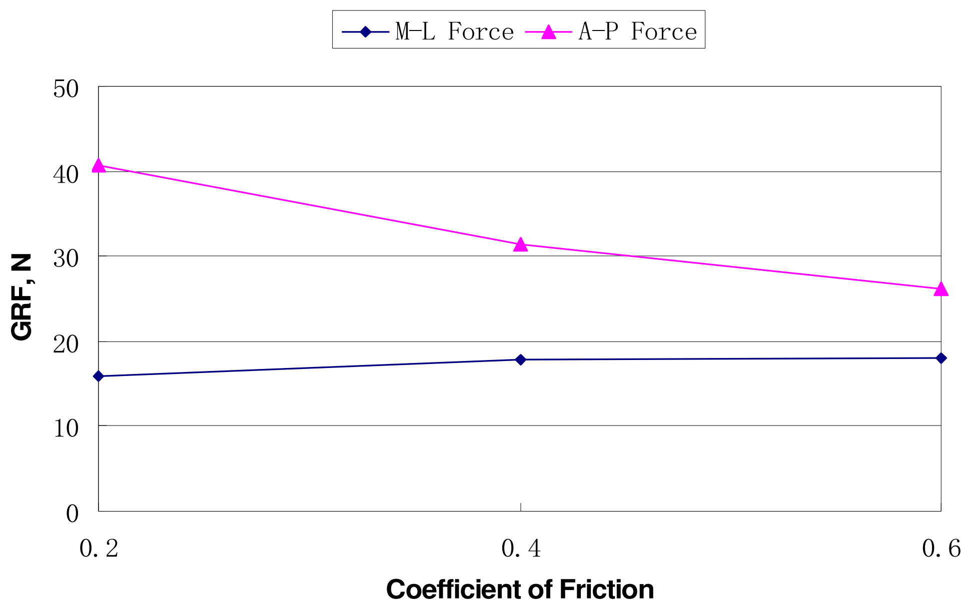

Figure 4-33. Ground reaction forces in A-P direction and M-L direction with different coefficient of friction (0.6, 0.4, and 0.2).

4.4 Walking with High-heeled Shoes

4.4.1 FE Simulation on Mid-stance Phase

In this study, the mid-stance phase during walking with 2-inch HHS was simulated by applying same loading steps but with different magnitude of musculotendon forces and location of GRF. With the total GRF maintained at 513 N (95% of BW), Achilles tendon forces was applied based on the sensitivity study on the effect of Achilles tendon force from 100% to 200% of half BW (270 N), at interval of 5%. It was found that Achilles tendon force of 155% of half BW was proper in term of the closest of centre of GRF. Only the Achilles tendon tension was considered on the sensitivity study while all intrinsic and the rest of the extrinsic muscle forces were neglected because triceps surae played a major role in the control of COP in A-P direction.

The comparison between plantar pressure distributions obtained from F-scan measurement and FE prediction is shown in figure 4-34. The model predicted peak plantar pressure of 0.23, 0.07, 0.16, 0.09, 0.13, 0.12, and 0.08 MPa accordingly at the heel region, the first toe region and from the first to the fifth metatarsal head regions, respectively, while the corresponding F-scan measured peak pressure were 0.22, 0.09, 0.08, 0.09, 0.18, 0.11, and 0.04 MPa. The contact area from FE prediction was 69.1 cm^2, compared to 43.4 cm^2 from F-scan measurement at mid-stance phase of gait with 2-inch HHS. The center of GRF measured from foot platform was 49 mm anterior, 15 mm lateral from the lateral malleolus. The predicted center of GRF was less than 3 mm anterior deviation and 3 mm medial deviation from the applied GRF location.

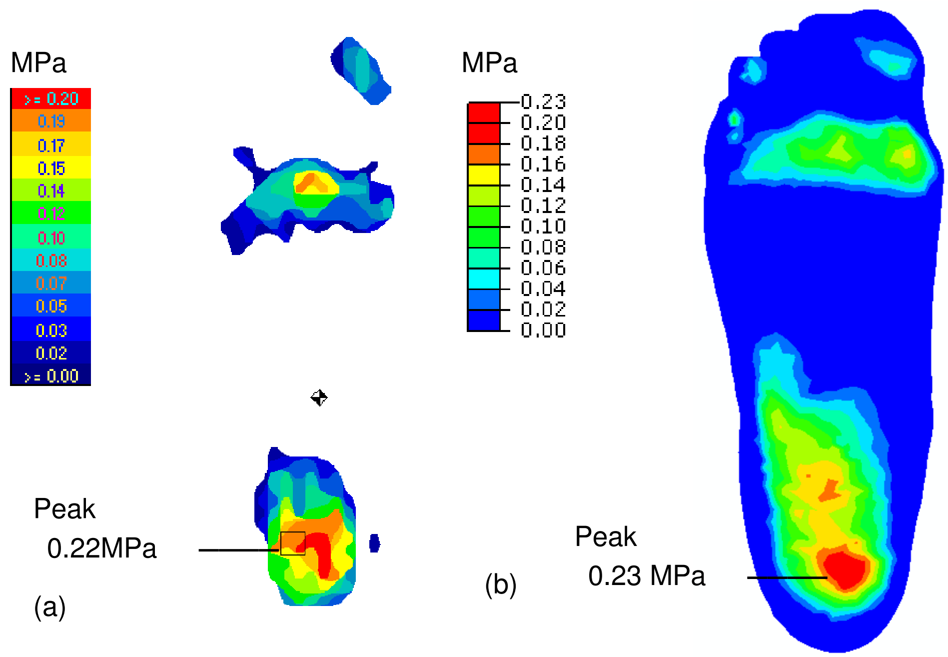

Figure 4-34. Plantar pressure distributions at mid-stance phase of gait with 2-inch HHS: (a) F-scan measurements and (b) FE prediction.

Peak A-P shear stress of 55.8 KPa was predicted at the posterior heel region and peak M-L shear stress of 48.2 KPa was predicted at the medial heel region (Fig. 4-35). In the forefoot region, peak shear stress of 38.7 KPa in A-P direction and 31.7 KPa in M-L direction were predicted around the soft tissue beneath the forefoot, especially at the first metatarsal head.

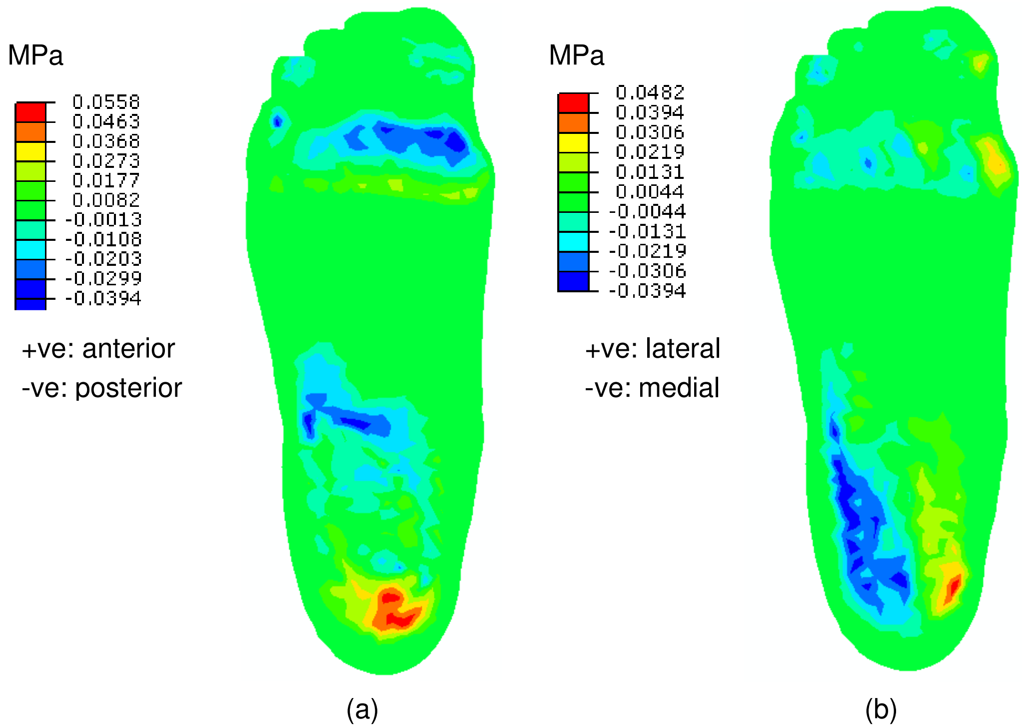

Figure 4-35. FE predicted plantar shear stresses: (a) A-P direction and (b) M-L direction.

Figure 4-36 depicts the von Mises stress of the foot bones at mid-stance phase of gait with 2-inch HHS. Major bony stresses at balanced standing and mid-stance phase were compared in figure 4-37.

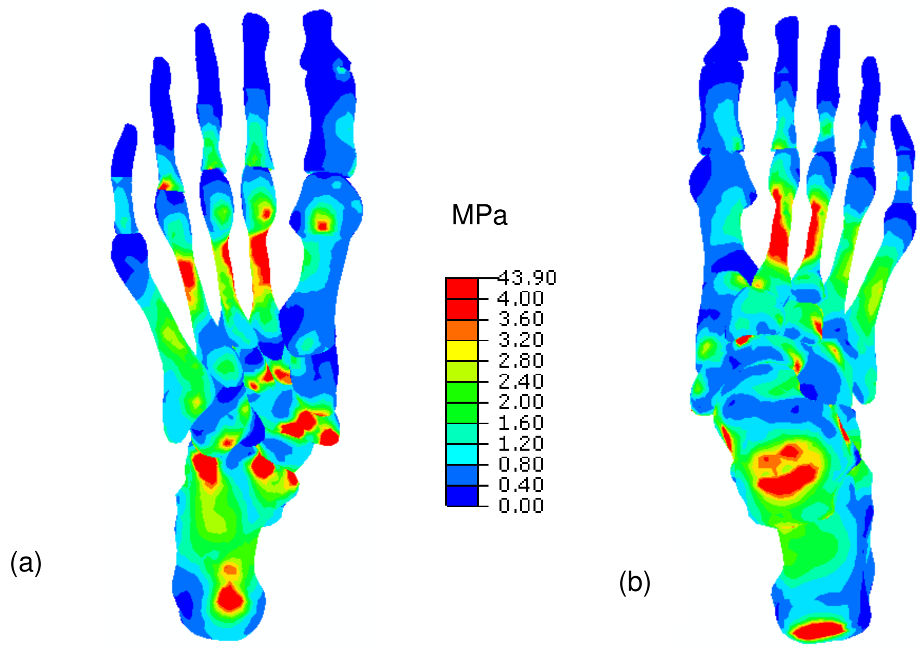

Figure 4-36. FE predicted von Mises stress of the foot bones at mid-stance phase of gait with 2-inch HHS: (a) bottom and (b) top view.

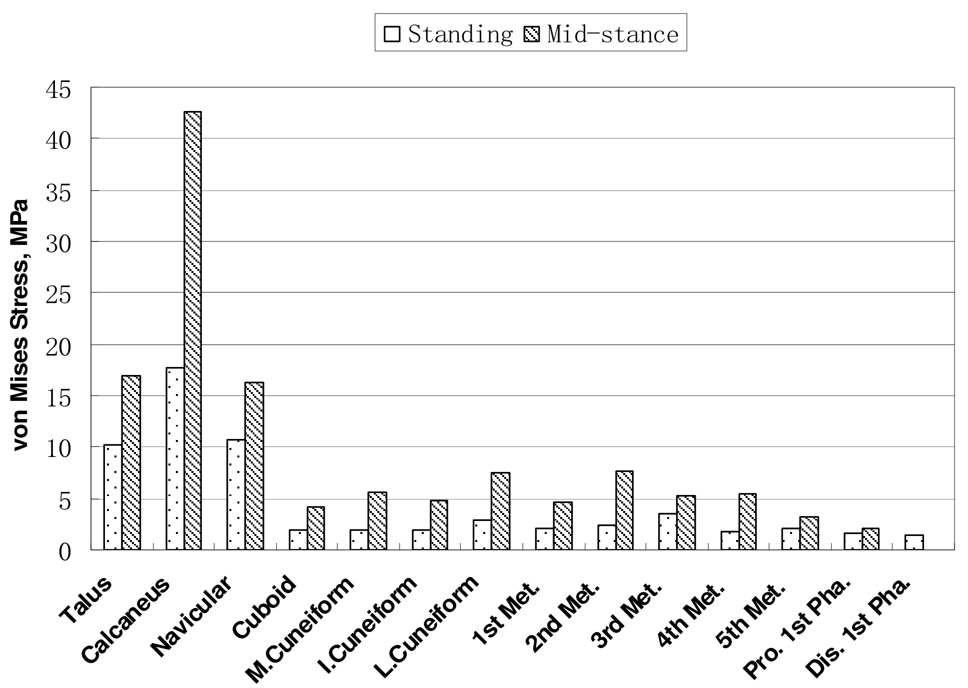

Figure 4-37. FE predicted von Mises stresses of foot bony structures at standing and mid-stance.

The predicted medial longitudinal arch was decreased by 11.7 mm at mid-stance phase. The predicted peak and average strain on five rays of plantar fascia segment ranged was 1.6% and 0.9%, respectively. Total tension forces of plantar fascia were 198 N.

4.4.2 Gait Analysis Experiment

After walking with each shoe condition, subjective ratings related to comfort were completed by totally five subjects. One way ANOVA using Student-Newman-Keuls adjustment for post hoc multiple comparisons was performed on subjective questionnaires.

Table 4-1. Subjective comfort ratings across heel conditions.

Body Area	Subject ratings Least (0)-------Most(6)			Main Effects	
	Flat Mean (SD)	2-inch Mean (SD)	4-inch Mean (SD)	F Value	P Value
Easiness in walking	4.8(0.4)	5(0.7)	3.9(1.5)**	60.286	0.0000
Easiness in balancing	5.2(0.8)	4.6(1.1)	4.1(1.6)**	9.879	0.0029
Total comfort	3.6(1.1)	4.6(0.5)	3.2(1.6)**	16.750	0.0003
Plantar forefoot comfort	4.2(0.4)	4.0(1.0)	3.0(1.8)**	28.737	0.0000
Plantar heel comfort	3.8(1.3)	4.4(0.9)	3.6(1.2)**	4.500	0.0348
Dorsal vamp region comfort	1.4(1.1)	3.4(1.1)	2.1(1.5)*	3.714	0.0555
Heel counter comfort	4.0(1.2)	4.0(1.0)	3.7(1.0)	1.000	0.3966
Toe comfort	2.0(1.0)	3.4(1.5)	2.5(1.2)	2.457	0.1275
Knee comfort	4.4(0.5)	4.2(0.8)	3.9(0.9)**	5.733	0.0179
Lower back comfort	4.4(0.5)	4.4(0.5)	4.1(0.7)	2.286	0.1442

**Significantly different from both other conditions in post hoc tests ($p<0.05$).

*Significantly different from 2-inch conditions in post hoc tests ($p<0.05$).

The foot pressure distributions, kinematic data and GRF of the subject who volunteered for MRI scan were analyzed for FE loading condition. The gait kinematic data was analyzed (Table. 4-2).

Table 4-2. Temporal data of high-heeled gait.

Measure	Flat Mean (SD)	2-inch Mean (SD)	4-inch Mean (SD)	p Value
Cadence (steps/min)	87.41 (1.75)	87.83 (1.69)	88.48 (1.80)	0.630
Stride length (m)	1.15 (0.01)	1.14 (0.02)	1.17 (0.03)	0.102
Velocity (m/sec)	0.84 (0.02)	0.83 (0.01)	0.86 (0.02)*	0.029
% Stance	63.11 (0.78)	63.42 (1.54)	65.33 (1.80)	0.063

* Significantly different from 2-inch conditions in post hoc tests ($p<0.05$).

Ground reaction forces in vertical and A-P direction with different HHS were tabulated in Table 4-3. Fz1 represents the first peak vertical GRF during stance, Fz2 represents the second peak vertical GRF during stance, Fzmin represents the minimum vertical GRF between the first and second peak vertical GRF during stance.

Table 4-3. GRF variables across heel conditions.

Measure	Flat Mean (SD)	2-inch Mean (SD)	4-inch Mean (SD)	p Value
Maximal Braking Force	-0.12(0.01)	-0.14(0.01)	-0.14(0.02)#	0.045
Maximal Propulsive Force	0.15(0.00)	0.18(0.01)**	0.15(0.01)	0.000
Fz1	1.10(0.03)	1.14(0.02)**	1.07(0.02)	0.004
Fz2	1.17(0.03)	1.20(0.01)	1.00(0.02)**	0.000
Fzmin	0.97(0.02)	0.95(0.03)	0.84(0.02)**	0.000

** Significantly different from both other conditions in post hoc tests ($p<0.05$).

* Significantly different from 2-inch conditions in post hoc tests ($p<0.05$).

Significantly different from 0-inch conditions in post hoc tests ($p<0.05$).

Peak plantar foot pressure during walking obtained from F-scan measurement is compared in figure 4-38. It was found that peak pressure in the heel region decreased significantly ($p<0.05$) with the HHS. Pressure-time integral of forefoot increased significantly ($p<0.05$) with heel height increase (Fig. 4-39).

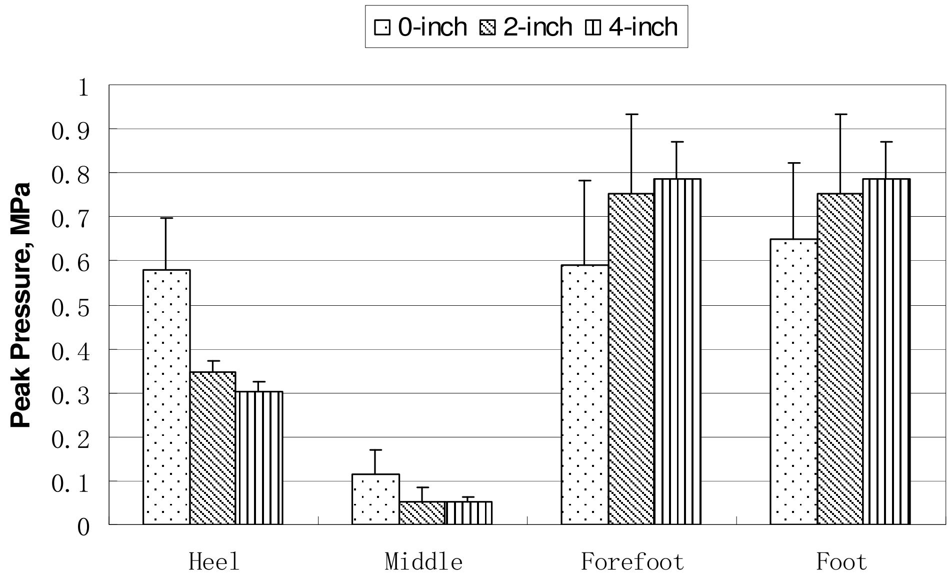

Figure 4-38. Peak pressure during walking with different heel height shoes.

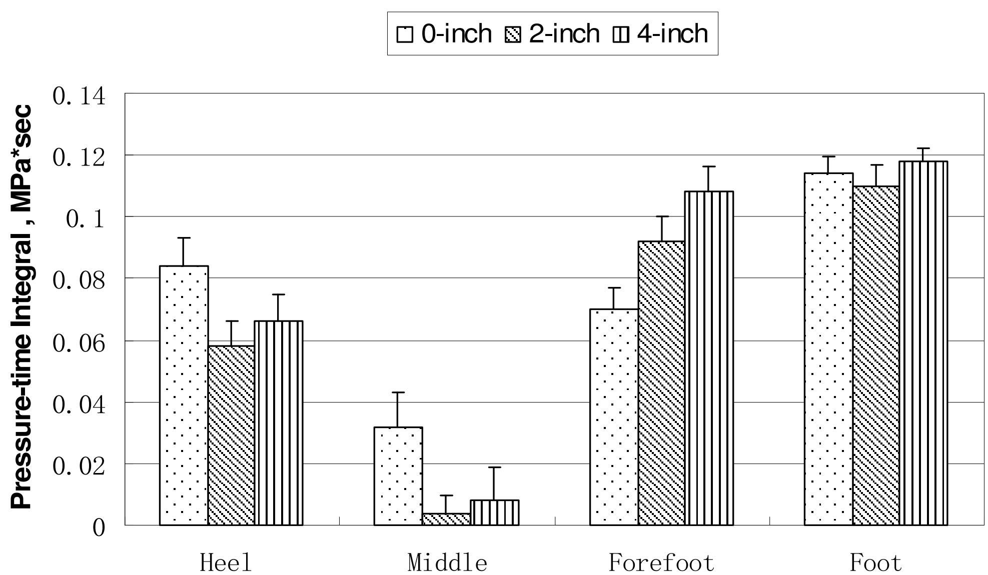

Figure 4-39. Pressure-time integral during walking with different heel height shoes.

The maximum contact areas during walking of heel, midfoot and forefoot regions are compared in figure 4-40. It was found that maximum contact areas of the forefoot and the midfoot region of 0-inch condition were significantly different ($p<0.05$) from both other conditions in post hoc tests, while maximum contact area of the heel region of 4-inch condition was significantly different ($p<0.05$) from both other conditions in post hoc tests.

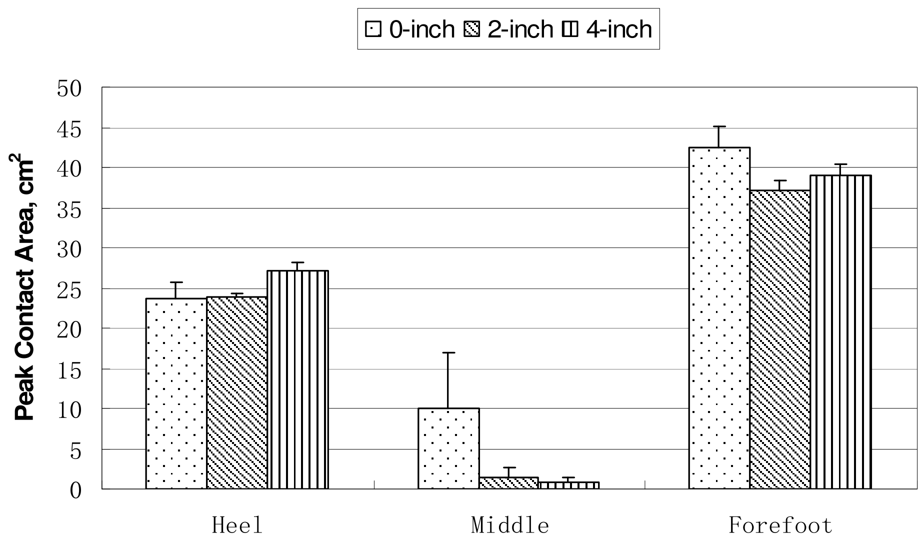

Figure 4-40. Maximum contact area of foot during walking with different heel height shoes.

Dorsal pressure distributions of foot were obtained from Tekscan systems. Peak pressures and forces at the medial and dorsal region of the first ray were significantly different ($p<0.05$) among all conditions (Fig. 4-41).

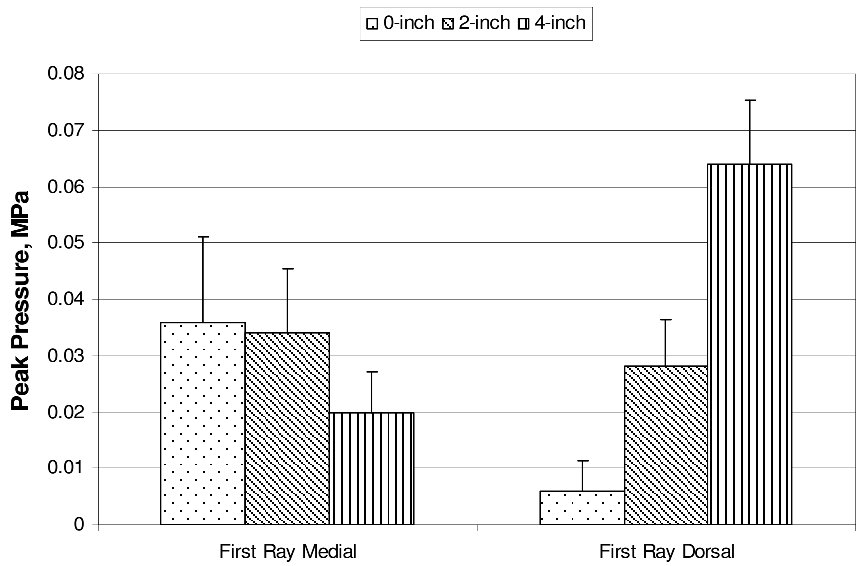

(a)

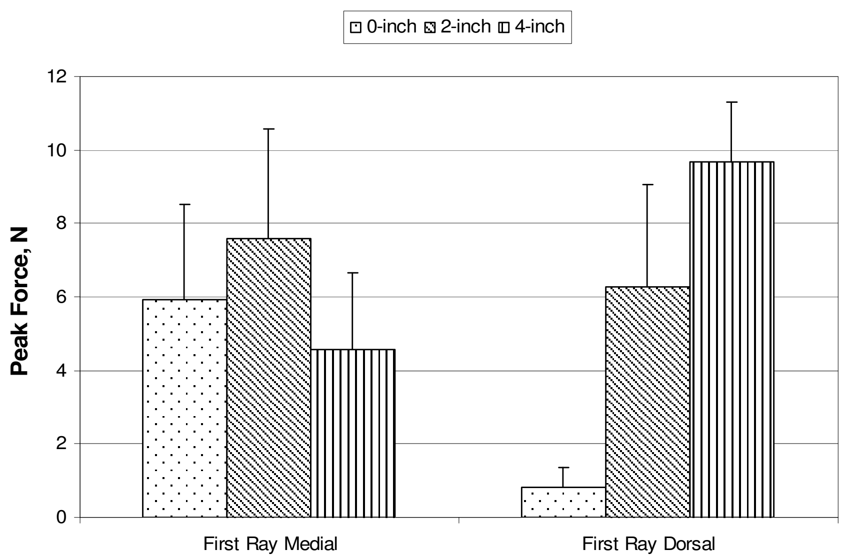

(b)

Figure 4-41. Dorsal contact at the first ray: (a) peak pressure and (b) peak force.

CHAPTER V DISCUSSION

Well validated computational model is a powerful tool which could predict plantar contact pressure as well as internal stresses within the bony and soft tissue structures. Combinations of FE modelling and experimentation have been extensively used, and proved to be effective to study the biomechanical behavior of the ankle–foot complex and supports. This is certainly a prerequisite to further enhance the understanding of foot/footwear biomechanics and the design of proper footwear.

5.1 Validation of FE Model of Foot

5.1.1 Balanced Standing on Flat Support

To validate the FE model of a female foot, the loading condition of balanced standing with flat support was firstly employed. Achilles tendon forces play an important role in the control of COP in A-P direction. Achilles tendon forces of 75% of the total weight on the foot (270N) were found to provide the closest match of the measured COP of the subject during balanced standing. Achilles tendon force of 75% of the total weight during balanced standing was comparable to the analytical assumptions (Kim and Voloshin, 1995; Arangio et al., 2000) which estimated Achilles tensions ranging from about half to two-third the weight on the foot. This loading condition was consistent with the reported results by Cheung et al. (2004).

The FE predicted plantar pressure distribution pattern was, in general, comparable to experiment measurement from pressure sensitive sensors. The high plantar pressure from F-scan measurement and FE prediction both concentrated at the central heel region and metatarsal heads. However, the predicted value of peak pressure was 9.5% higher than that of F-scan measurement.

The difference in resolution between pressure measurement and the FE prediction and the actual minimal load threshold of the F-scan system may influence the reading. Having a spatial resolution of 4 sensors per cm^2, F-scan sensors recorded an average pressure for an area of 25 mm^2. By contrast, the FE analysis provided solutions of nodal contact pressure rather than an average pressure calculated from nodal force per element surface area. Thus the predicted values were expected to be greater than the measured peak plantar pressure. Although the contact area pattern was in general consistent with experimental measurement, predicted contact area in the midfoot region was obviously larger than that of experimental measurement. The total plantar contact area by the FE prediction was 71.3% larger than that of F-scan measurement. The difference in sensitivity range between prediction and experimental measurement may influence readings. The range of sensitivity of F-scan system may not fully cover relative low pressure region when its target pressure was high pressure.

The high plantar shear stress in both A-P and M-L directions were at the heel region and beneath the medial metatarsal heads. This finding complied with the frequent observation of plantar foot ulcers at the medial forefoot and the heel regions of diabetic patients (Mueller et al., 1994; Raspovic et al., 2000). The predicted shear stress was considered to be a direct contribution to tissue breakdown of the diabetic feet (Lord and Hosein, 2000).

For foot deformation comparisons, the predicted medial longitudinal arch deformation (17.8%) was comparable to the volunteer measurement (12.9%) during balanced standing with flat support. The pronation angle of rearfoot from FE prediction was only 0.5 degree discrepancy from that of measurement.

Internal biomechanical information of foot from FE predictions was compared to that of the cadaveric measurements and previous FE analyses in the literatures. 55.9% of the applied load (270N) was sustained by the plantar fascia by the model predicted, which complied with the prediction (47%) reported in the literature (Wright and Rennels, 1964). The average strains (0.7%) predicted by the FE model agreed with the experimental measurements with the strain of 0.5% reported by Kogler et al. (1995). Using an implanted microstrain transducer, Kogler et al. (1995) measured the plantar fascia strain of cadaveric specimens with a similar magnitude of compressive loading at the bottom of foot. The high tension predicted in the plantar fascia suggested that it is one of the major stabilizers of the medial longitudinal arch during walking.

The prediction of peak von Mises stress showed that the calcaneus and the mid-shafts of the second to the fourth metatarsals were the most vulnerable regions. The confined positions of these metatarsals are probably the direct cause of stress concentration. Besides metatarsal bones, the junction of the ankle and subtalar and together with the insertion areas of the plantar fascia were the sites of high stress under balanced standing. Those sites were possible locations of stress failure under weight-bearing, and consistent with Cheung et al. (2004) ‘s report but with smaller magnitudes.

5.1.2 Pure Compression

Comparisons between pure compression simulation and cadaveric experiment could further validate the FE model’s load-deformation characteristics from initial to fully BW loaded condition. The results from maximum vertical compressive force (540N) were compared to previous pure compression study up to 700N, which was the full BW of volunteer of Cheung‘s FE foot models.

Figure 5-1 shows vertical deformation comparison among FE prediction from this study, cadaveric experiment and FE prediction in previous study (Cheung et al., 2005).

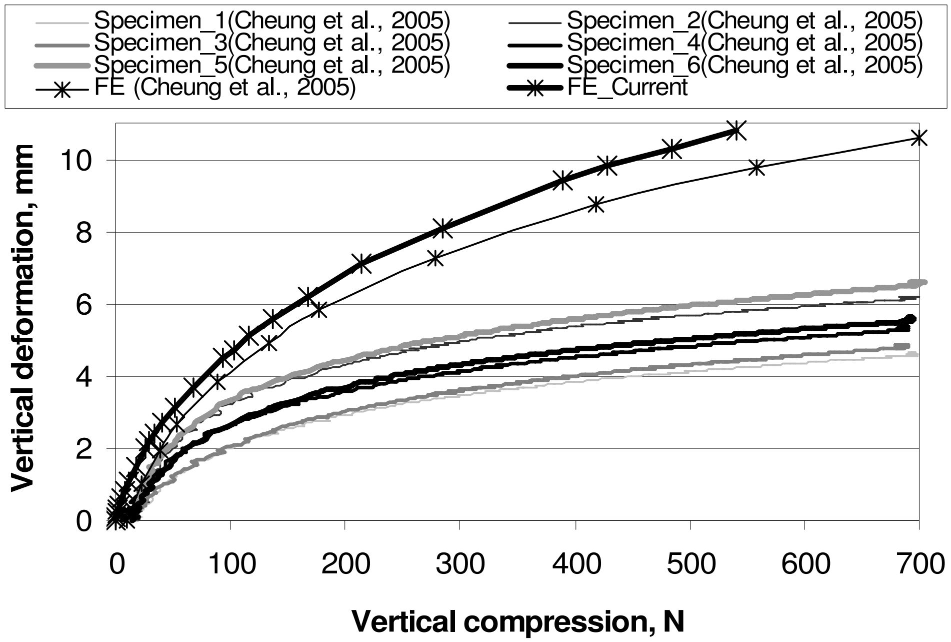

Figure 5-1. The vertical deformation under vertical compressive loading obtained from FE prediction in this study and cadaveric experimental measurements and FE prediction from literature (Cheung et al., 2005).

Under pure compressive loading, the FE model in this study predicted a similar profile but a larger magnitude of vertical deformation than the cadaveric foot measurements and slightly larger than prediction in the literature (Cheung et al., 2005). The discrepancy between FE prediction in this study and cadaveric experimental measurement might be due to the fact of neglecting the stabilizing effects from the structural interactions between the joints and the ligamentous and muscular tissues, which reduced the joint stiffness of the ankle–foot structures. Besides, the mechanical properties of the foot soft tissues and stiffened foot structure might be changed by the process of freezing and thawing of the cadaveric specimens. Moreover, FE model of a female foot was used in this study while gender of specimens in the literature was not identified.

Comparison of strain of plantar fascia between the results from this study and literature is showed in figure 5-2.

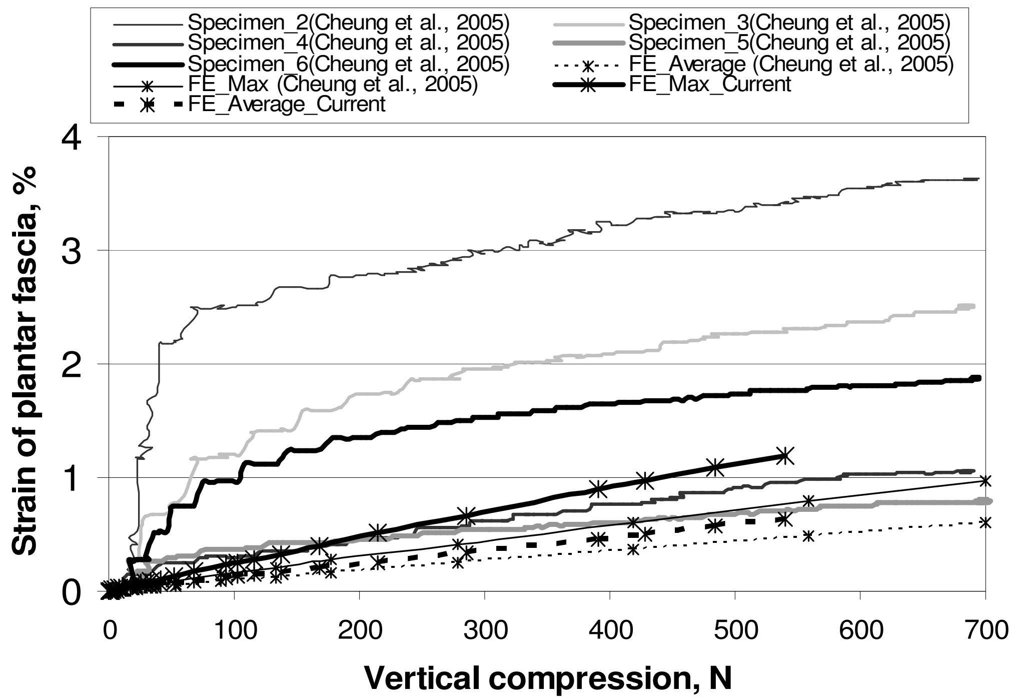

Figure 5-2. The strain of plantar fascia under vertical compressive loading obtained from FE prediction in this study and cadaveric experimental measurements and FE prediction from literature (Cheung et al., 2005).

The FE prediction in this study had a relatively low and linear response of increased fascia strain under vertical compression compared to cadaveric experimental measurement. The assumption of linear elastic material property and simplified geometry of the plantar fascia as linear truss structures might lead to an underestimation of predicted plantar fascia strain. Besides, the discrepancy might result from the neglect of the aforementioned soft tissue restraint on the foot joints. The strain profile of the plantar fascia from FE prediction in this study was in good agreement with the strain measurements in the literature (Kogler et al., 1995, 1996). Using an implanted microstrain transducer, Kogler et al. (1995, 1996) reported average plantar fascia strains of 1.46% and 3.54% in the tested foot with vertical compression of 675 N.

Achilles tendon force played a key role in adjustment of plantar pressure distribution because it acted the most important moment arm to achieve an equilibrium balanced standing position (Basmajian and Stecko, 1963). Without Achilles tendon force, peak pressure would more concentrate in the heel region, which was consistent with the reported finding (Kim et al., 2003).

In general, based on the balanced standing and pure compression simulations, the predictions from current FE model of a female foot were in good agreement with experimental validation measurements and previous FE analyses. Moreover, further comparisons between FE predictions and experimental measurements would be employed as well.

5.2 Effects of Heel Height on the Foot

Societal and fashion customs encourage the continued use of HHS despite concerns regarding their detrimental effects on lower-extremity. Wearing HHS may cause discomfort and eventually lead to foot problems such as hallux valgus and tight heel cord problems.

In this study, different high-heeled foot supports (1-inch, 2-inch and 3-inch) were used to investigate the effects of heel height on the foot during balanced standing. Achilles tendon force of 65%, 80%, and 160% of half BW was applied for 1-inch, 2-inch and 3-inch high-heeled foot supports respectively. The trend of increased forces of Achilles tendon represented more muscle EMG activities, which was in general consistent with those of previous studies. The increase of muscle force could be a compensating response for the more positive-inverting movements of the GRF while standing on high-heeled foot supports (Henderson and Piazza, 2004). While other studies reported there were no significant differences in EMG activity of the gastrocnemius (Stefanyshyn et al., 2000). Lee et al. (1990) found a progressive negative linear relationship with increasing heel height for EMG activity of the gastrocnemius. The inconsistent of previous results may be due to the difference trend of activities of lateral and medial gastrocnemius with wearing HHS (Gefen et al., 2002).

Wearing HHS prevents normal stretching of the gastrocnemius and soleus muscles and results in abnormal forefoot load (Tower et al., 2003). Keeping the Achilles tendon from fully stretching may lead to tight heel cords.

The predicted medial longitudinal arch deformation reduced with heel elevation, which agreed with trend from measurement, but with larger magnitude up to 2.4 mm. The results from this study are partially agreeable with those of previous studies. In the study of unilateral standing on cork plates of various heights (0 to 40 mm), Shimizu and

Andrew (1999) also found that heel elevation raised the medial longitudinal arch. Ricci and Karpovich (1964) reported that the high heels caused an increase in arch height after one day wearing it. These results suggest that elevating the heel of a shoe could help to reduce arch deformation of the weight-bearing feet. However this finding can hardly be interpreted as an encouragement of wearing HHS.

The plantar pressure distribution patterns from FE predictions were in good agreement with the F-scan measurements. The peak pressure shifted from the heel region to the forefoot region, while high pressure at forefoot kept at the central of metatarsal heads. Loading in plantarflexion allows excessive direct loading of the metatarsal heads and is thought to predispose to Freiberg's infraction or osteonecrosis of the metatarsal heads. However, during unilateral standing and walking with high heels, peak pressure in the forefoot region would shift from the central to the medial side (Shimizu and Andrew, 1999; Mandato and Nester, 1999). The discrepancy may be due to different experiment protocols. In this study, the volunteer was required to align her feet along the middle line of high-heeled foot supports during balanced standing while other studies were either at unilateral standing. Compared to flat supporting, standing on low high-heeled supports (<3 inch) could reduce peak plantar pressure. This result could be explained by the increased contact areas at forefoot and midfoot and redistributed plantar pressure.

Heel elevation with shoe modification and arch insole insert has been used as a conservative treatment strategy for plantar fasciitis to reduce the strain in plantar fascia

(Gordon, 1984; Cole et al., 2005; Marshall, 1988). From the FE predictions, the peak strain of plantar fascia reduced from 1.3% to the minimum values (0.6%) at 2-inch condition and increased rapidly at 3-inch condition (2.8%). Kogler et al. (2001) analyzed the effect of platform with shank curve at various heel heights in the cadaveric foot specimens and found that the strain in the plantar fascia decreased with an increase in heel height. However, platform with heel elevation block did not significantly influence the strain in plantar fasciitis and suggested that the influence of heel elevation on loading of the plantar fascia may be dependent on individual variation and foot structure differences. Reduced tensile strain in the plantar fascia may contribute to alleviating pain and inflammation. Current developed model was limited to a single female subject and cannot be used to predict the effects of difference of foot structures. The prediction of ligaments and plantar fascia strain was likely to be underestimated due to simplification of material properties and the windlass mechanism. The effect of foot structure difference was not considered in current study, which likely led to underestimation of peak plantar fascia tension and strain. Elevation of shoe heel without arch support may not provide proper support in the heel region and plantar fasciitis may be resulted at the arch region over time. The function of arch support could be investigated and included in future study.

With heel elevation of foot supports and increased Achilles tendon forces, the predicted von Mises stress of the rearfoot bones increased. The peak bony stresses among five metatarsals shifted from the mid-shaft of the fourth metatarsal to the third metatarsal with heel elevation. While most midfoot bones (cuboid and cuneiforms) sustained similar stresses from flat support to 2-inch foot support. Metatarsals reduced stresses from flat support to 2-inch foot support. At 3-inch condition, stresses of almost all bones were significantly increased because the foot was hyper-flexed and peak plantar pressure shifted from the heel region to the forefoot region. However, stresses of medial cuneiform increased abruptly at 3-inch condition. Wearing HHS higher than 2-inch would likely cause stress or fatigue failure and subsequent forefoot pain because of the intensified stresses in the central metatarsals, plantar site of calcaneocuboid joint junction, and forefoot plantar peak pressure. Gefen (2002) found that in general, HHS increased the load on the forefoot and relieved load on the rearfoot compared to that of flat shoes. Wang and Lu (2006) reported that flat shoes increased tensile stress while HHS only induced compressive stress of the second metatarsal. From this point of view, HHS do not increase load situation of the second metatarsal, thus leading to fewer problems in bone fractures. It is a typical claim that shoes with heel height less than 2 inches are safe to wear (Ebbeling et al., 1994). However, even moderate-heeled shoes (1.5-inch) increased knee torques significantly. The knee torques were thought to be relevant in the development and/or progression of knee OA (Kerrigan et al., 2005).

With heel elevation, the total plantar contact area had a maximum of 9.2% reduction for FE predictions and 14.5% of reduction for F-scan measurements, respectively. The FE predicted decreased trend of plantar foot contact area from flat support to 3-inch high-heeled support in general agreed with F-scan measurement but with constant larger magnitude. The discrepancy between prediction and measurement may result from the low measured pressure region in the midfoot region.

Shoes with elevated heel will dorsiflex the first MTP joint, the joint may become symptomatic with stiffness and pain. The FE predictions showed that peak contact pressure increased significantly at the first MTP joint with heel elevation compared to that of flat support. The cadaveric measurements obtained the same trend of FE predictions. However, the highest values of peak pressure and force between simulated cases and measurement were inconsistent. The trends of contact and force between experimental measurement and FE prediction were different. These discrepancies may be due to different muscle loading condition between FE simulation and cadaveric experiment. It should be noted that limited specimen was used in cadaveric experiment. Increasing the number of specimens would minimize the foot structures difference. Interactions beneath metatarsal heads and sesamoids were not considered in current FE model.

In cadaveric study of compressive loading, it was found that applying Achilles tendon forces increased pressure, force and contact area at the first MTP joint. Pronounced contact interaction could be induced by intensified strain of plantar fascia. Carlson et al. (2000) measured an increased plantar fascia strain with increasing loading on the Achilles tendon under static loading conditions of the foot. Cheung et al. (2006) predicted consistent results as well. In cadaveric study of simulating cyclic sagittal movement, the first MTP joint had small movement both in sagittal plane and transverse plane with and without HHS. No noticeable rotation movement in transverse plane of the first MTP segment was predicted from the FE predictions of static standing on flat support and 2-inch HHS.

During high-heeled standing, the first MTP joint was hyper-extended. Sussman and D'Amico (1984) reported the relationship of heel height and degrees of dorsiflexion at the MTP joint. The dorsiflexion angle at the first MTP joint was 19.8, 34.0, 48.0 and 62.5 degrees for 1-inch, 2-inch, 3-inch, and 4-inch respectively. The FE predicted soft tissue stress at the dorsal region on MTP joints was increased. The increased forefoot stress especially at the first MTP segment during prolonged high-heeled standing may contribute to progressive hallux valgus. McBride et al. (1991) reported MTP joint reaction force was twice as large in high-heeled shoes compared to walking with barefoot. Dorsiflexion and the high tissue stress at the dorsal first MTP joint would cause stretching of the capsule and synovial attachment at the great toe. Injury to the soft tissue structures around the first MTP joint may cause pain at this joint. The peak von Mises stress at the metatarsals shift from the fourth metatarsal to the third metatarsal.

In current FE simulation, the upper and counter parts of HHS were not included and the loading at the toe region may be underestimated. Obviously, a tight fitting toe box will apply additional pressure to the toes and force them into an unnatural shape which causes discomfort and eventually lead to foot deformity (Rossi and Tennant, 1984). Wearing HHS, the toes are shifted forward in the shoe and become even more cramped quarters for toes. HHS may contribute to the formation of hallux valgus since the wearers pronate during propulsion. Hallux valgus deformity occurs primarily in shod populations and the deviation of the hallux occurs primarily in the transverse plane.

Hallux valgus develops slowly and results from the gradual dislocation of the joint in the transverse plane. In this study, transverse intermetatarsal ligament strains did not change significantly compared to that of horizontal support and no significant strain difference between medial and lateral collateral ligaments of the first metatarsal was found. The stabilizing forces for varus and valgus about the first MTP joint is provided by the capsuloligamentous soft tissue structures (Childs, 2006). Kura et al. (1998) showed that the medial capsule rather than the metatarsal ligament stabilized the hallux and the transverse ligament did not noticeably cause hallux valgus during in vitro study. Phillips (1988) stated that even without medial stabilizing structures, the lateral joint capsule and collateral ligaments tighten and the adductor hallucis muscle acts unopposed which will exacerbate the deformity. Thus the restraint by the tight fitting toe box of HHS and the imbalanced muscle forces deforming the joint may play an important role in hallux valgus. Heel elevation could be a triggering factor. Further improvement of FE model including toe box in addition to experimental validations are needed before a solid conclusion can be made.

5.3 Effects of Outsole Stiffness and Coefficient of Friction on the Foot

5.3.1 Validation FE Predicted Balanced Standing on HHS

The sensitivity study on different designs of HHS conducted with the simulated loading condition of balanced standing with conventional 2-inch HHS was employed. Same muscle forces used for 2-inch high-heeled foot support were applied to 2-inch HHS, because HHS and foot support had the same shank profile and toe spring.

To prevent toe jamming and allow foot extension and plantar-flexion freely during walking, sufficient space of HHS around MTP joint would be reserved. Although the foot was well stepped on the HHS, the MTP joint might not perfectly match the contour of the shank curve.

The FE predicted plantar pressure distribution was in good agreement with that of F-scan measurement. Similar von Mises stress distribution of foot bony structures was obtained. While predicted plantar pressure distributions between HHS and foot support condition was not exactly the same, the predicted arch deformation with 2-inch HHS was 7.8% smaller than that with 2-inch foot support. Contact area with 2-inch HHS was 12.2% larger than that with 2-inch foot support. The differences may be due to the different material properties of supports and deformation of HHS.

5.3.2 Effects of Outsole Stiffness

The outsole stiffness is largely determined by the materials of outsole itself and shankpiece. In conventional shoe manufacturing, steel shankpiece embedded into outsole is widely used to maintain shank contour of HHS.

There were a few FE analyses explored footwear sole design (Lemmon et al., 1997; Chen et al., 2003; Verdejo R et al., 2005; Cheung and Zhang, 2008) and their studies mainly focused on general characteristics of footwear design. This study could be a pioneer having 3D FE model of a female foot to evaluate the effects of outsole stiffness on the biomechanical load-bearing characteristics of plantar foot and internal bony structures.

The model predicted noticeable shoe deformations with PU and EVA outsole conditions while plantar pressure distributions in all simulated cases were agreement with conventional design. The space at metatarsals heads and toe spring angle with PU and EVA conditions were disappeared by the FE predictions. It is possible that the shoe deformation and foot responses may correlate to comfort experience. The result suggests that the outsole stiffness has minor effects on the plantar pressure distribution during balanced standing compared to heel height variation. Previous studies from experimental approaches and FE simulations showed that the contour of insole had more important role in reduction of peak pressure and redistribution of plantar pressure than that of the stiffness of insole (Chen et al., 2003; Cheung and Zhang, 2008).

With regards to simulations of using HDPE and TPR outsole, no significant variations of either peak plantar pressure or internal stress/stain were found. However, the outsole stiffness had an insignificant influence on the total contact area but had pronounced impact on the strain and tension of plantar fascia on outsole using PU and EVA. The peak strain and total tension force of plantar fascia increased 16.7% and 9.9% with the softest outsole. Peak von Mises stress of bony structures decreased 17.3% while central metatarsal bones experienced increased stresses. The results showed that inconsistence compared with common design concept because steel shankpiece had no obvious role in maintaining shank contour by FE predictions. However, compared FE predictions with and without steel shankpiece, it was found that steel shankpiece sustained most of the stress. Therefore, steel shankpiece could protect over-deformation and extend the life time of HHS, especially during walking.

Stiffness of sole has been linked to balance, especially for elderly. Robbins et al. (1997) reported that shoes with thin hard soles provided better stability for the elderly men than those with thick soft midsoles. Under assessment of static balance by body sway test, Lord and Bashford (1996) found that bare feet and walking shoes maximize balance, whereas high-heeled shoes constitute a needless balance hazard for older women.

It should be noticed that maximal deformation of outsole occurs at late mid-stance and push off phase of gait. Further investigation during gait simulation should be done to get more concrete conclusion.

5.3.3 Effects of Coefficient of Friction

Interfacial friction plays an important role in the stability of whole body and in local stresses around the contact areas as well. Plantar contact pressure/shear stress has a clinical relevance to various foot problems, especially plantar ulceration in neuropathic foot. A number of studies have investigated the role of footwear in preventing foot lesions (Litzelman et al., 1997; Maciejewshi et al., 2004). It was found that appropriate footwear helped to redistribute plantar pressure and reduce peak plantar pressure and shear. Little investigation has been done on plantar shear stress due to the lagged technology for experimental measurement (Tappin and Robertson, 1991; Hosein and Lord, 2000). Since direct measurement of shear stress in situ is difficult, researchers turned to numerical modelling methods. Several FE analyses have been successfully implemented to evaluate the plantar pressure and shear stress distributions (Dai et al., 2005; Cheung et al., 2005).

In this sensitivity study, three different coefficients of friction were employed to investigate its effects on the biomechanical response of foot during balanced standing. From the FE predictions, the plantar peak pressure increased 1.7% with the reduction of coefficient of friction from 0.6 to 0.2. Both high A-P and M-L shear stresses were beneath the heel region, metatarsal heads and big toe. This finding complies with clinical observations that the heel region and metatarsal heads are the most common incidence sites of ulceration or callus. Although the FE predicted shear stress distributions were similar, the peak shear stress both in A-P direction and M-L direction decreased 32.0% and 26.5%, respectively, with the reduction of coefficient of friction to 0.2. Hosein and lord (2000) reported that during walking, heel region and metatarsal heads experienced maximum shear stress ranged from 38.5 to 51.4 KPa, which had the same range of magnitude with this study.

Since the average A-P shear stress increased with the reduction of coefficient of friction, the GRF in A-P direction was found to increase 55.5% with the reduction of coefficient of friction from 0.6 to 0.2. Dai et al. (2005) predicted that with wearing sock, the peak shear force was reduced from 3.1 N for barefoot to 0.88 N at the rearfoot, and from 10.61 to 1.61 N at the forefoot, respectively.

5.4 Walking with High-heeled Shoes

5.4.1 FE Simulation on Mid-stance Phase

In this study, 72.5% of BW was applied by Achilles tendon force during mid-stance phase based on sensitivity test on its effects on COP. Cheung and Zhang (2007) calculated 100% BW of Achilles tendon forces for mid-stance phase simulation of barefoot walking. Previous studies from cadaveric experiments (Sharkey and Hamel, 1998; Hansen et al., 2001) reported Achilles forces ranged from 143% to 186% BW at GRF of 75% BW (700 N) during 40% of barefoot gait cycle. Esenyel et al. (2003) reported that with HHS the plantar flexor moment reduced till terminal stance compared to low-heeled shoes and 29% reduced concentric push-off work. The magnitude of Achilles tendon forces in general agreed with previous experiments findings.

The FE predicted peak plantar pressure was in good agreement with that of F-scan measurement. For forefoot pressure distribution, the peak plantar pressure was predicted at the first metatarsal head while from F-scan measurement it was found at the third metatarsal head. The discrepancy may be due to the assumption that the same other extrinsic muscle forces were generated for 2-inch HHS mid-stance phase of walking and standing. The FE predicted peak plantar pressure increased 35.7% and 128.6% for the heel region and the forefoot region, respectively. Moreover, from the FE predictions, peak A-P and M-L shear stress in the forefoot region shifted from the soft tissue beneath the big toe to the first metatarsal head.

Within expectation for comparing mid-stance phase to standing from the FE predictions, arch deformation increased 98.3% from 5.9 mm to 11.7 mm. Tension and peak strain of plantar fascia increased 243.6% and 250.5%, respectively. While comparing walking with 2-inch HHS to balanced standing on flat support, tension force of plantar fascia increased by 31.1%.

5.4.2 Gait Analysis Experiment

Subjective comfort ratings across heel conditions revealed that walking with 4-inch HHS could significantly ($p<0.05$) influence the easiness of walking, easiness in balancing, total comfort, plantar forefoot comfort, plantar heel comfort and knee comfort. However, no significantly different comfort perceptions were noticed between flat shoes and 2-inch HHS. For the same volunteer, no significant difference was found in cadence, stride length and stance percentage. The subject walked slightly slowly at 4-inch HHS condition among all situations.

The maximal propulsive force and Fz1 of 2-inch condition was significantly different from both other two conditions, and Fz2 and Fzmin of 4-inch condition were significantly different from both other two conditions. Maximal braking force of 4-inch condition was significantly different from that of 0-inch condition. This finding was in partial agreement with previous studies. Significant increase in maximal braking and propulsive force was found, which was consistent with previous finding (Snow and Williams, 1994). Wang et al. (2001) observed that HHS generated smaller Fz1 but larger Fz2 compared to flat leather shoes. Stefanyshyn et al. (2000) found that Fz1, maximal propulsive and braking force increased as heel height increased, whereas Fz2 was the highest for shoe with 3.7 cm heel height throughout all conditions. Age and experience of wearing HHS could contribute to the disagreement from previous studies.

With the increase of heel height from 0-inch to 4-inch, peak pressure and pressure-time integral in the forefoot region increased significantly by 33% and 54%, respectively, whereas corresponding values of the heel region decreased. The measured results trend was generally in accordance with previous reports (Mandato and Nester, 1999; Speksnijer et al., 2005). Mandato and Nester found that the peak forefoot pressure increase 63% with heel height changed from 0-inch to 2-inch, and 30% with heel height changed from 2-inch to 3-inch. Speksnijer et al. (2005) reported that peak pressures of forefoot increased approximately 30-50%, and pressure-time integral increase by 48% with HHS compared to flat shoes.

FE predictions accompanied with experimental measurements were combined with subjective comfort ratings to study the association between the quantitative measurements and comfort in shoe design. Wearing higher heels would increase the discomfort and pain of subjects, whereas reflected by increase pressure-time integral in the experimental studies and peak pressure in the FE prediction. In fact, current subjective comfort rating questionnaires only serve as an accessory in better understanding on the comfort in shoe designs. A more holistic and systematic research could be organized to in-depth study the association between qualitative comfort to biomedical quantities.

Maximum peak dorsal contact pressure coincided with dorsiflexion of the foot, and occurred above the MTP joint at the flex-line of HHS. This finding was consistent with previous study (Jordan et al., 1996) with the same range of dorsal pressure (50 kPa). It should be noticed that the dorsal contact pressure was significantly influenced by dimensional difference between foot and shoe individually. Further study related to relationship between fit and dorsal pressure should be done.

5.5 Limitations of FE Simulation and this Study

5.5.1 Limitations of FE Simulation

A number of assumptions were made in current FE model to simplify the analysis. Therefore, the predictions of this study should be interpreted with the limitations inherent to FE modelling. A number of assumptions may contribute to prediction errors. The material properties for the bony and ligamentous structures were assumed to be homogeneous and linearly elastic. Due to the composition of trabecular and cortical bone, the outermost layer, cortical bone, has a higher stiffness, compared with that of the average value, thus, the predicted peak pressure would be less compared to that of the real scenario. The use of linear truss elements of ligaments and plantar fascia was a gross assumption. Ligaments with the four lateral toes and other connective tissues such the joint capsules were not considered. The surface interactions between bony, ligamentous and musculotendon structures were not considered as well. These structural simplifications of current FE model would result in a reduction of joint stiffness and an increase of medial longitudinal arch deformation. The encapsulated bulk soft tissues were assigned with the same hyperelastic material without considering variations among different sites, such as metatarsal heads and fat pad. This simplification would result in larger discrepancy of peak plantar pressure and foot deformation. In future study, the viscoelastic and anisotropic material properties for different sites of soft tissues could be considered. Linearly elastic material properties were assigned to HHS and foot supports in current FE model. Deformations of footwear are relatively large, it is suggested to assign the nonlinear stress-strain curve to shoe material to simulate large deformation situation (Shiang, 1997). The accuracy of estimating the plantar pressure may decrease at large deformation conditions.

Axial connector elements were used to simulate the musculotendon forces, but the muscles may have several heads and origins, the fibers are not in line in actual foot structures. In addition, the trends of activities of lateral and medial gastrocnemius were different when wearing HHS (Gefen et al., 2002). Imbalance load of gastrocnemius was not considered in current FE model, so the accuracy of FE prediction may further decrease. Extrinsic muscle forces for mid-stance phase condition were linearly estimated from EMG data at normal walking condition; real muscle force at HHS situation should be applied in future study. Joint contact coefficient of friction was not frictionless. Frictionless surface to surface contact assumption may overestimate the movement of joints.

Besides the simplifications of the structural and material properties of the foot, the following loading and boundary conditions assumptions made for current FE simulations would affect the accuracy of the FE predictions. Firstly, only the major extrinsic muscle forces were considered while other intrinsic muscle forces were ignored. Fiolkowski et al. (2003) found that the intrinsic muscles might play an important role in supporting the medial longitudinal arch. Therefore, current FE predicted foot responses likely underestimated the stiffness of the actual foot structure.

The geometrically complex bony and soft tissue structures could use automatic meshing algorithm with the tetrahedral elements. The accuracy of the FE predictions can be increased with the use of hexahedral elements, which provide better accuracy under larger deformation. To what extent the accuracy of current FE mesh could provide was not yet known and rigorous convergence and sensitivity tests on the element types and mesh density should be conducted before a conclusion can be made.

The geometrical model is based on one healthy subject. Nevertheless, the results obtained from current model could provide a better understanding of foot biomechanics. Foot pathology or deformity could further be investigated by developing more sophisticated model for specific purpose.

All of the aforementioned limitations can influence the accuracy of FE predictions, but the relative differences between comparisons under different conditions are less likely affected due to systematic nature of these assumptions. Therefore, the predictions should be interpreted on the percentage changes caused by the altered conditions, rather than absolute values.

5.5.2 Limitations of this Study

There are several limitations in this study. Firstly the developed model represented a normal arch configuration whilst the arch stability or stiffness is individualized with different foot structures. Owing to the use of single model, the generalization of current FE prediction remains questionable. Improvement on certain aspects of the FE model and more comprehensive simulations of various physiological loading conditions on different foot types in addition to experimental validations are needed to obtain a more representative and generalized solution.

Secondly, to simplify the FE simulations, toe box, heel counter and vamp of HHS were not considered in current FE model. However, toe box, especially for pointed toe box, has an important role in developing forefoot deformities and problems. Pointed toe box constricted toes, which may eventually deform the foot. The same thing happens if women wear high-heeled shoed that slide the foot forward. In addition, only one conventional style of HHS was considered. It was considered the width of heel could influence the balance during high-heeled walking, therefore more type of HHS would offer insight of this field. Positions of foot on the HHS were not consistent with the experiment. Spears et al. (2007) found that well-fitted counter with heel pad could effectively reduce heel pad stress. Therefore, plantar pressure and internal stress could be overestimated without the simulation of heel counter.

Thirdly, only balanced standing and the mid-stance phase were simulated while high load-bearing stance phases such as push off and heel strike were essential for understanding the real walking condition. Static condition was considered in all simulations and the biomechanical effects of inertial forces and history of loading during the dynamic conditions cannot be addressed. Simulation of balanced standing with 4-inch heel elevated foot support was not computationally feasible for the current FE model conducted because of the excessive tissue deformation involved around the ankle joint.

Limited specimens were used in cadaver experiment. The number of specimens should be sufficient in future study. Axial compressive load and musculotendon loadings were scaled down compared to FE prescribed loading conditions because the limitation of equipment.

Subject number of gait analysis was small, large recruitment should be carried out to obtain concrete conclusion. Comfort evaluation of subjects' wearing HHS was from a short term perception, and long term effect was not considered in this study. Moreover, in gait experiment, extra load on the right foot by Tekscan data sockets and Vicon makers would influence natural gait. Since only mid-stance phase was simulated in current FE model, kinematic and kinetic data from Vicon system were not included in this study. Kinematic and kinetic analyses of gait will be conducted, because those data are important for gait simulation input in future study.

CHAPTER VI CONCLUSIONS and FUTURE WORK

6.1 Conclusions

Numerous experimental techniques were developed and employed to investigate the biomechanical interactions of foot and footwear. However, direct biomechanical measurement of internal stress and strain on bony, ligamentous and soft tissue structures of the foot remains unavailable or highly invasive. In this study, a comprehensive FE model of a female foot with HHS was developed. The model used real 3D foot geometry, and incorporated nonlinear material properties, large deformations and interfacial slip/friction conditions. The computational model was validated and the FE predictions were in good agreement with experimental measurements.

From the FE predictions on the parametric study on heel height from 0-inch to 3-inch, an increase in heel height resulted in a decrease in arch deformation from 8.8 mm to 1.1 mm, which was consistent with measured deformations. The results imply that wearing HHS may help reduce arch deformation of the weight-bearing feet. There was a general increase in predicted maximum von Mises stress of foot bones with increasing heel height of foot supports from 0-inch to 3-inch. In the forefoot region, relatively high von Mises stresses concentrated at the second to the fourth metatarsals. With 2-inch high-heeled foot support, the strain and total tension force in the plantar fascia was minimum in all calculated cases. Moderate heel elevation may help to reduce the strain of in plantar fascia. This finding copes with existing conservative treatment strategy for plantar fasciitis to reduce the strain in plantar fascia. Comparing the FE predictions of static standing on flat support and HHS, no noticeable rotation movement in transverse plane of the first MTP segment was found, which was consistent with cadaveric experiment. A pronounced increase in peak von Mises stress in the first MTP joint was predicted in HHS condition compared to flat support. Therefore, heel elevation was not found to be a direct biomechanical risk factor for hallux valgus deformity. However, combined effects with tight toe box may impose risk of hallux valgus deformity. Heel elevation could be a triggering factor and should be confirmed in further study.

For the parametric study on outsole stiffness, comparison of von Mises stress in outsole with and without shankpiece suggested that embedded steel shankpiece is an important component of HHS, which sustains most of the loading of outsole and prevents outsole from collapsing and distorting. The forefoot and midfoot were in a relatively plantarflexed position with the softer outsole.

For the parametric study on the coefficient of friction, the model predicted that reduction of coefficient of friction will result in reduction in peak shear stress, whereas the peak plantar pressures remain approximately the same. The GRF in A-P direction increased significantly with the reduction of coefficient of friction.

Comparing mid-stance phase to standing from the FE predictions, arch deformation increased 98.3% from 5.9 mm to 11.7 mm. Tension and peak strain of plantar fascia increased 243.6% and 250.5%, respectively. While comparing walking with 2-inch HHS to balanced standing on flat support, tension force of plantar fascia increased by 31.1%. Results from gait analysis showed that increasing heel height from 0-inch to 4-inch increased the peak pressure and pressure-time integral in the forefoot region significantly by 33% and 54%, respectively, whereas corresponding values in the heel region decreased. For the GRF, the maximal propulsive force and maximal braking force with HHS were larger than those of the flat condition. The results imply that wearing HHS may be a possible risk factor of metatarsalgia.

Current FE predictions were carried out with HHS without the shoe upper structures such as toe box and heel counter. In addition, stance phases such as heel strike and push off were not simulated in this study. Therefore, further investigations and simulations should be conducted before a solid conclusion about the biomechanical effects of wearing HHS can be made. The biomechanical information on the effects of different parameters, such as heel height, material properties and friction of HHS obtained from this study will be useful for better understanding HHS related foot problems and designing proper HHS.

6.2 Directions for Further Studies

Several further studies can be done, which are directed to the improvement of current FE model. Advanced material model such as anisotropic, and viscoelastic models can be employed in the FE model to enable a realistic simulation of the mechanical behavior of the foot soft tissue. Three dimensional structural modeling of the ligamentous and musculotendon structures can be incorporated to simulate more accurately the stabilizing role provided by these structures and the interactions with the bony and encapsulated soft tissue structures. The hyaline cartilage of the contacting joint surfaces and associated joint capsules can be incorporated to refine the simulation of the foot joints.

Since pointed toe box may contribute to progressive foot deformity. Shoe components such as toe box and heel counter should be included in future FE analysis (Fig. 6-1). In addition, high weight-bearing stance instances such as heel strike and push off should be investigated (Fig. 6-2). Investigations on the other design factors of HHS such as different shank profiles, heel width, toe box shape and distributions of sole stiffness can be done.

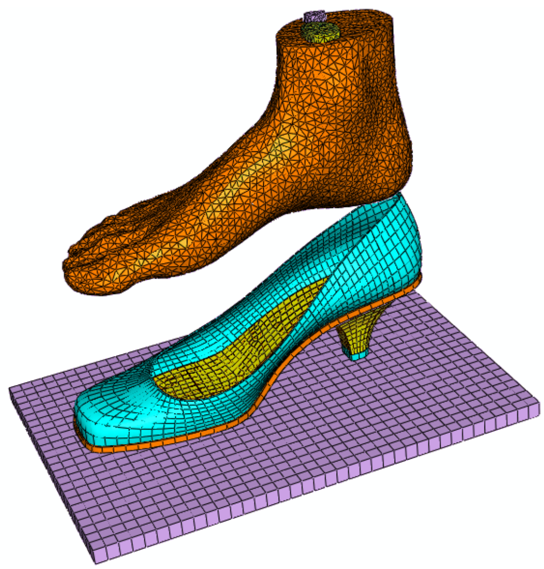

Figure 6-1. FE model of foot with whole HHS.

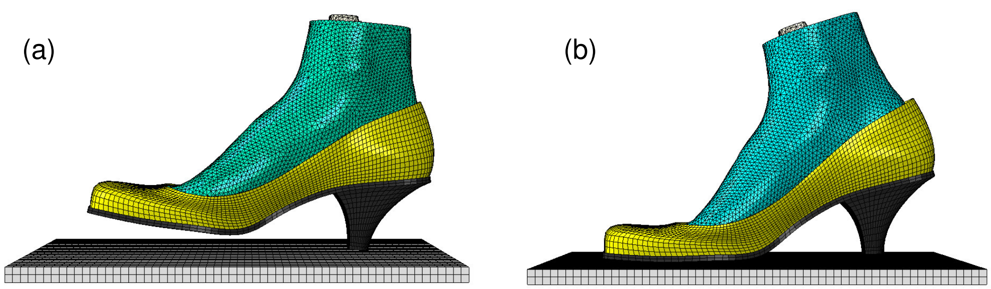

Figure 6-2. Walking with HHS: (a) heel strike and (b) push off.

Since level of discomfort and pressure tolerance of the foot may be different, further study is needed to study relationship between comfort rating and pressure tolerance level on the whole skin surface of the foot. Guidelines on the clearances between different feet and shoes could be estimated. Cadaveric experiment focusing on the biomechanical interactions of HHS and foot was limited; the pathomechanics of HHS related foot deformity development could be further investigated by comprehensive cadaveric experiment.

The female foot shows apparent difference in terms of geometry compared with the male foot constructed by our research team. Gender difference in foot / footwear biomechanics during walking could be investigated by comparison the results from current model with previous male models.

Furthermore, it was reported that HHS could lead to the development and progression of knee OA (Kerrigan et al., 2005). Current FE model can be extended to the knee joint level (Fig. 6-3).

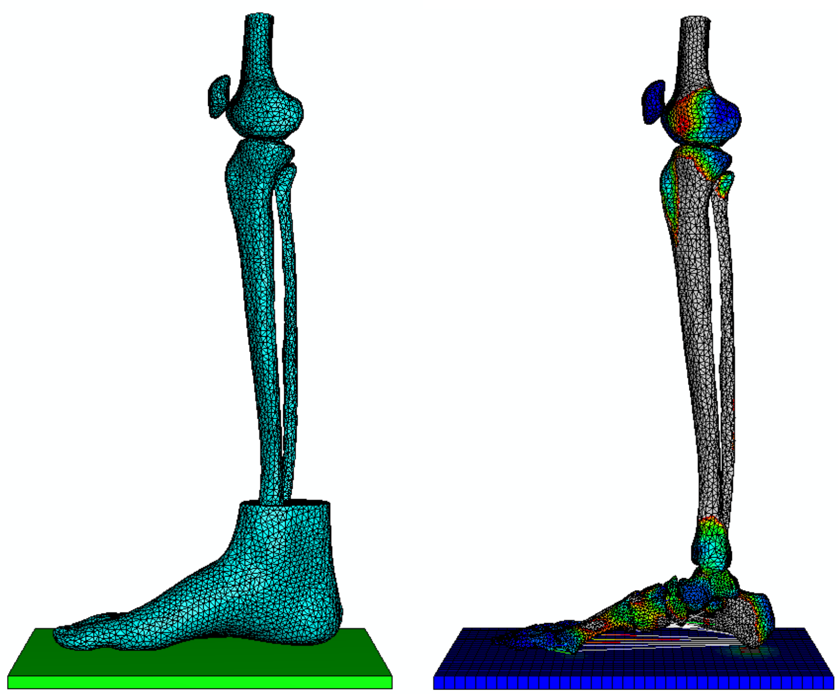

Figure 6-3.FE model of the knee-ankle-foot structures.

APPENDIX

Subject No: **Heel height:** **Date:**

Subjective Questionnaires

Subject should complete subjective ratings on following aspects of wearing shoes with different heel height by ticking the proper number.

1. **Easiness in Walking (Least to Most)**

0 1 2 3 4 5 6

2. **Easiness in Balancing (Least to Most)**

0 1 2 3 4 5 6

3. **Total Comfort (Least to Most)**

0 1 2 3 4 5 6

4. **Plantar Forefoot Comfort (Least to Most)**

0 1 2 3 4 5 6

5. **Plantar Heel Comfort (Least to Most)**

0 1 2 3 4 5 6

6. **Dorsal Vamp Region Comfort (Least to Most)**

0 1 2 3 4 5 6

7. **Heel Counter Comfort (Least to Most)**

0 1 2 3 4 5 6

8. **Toe Comfort (Least to Most)**

0 1 2 3 4 5 6

9. **Knee Comfort (Least to Most)**

0 1 2 3 4 5 6

10. **Lower Back Comfort (Least to Most)**

0 1 2 3 4 5 6

REFERENCES

1. ABAQUS theory and user's manual, version 6.7, 2007. Hibbitt, Karlsson and Sorensen Inc., Pawtucket, RI, USA.
2. Adrian KC, 1991. American last making: procedures, scale comparisons, sizing and grading information, basic shell layout, bottom equipment standards. Shoe trades publishing, Arlington, MA.
3. Adrian MJ, Karpovich PV, 1966. Foot instability during walking in shoes with high heels. Res Q. 37,168-75.
4. American College of Foot and Ankle Surgeons, 2008. (http://www.footphysicians.com/)
5. Antues PJ, Dias GR, Coeiho AT, Rebeio F, Pereira T, 2008. Hyperelastic modelling of cork-polyurethane gel composites: non-linear FEA implementation in 3D foot model. Materials Science Forum. 4, 700-705.
6. Aquino A, Payne C, 1999. Function of the plantar fascia. The Foot.9, 73–78.
7. Tam A, Joneja A, Tang K, Yao ZY, 2007. A surface development method with application in footwear CAD/CAM. Computer-Aided Design and Applications. 4,1-4.
8. Arangio GA, Phillippy DC, Xiao D, Gu WK, Salathe EP, 2000. Subtalar pronation-relationship to the medial longitudinal arch loading in the normal foot. Foot Ankle Int. 21, 216–220.
9. Athanasiou KA, Liu GT, Lavery LA, Lanctot DR, Schenck RC, 1998. Biomechanical topography of human articular cartilage in the first metatarsophalangeal joint. Clin Orthop. 348, 269–281.
10. Baba K, 1974. Foot measurement for shoe construction with reference to the relationship between foot length, foot breadth, and ball girth. Human Ergonomics (Tokyo).3, 149-56.
11. Barani Z, Haghpanahi M, Katoozian H, 2005. Three dimensional stress analysis of diabetic insole: a finite element approach. Technology Health Care. 13, 185-192.
12. Basmajian JV, Stecko G, 1963. The role of muscles in arch support of the foot. J Bone Joint Surg Am. 45, 1184-1190.
13. Beimers L, Tuijthof GJ, Blankevoort L, Jonges R, Maas M, van Dijk CN, 2008. In-vivo range of motion of the subtalar joint using computed tomography. J Biomech.41, 1390-1397.
14. Bendix T, Srensen SS, Klausen K,1984. Lumbar curve, trunk muscles, and line of gravity with different heel height. Spine.9, 223-227.

15. Borg GAV, 1982. Psychophysical bases of exertion. Medicine and Science in Sports and Exercise. 14,377–38.

16. Brenna Maloney. 2008. Washington Post (http://www.washingtonpost.com)

17. Broch NL, Wyller T, Steen H, 2004. Effects of heel height and shoe shape on the compressive load between foot and base: a graphic analysis of principle. J Am Podiatr Med Assoc. 94.461-469.

18. Budhabhatti SP, Erdemir A, Petre M, Sferra J, Donley B, Cavanagh, P.R., 2007. Finite element modeling of the first ray of the foot: a tool for the design of interventions. Journal of Biomechanical Engineering. 129, 750-756.

19. Canale ST, Campbell WC. 1998. Campbell's Operative Orthopaedics, 2, 1420- 920, CV Mosby, St Louis,

20. Carlson RE, Fleming LL, Hutton WC, 2000. The biomechanical relationship between the tendoachilles, plantar fascia and metatarsophalangeal joint dorsiflexion angle. Foot Ankle Int. 21, 18-25.

21. Carol Frey, 1995.Pain and deformity in women's feet. J Musculoskel Med.12, 27-32.

22. Carol Frey, Francesca Thompson, Judith Smith, Melanies Sanders, Helen Horstman, 1993. American orthopaedic foot and ankle society women's shoe survey. Foot Ankle. 14, 78-81

23. CD Media Studio Inc., 2003

24. Chen WP, Ju CW, Tang FT, 2003. Effects of total contact insoles on the plantar stress redistribution: a finite element analysis. Clin Biomech.18, S17-24.

25. Cheng FT, Perng DB, 1999.A systematic approach for developing a foot size information. Int. J. of Industrial Ergonomics. 25, 171–185.

26. Cheung JT, Zhang M, 2008. Parametrical design of pressure-relieving foot orthoses using statistical–based finite element method. Med Eng Phys.30, 269-277.

27. Cheung JT, Zhang M, An KN, 2006. Effect of Achilles tendon loading on plantar fascia tension in the standing foot. Clin Biomech. 21, 194-203.

28. Cheung JT, Zhang M, 2005. A 3-dimensional finite element model of the human foot and ankle for insole design. Arch Phys Med Rehabil.86, 353-358.

29. Childs, S.G., 2006. The Pathogenesis and Biomechanics of Turf Toe. 25, 276-280.

30. Chu TM, Reddy NP, Padovan J, 1995.Three-dimensional finite element stress analysis of the polypropylene, ankle-foot orthosis: static analysis. Med Eng Phys.17, 372-379.

31. Cimmino MA, Parodi M, 2004. Risk factors for osteoarthritis. Seminars in Arthritis and Rheumatism. 34, 29-34.

32. Cobb J, Claremont D, 2001.An in-shoe laser Doppler sensor for assessing plantar blood flow in the diabetic foot. Med Eng Phys. 23, 417-425.

33. Cole C, Seto C, Gazewood J, 2005. Plantar fasciitis: evidence-based review of diagnosis and therapy. Am Fam Physician. 72, 2237-2242.

34. Coughlin MJ, 1994. The high cost of fashionable footwear. J Musculoskel Med.11, 40-53.

35. Dai XQ, Li Y, Zhang M, Cheung JT, 2006. Effect of Sock on biomechanics of foot during walking. Clin Biomech. 21, 314-321.

36. DiGiovanni J, Smith S, 1976. Normal biomechanics of the adult rearfoot. J Am Pod Assoc (JAPA). 66,812-24.

37. Dohi M, Mochimaru M, Kouchi M, 2002.The distribution of the tactile sensitivity of a foot and the softness of its skin, Proceedings of the 32nd Convention Meeting of Kanto Branch of the Japan Ergonomics Society.90-91.

38. Dul J. 1983. Development of a minimum-fatigue optimization technique for predicting individual muscle forces during human posture and movement with application to the ankle musculature during standing and walking. PhD thesis, Vanderbilt University;

39. Ebbeling CJ, Hamill J, Crussemeyer JA. 1994. Lower extremity mechanics and energy cost of walking in high-heeled shoes. J Orthop Sports Phys Ther. 19.190-196.

40. Erdemir A, Saucerman JJ, Lemmon D, Loppnow B, Turso B, Ulbrecht JS, Cavanagh PR, 2005. Local plantar pressure relief in therapeutic footwear: design guidelines from finite element models. J Biomech. 38, 1798-1806.

41. Esenyel M,Walsh K, Walden JG,Gitter A. 2003. Kinetics of high-heeled gait, J Am Podiatr Med Assoc.93,27-32.

42. Fiolkowski P, Brunt D, Bishop M, Woo R, Horodyski M, 2003. Intrinsic pedal musculature support of the medial longitudinal arch: an electromyography study. J Foot Ankle Surg. 42, 327-333.

43. Footsolutions Inc. 2007 (http://www.footsolutions.com).

44. Franklin ME, Chenier TC, Brauninger L, Cook H, Harris S. 1995 Effect of positive heel inclination on posture. J Orthop Sports Phys Ther.21. 94-99.

45. Frey C, Thompson F, Smith J, Sanders M, Horstman H, 1993. American Orthopaedic Foot and Ankle Society women's shoe survey. Foot Ankle. 14, 78-81.

46. Gao C, Abeysekera J,Hironen M, Gronqvist R, 2004. Slip resistant properties of footwear on ice. Ergonomics. 47,710–716.

47. Garca-Hernandez J, Heras S, Juan A, Paredes R, Nacher B, Alemany S, Alcantara E, Gonzalez JC, 2005. The MORFO3D Foot Database. J.S. Marques et al. (Eds.): IbPRIA , LNCS 3523, 658–665.

48. Gefen A, 2003. Plantar soft tissue loading under the medial metatarsals in the standing diabetic foot. Med Eng Phys. 25, 491-499.

49. Gefen A, Megido-Ravid M, Itzchak Y, Arcan M, 2002.Analysis of muscular fatigue and foot stability during high-heeled gait. Gait Posture.15, 56-63.

50. Gefen A, Megido-Ravid M, Itzchak Y, Arcan M, 2000. Biomechanical analysis of the three-dimensional foot structure during gait: a basic tool for clinical applications. J Biomechan Eng. 122,630-639.

51. Gollnick PD, Tipton CM, Karpovich PV. 1964. Electrogoniometric study of walking on high heels. Res Q. Oct; 35, SUPPL370-378.

52. González JC, Alcántara E,Bataller A,García AC, 2001.Physiological and subjective evaluation of footwear thermal response over time. Proc. of the 5th Symp. on Footwear Biomechanics, Zurich / Switzerland, (Eds. E. Hennig, A. Stacoff)

53. Goonetilleke RS, 1999. Footwear cushioning: relating objective and subjective measurements. Human Factors. 41,241-256.

54. Gordon GM, 1984. Evaluation and prevention of injuries. Clin Podiatry. 1, 401-416.

55. Goske S, Erdemir A, Petre M, Budhabhatti S, Cavanagh PR, 2006. Reduction of plantar heel pressures: Insole design using finite element analysis. J Biomech.39, 2363-2370.

56. Hansen ML, Otis JC, Kenneally SM, Deland JT, 2001.A closed-loop cadaveric foot and ankle loading model. J Biomech.34, 551-555.

57. Hanson JP, Redfern MS, Mazumdar M, 1999. Predicting slips and falls considering required and available friction. Ergonomics. 42, 1619–1633.

58. Henderson, PD, Piazza, SJ, 2004. A biomechanical evaluation of standing in high-heeled shoes. Penn. State McNair J. 11, 25–38.

59. Hsu YC, Gung YW, Shih SL, Feng CK, Wei SH, Yu CH, Chen CS, 2008. Using an optimization approach to design an insole for lowering plantar fascia stress-a finite element study. Annals of Biomedical Engineering. 36, 1345-1352.

60. Interactive Foot and Ankle, 1999

61. ISO 9407:1991. Shoe sizes --- Mondopoint system for sizing and marking. International Organization for Standardization. (www. iso.org).

62. Jacob S, Patil MK, 1999. Stress analysis in three-dimensional foot models of normal and diabetic neuropathy. Front Med Bio Eng.9, 211-227.

63. Jeffery TE and Thurston LL, 1955. A factorial analysis of foot measurements. Natick, Massachusetts: US Army.

64. Jordan C, Payton CJ, Bartlett RM,1996. Perceived comfort and pressure distribution in causal footwear. Abstract of fifth EMD user meeting, S5.

65. Joseph J, 1968.The pattern of activity of some muscles in women walking on high heels. Ann Phys Med. 9,295-299.

66. Joseph J, 1963. Some aspects of the functional anatomy of the foot. Ann Phys Med 7, 26-30.

67. Kato T, Watanabe S, 1981. The etiology of hallux valgus in Japan. Clin Orthop. 157, 78-81.

68. Kawabata A, Tokura H, 1993. Effects of two kinds of sports shoes with different structure on thermoregulatory responses. Ann Phys Anthrop. 12,165-171.

69. Kerrigan CD. Johansson JL. Bryant MG. Boxer JA, 2005. Moderate-heeled shoes and knee joint torques relevant to the development and progression of knee osteoarthritis. Arch Phys Med Rehabil. 86,871-875.

70. Kerrigan DC, Todd MK, Riley PO, 1998. Knee osteoarthritis and high-heeled shoes. Lancet.351, 1399-1401.

71. Kim KJ, Kitaoka HB, Luo ZP, Ozeki S, Berglund LJ, Kaufman KR, et al. 2001. An in vitro simulation of the stance phase in human gait. J Musculoskel Res.5, 113–21.

72. Kim KJ, Uchiyama E, Kitaoka HB, An KN, 2003. An in vitro study of individual ankle muscle actions on the center of pressure. Gait Posture 17, 125–131.

73. Kim W, Voloshin AS, 1995. Role of plantar fascia in the load bearing capacity of the human foot. J. Biomech. 28, 1025–1033.

74. Kirby KA, 2001. What future direction should podiatric biomechanics take? Clinics in Podiatric Med Surg. 18,719-723.

75. Kogler GF, Veer FB, Verhulst SJ, Solomonidis SE, Paul JP, 2001. The effect of heel elevation on strain within the plantar aponeurosis: In vitro study. Foot Ankle Int, 22, 433-439.

76. Kogler GF, Solomonidis SE, Paul JP, 1995. In vitro method for quantifying the effectiveness of the longitudinal arch support mechanism of a foot orthosis. Clin Biomech. 10, 225–245.

77. Kogler GF, Solomonidis SE, Paul JP, 1996. Biomechanics of longitudinal arch support mechanisms in foot orthoses and their effect on plantar aponeurosis strain. Clin Biomech. 11, 243–252.

78. Kos L, Duhovnik J, 2002. A system for footwear fitting analysis, Int. Design Conference – Design

79. Kura H, Luo Z.P., Kitaoka HB, An KN, 1998. Role of medial capsule and transverse metatarsal ligament in hallux valgus deformity. 354, 235-240.

80. Kurz B, 1992. Schuh Technik, July/August.

81. Lam SF, Hodgson AR, 1958. A comparison of foot forms among the non-shoe and shoe-wearing Chinese population. J Bone Joint Surg Am. 40, 1058-1062.

82. Lee YH, Hong WH, 2005. Effects of shoe inserts and heel height on foot pressure, impact force, and perceived comfort during walking. Applied Ergonomics. 36,355–362.

83. Lee, KH, Matteliano A, Medige J, Smiehorowski T, 1990. Electromyographic changes of leg muscles with heel lifts in women: therapeutic implications. Archives of Physical Medicine and Rehabilitation. 71, 31-33.

84. Lemmon D, Shiang TY, Hashmi A, Ulbrecht JS, Cavanagh PR, 1997. The effect of insoles in therapeutic footwear: a finite-element approach. J Biomech. 30, 615-620.

85. Lewis G, 2003. Finite element analysis of a model of a therapeutic shoe: effect of material selection for the outsole. Biomed Mater Eng. 13, 75-81.

86. Li KW, Chen CJ, 2004. The effect of shoe soling tread groove width on the coefficient of friction with different sole materials, floors, and contaminants. Applied Ergonomics.35, 499–507.

87. Linder M, Saltzman CL, 1998. A history of medical scientists on high heels. Int. J of Health Services, 28,201-225.

88. Litzelman DK, Marriott DJ, Vinicor F, 1997. The role of footwear in the prevention of foot lesions in patients with NIDDM. Diabetes Care. 20, 156–162.

89. Llana S, Brizuela G, Durc JV, Garcia AC,2002.A study of the discomfort associated with tennis shoes, Journal of Sports Sciences.20, 671- 679.

90. Lord M, Hosein R, 2000. A study of in-shoe plantar shear in patients with diabetic neuropathy. Clin Biomech. 15,278–283.

91. Lord SR, Bashford GM. 1996. Shoe characteristics and balance in older women. J American Geriatrics Society. 44. 429-433.

92. Lord SR, Bashford GM, Howland A, Munroe BJ, 1999. Effects of Shoe Collar Height and Sole Hardness on Balance in Older Women. J Am Geriatri Soc. 47,681-684.

93. Luximon A, Goonetilleke RS, 2001. A fit metric for footwear customization. Proceedings of the 2001 world congress on mass customization and personalization. Hong Kong.

94. Maciejewshi ML, Reiber GE, Simth DG, Wallace C, Hayes S, Boyko EJ, 2004. Effectiveness of diabetic therapeutic footwear in preventing reulceration. Diabetes Care. 27, 1774–1782.

95. Mandato MG, Nester E, 1999. The effects of increasing heel height on forefoot peak pressure. Journal of the American Podiatric Medical Association. 89. 75-80.

96. Manna I, Pradhan D, Ghosh S, Kar SK, Dhara P, 2001. A comparative study of foot dimension between adult male and female and evaluation of foot hazards due to using of footwear. J Physiol Anthropol Appl Human Sci.20, 241-246.

97. Marshall P, 1988. The rehabilitation of overuse foot injuries in athletes and dancers. Clinics in Sports Medicine. 7, 175-191.

98. Mayo Clinic. Foot problems in women: High heels and your health, 2006, (http://www.mayoclinic.com).

99. McBride ID, Wyss UP, Cooke TV, Chir B, Murphy L, Phillips J, Olney S, 1991. First metatarsophangeal joint reaction forces during high-heel gait. Foot Ankle. 11, 282-288.

100. McPhoil TG, 1988. Footwear. Physical Therapy. 68,1857-1865.

101. Merrifield HH, 1971. Female gait pattern in shoes with different heel height. Ergonomics.14, 411-417.

102. Miller JE, Nigg BM, Liu W, Stefanyshyn DJ, Nurse MA.2000.Influence of foot, leg and shoe characteristics on subjective comfort. Foot Ankle Int. 21, 7 59-767.

103. Mundermann A, Nigg BM, Stefanyshyn DJ, Humble RN, Daren J, 2003. Orthotic comfort is related to kinematics, kinetics, and EMG in recreational runners, Med Sci Sports Exerc. 35, 1710-1719.

104. Mundermann A, Nigg BM, Stefanyshyn DJ, Humble RN, 2002. Development of a reliable method to assess footwear comfort during running. Gait and Posture.16, 38–44.

105. Mundermann A, Nigg BM, Stefanyshyn DJ, Humble RN, A reliable measure to assess footwear comfort. Proc. of the 5th Symp. on Footwear Biomechanics, 2001, Zurich / Switzerland, (Eds. E. Hennig, A. Stacoff). 64.

106. Nakamura S, Crowninshield RD, Cooper RR, 1981. An analysis of soft tissue loading in the foot—a preliminary report. Bull Prosthet Res. 18, 27–34.

107. Nielsen R, Gavhed DCE, Nilsson H, 1989.Thermal function of a clothing ensemble during work: dependency on inner clothing layer fit. Ergonomics. 32,1581-1594.

108. Nigg BM, Denoth J, ker B, Luethi S, Smith D, Stacoff A. 1984. Load, sport shoes and playing surfaces. In sport shoes and playing surfaces (edited by Frederick EC), 1-23. Champaign,IL: Human Kinetics.

109. Nyska M, McCabe C, Linge K, Klenerman L,1996.Plantar foot pressures during treadmill walking with high-heel and low-heel shoes. Foot Ankle Int.17, 662–666.

110. Opila KA, Wagner SS, Schiowitz S, Chen J, 1988. Postural alignment in barefoot and high-heeled stance. Spine. 13, 542-547.

111. Opila-Correia KA, 1990(a). Kinematics of high-heeled gait. Archives of physical medicine and rehabilitation. 71,304.

112. Opila-Correia, KA, 1990 (b). Kinematics of high-heeled gait with consideration for age and experience of wearers. Archives of Physical Medicine and Rehabilitation.71, 905-909.

113. Orthcoastfootcare (www.orthcoastfootcare.com)

114. Penrose JM, Holt GM, Beaugonin M, Hose DR, 2002. Development of an accurate three-dimensional finite element knee model. Comput Methods Biomech Biomed Eng. 5, 291-300.

115. Perry J. 1992. Gait analysis: normal and pathological function. Thorofare, NJ: SLACK;

116. Brownrigg P, 1996. The foot and footwear. Australian Family Physician. 25,895—899.

117. Phillips D, 1988. Biomechanics in Hallux Valgus and forefoot surgery. In: Hetherington, VJ (Ed.), Churchill Livingstone, New York 39.

118. Purvis AJ. Tunstall H, 2004. Effect of sock type on foot skin temperature and thermal demand during exercise. Ergonomics. 47, 1657-1668.

119. Quimby HR. The Story of Lasts, in: National Shoe Manufacturers Association, New York 1944.

120. Ravindra S. Goonetilleke and Ameersing Luximon, 2001. Computer-Aided Ergonomics and Safety Conference.

121. Ricci B, Karpoich PV, 1964. Effect of height of the heel upon the foot. Res Q. 35, SUPPL385-388.

122. Robbins S, Gouw GJ, McLaren J, 1992.Shoe sole thickness and hardness influence balance in older men. J Am Geriatr Soc. 40, 1089-1094. .

123. Rossi WA, Tennant, 1984. Professional shoe fitting. New York, NY, National Shoe Retailer Association.

124. Rossi WA, 1983. The high incidence of mismated feet in the population. Foot Ankle. 4,105-112.

125. Schlager, 1994. How Products Are Made, MI, USA, Gale Group.

126. Schols EHM, Eijnde WAJ, Heus R,2004.A method for assessing thermal comfort of shoes using a ‘‘sweating’’ foot. Eur J Appl Physiol. 92,706–709.

127. Shackel B, Chidsey KD, Shipley P, 1969. The assessment of chair comfort. Ergonomics.12, 269-306.

128. Sharkey NA, Hamel AJ, 1998. A dynamic cadaver model of the stance phase of gait: performance characteristics and kinetic validation. Clin Biomech.13, 420–433.

129. Shiang TY, 1997. The nonlinear finite element analysis and plantar pressure measurement for various shoe soles in heel region. Proc Nat Sci Counc Repub China B. 21, 168-174.

130. Shiina Y, Hamamoto Y, Okumura K, 2006. Fracture of soft cellular solids--Case of non-crosslinked polyethylene foam. Europhys Lett. 76, 588-594.

131. Shimizu M, Andrew PD, 1999. Effect of heel height on the foot in unilateral standing. J Phys Ther Sci. 11, 95–100.

132. Shorten MR, 1998. Finite element modeling of soccer shoe soles. Proceedings of World Cup Scientific Congress. Lyons, France.

133. Siegler S, Block J, Schneck CD, 1988. The mechanical characteristics of the collateral ligaments of the human ankle joint. Foot Ankle. 8, 234-242.

134. Sivamani RK, Goodman J, Gitis NV, Maibach HI. 2003. Coefficient of friction tribological studies in man - an overview. Skin Res Technol. 9, 227-234.

135. Slater K, 1985. Human comfort. Springfield: Thomas.

136. Smith EO, Helms WS, 1999. Natural selection and high heels. Foot Ankle Int. 20, 55-57.

137. Sobel E, Levitz SJ, Caselli MA, Christos PJ, Rosenblum J. 2001. The effect of customized insoles on the reduction of postwork discomfort. J Am Podiatr Med Assoc. 91, 515-20.

138. Spears IR, Miller –Young JE, Sharma J, Ker RF, Smith FW. 2007. J Biomech. 40, 2774-2780.

139. Speirs AD, Heller MO, Duda GN, Taylor WR, 2007. Physiologically based boundary conditions in finite element modelling. J Biomech. 40,2318-2323.

140. Speksnijder CM, Munckhof R, Moonen S, Walenkamp G, 2005.The higher the heel the higher the forefoot-pressure in ten healthy women. The Foot.15, 17–21.

141. Stefanyshyn DJ, Nigg BM, Fisher V, O'Flynn B, Liu W. 2000.The influence of high heeled shoes on kinematics, kinetics and muscle EMG of normal female gait. J Appl Biomech. 16. 309-319.

142. Stephens MM, 1992. Heel pain: shoes, exertion, and Haglund's deformity. The Physician and Sports Medicine. 20, 87-95.

143. Sussman RE, D'Amico JC, 1984. The influence of the height of the heel o the first metatarsophalangeal joint. J Am Podiatry Assoc. 74, 504-508.

144. Syngellakis S, Arnold MA, Rassoulian H, 2000. Assessment of the non-linear behavior of plastic ankle foot orthoses by the finite element method. Proc Inst Mech Eng. 214, 527-539.

145. Tappin JW, Robertson KP, 1991. Study of the relative timing of shear forces on the sole of the forefoot during walking. Journal of Biomedical Engineering.13, 39–42.

146. Thompson FM, Coughlin MJ, 1994. The high price of high-fashion footwear. J Bone Joint Surg. 76A, 1586-1593.

147. The Gallup Organization Inc., 1986. Women's attitudes and usage of high-heeled shoes. The Gallup Organization Inc. Surrey, England.

148. Tower JD, Deible CT, Golla SK, 2003. Foot and ankle biomechanics. Seminars in musculoskeletal radiology. 7, 67-74.

149. Verdejo R, Mills NJ, 2004. Heel-shoe interactions and the durability of EVA foam running-shoe midsoles. J Biomech. 37, 1379-1386.

150. Viceconti M, Olsen S, Nolte LP, Burton K, 2005. Extracting clinically relevant data from finite element simulations. Clin Biomech. 20, 451–454.

151. Wang B, Lu G, 2006. Key engineering materials. Trans Publication, Switzerland. 275-280.

152. Wang YT, Pascoe DD, Kim CK. 2001. Force patterns of heel strike and toe off on different heel heights in normal walking. Foot Ankle Int. 22,486-492.

153. Witana CP, Feng J, Goonetilleke RS.2004. Dimensional differences for evaluating the quality of footwear fit. Ergonomics. 47, 1301-1317.

154. Wright D, Rennels D, 1964. A study of the elastic properties of plantar fascia. Journal of Bone and Joint Surgery—American Volume 46, 482–492.

155. Wright DG, Rennels DC, 1964. A study of the elastic properties of plantar fascia. J Bone Joint Surg Am. 46, 482-92.

156. Wu G, Siegler S, Allard P, Kirtley C, Leardini A, Rosenbaum D, Whittle M, D'Lima DD, Cristofolini L, Witte H, Schmid O, Stokes I; Standardization and Terminology Committee of the International Society of Biomechanics, 2002. ISB recommendation on definitions of joint coordinate system of various joints for the reporting of human joint motion--part I: ankle, hip, and spine. J Biomech. 35, 543-548.

157. Wunderlich RE, Cavanagh PR, 2001.Gender differences in adult foot shape: implications for shoe design. Med Sci Sports Exerc. 33,605-611.

158. Zhang M, Mak AF, 1999. In vivo skin frictional properties. Prosthet Orthot Int. 23, 135-141.